University of Sussex

Analysis of Homologous Recombination Restarted Replication Forks in *S. pombe*

Alice Budden

Genome Damage and Stability PhD

September 2020

Declaration

I hereby declare that this thesis has not been and will not be, submitted in whole or in part to another University for the award of any other degree.

Signature:……

Acknowledgements

Firstly, a huge thanks goes to Tony Carr for allowing me to take on this PhD and giving me his time in guiding me through the years and trying to pass on some of his incomprehensible knowledge. A lot of credit has to also go to Jo Murray for suggesting I apply for the position in the first place.

A massive shout out has to go to Karel Naiman for giving me endless amounts of his time supporting me throughout my entire PhD in respect to helping with experiments, general discussion, and so much support to help me be the best I can be. Loads of thanks has to go to everyone in the Carr lab who have also supported me hugely both experimentally, and well… just mentally. Owen, Tom, Adam, Dave, Marie and Rob have all played a large role in supporting me throughout this PhD, as well as providing a lot of banter and some entertaining pranks along the way. Not forgetting so many other people in the whole GDSC that have helped me through these years. In particular the "Ladies that Lunch" crew, with Rose always on hand in times of need.

Outside of science I have a load of other people to thank for keeping me sane. Well maybe sane is a strong word, but anyway. Particular thanks to my housemates Andy and Fab for sticking with me during my 8 years in Brighton, the endless good times, support, and just general release from stress has been top notch. Not forgetting the rest of S Club, always there to lift my spirits through this last stretch. I also cannot thank my family enough, my Dad, Mandy, Chloe, and Jade, have been incredible. Thanks for always being there for me, supporting me, providing me with a sense of normality, all the Sunday clubs, and visits to Brighton.

And lastly, I'd like to thank the pubs of Brighton, they may have taken a lot of my money, but they've always been there for me (well minus three months of lockdown, that was a tough three months). So for that, thank you.

Abstract

Natural impediments to DNA replication such as replication fork barrier's (RFB's), replication-transcription collisions, or secondary structure forming sequences, can result in replication stress and contribute to genomic instability. This project utilizes the *Schizosaccharomyces pombe* replication fork barrier, *RTS1*, known to result in replication fork stalling that requires homologous recombination (HR) for restart. The HR- restarted replication fork uses Polymerase δ to synthesise both DNA strands and is known to be error-prone in nature, resulting in both replication fork slippage and gross chromosomal rearrangements. This project produces an optimized system for studying the HR-restarted replication fork at *RTS1*. By utilizing methods including Pu-Seq, and a genetic replication slippage assay, we are able to investigate both polymerase usage between strands and replication fidelity, respectively. Break induced replication (BIR) in *Saccharomyces cerevisiae* is another replication fork restart method often compared to HR-restart at *RTS1* in *S. pombe*. Pol32 and its interaction with PCNA are essential for restart using BIR, however, we provide evidence using Cdc27 (*Sc*Pol32) that this interaction is important to a lesser extent during HR-restart at *RTS1*. Additionally, the necessity of the protein Rtf2 for efficient replication fork stalling at *RTS1* has been confirmed. Rtf2 and its removal from stalled replication forks has recently been implicated in maintaining genome stability in human cells. Additional methods used including ChIP-qPCR, Co-IP and mass spectrometry has allowed further investigation into proteins involved in the restarted replication fork.

List of Figures

List of Tables

List of Abbreviations

ATP	Adenosine triphosphate
BIR	Break induced replication
CPT	Camptothecin
DAPI	4’6-diamino-2-phenylindole
DNA	Deoxyribonucleic acid
DSB	Double strand break
dsDNA	Double stranded deoxyribonucleic acid
FACS	Fluorescence activated cell sorting
HR	Homologous recombination
HU	Hydroxyurea
MMS	Methylmethane sulfonate
MS	Mass spectrometry
NHEJ	Non-homologous end joining
PBS	Phosphate buffered saline
rDNA	Ribosomal DNA
RF	Replication fork
RFB	Replication fork barrier
RNA	Ribonucleic acid
rNTP	Ribonucleoside triphosphate
rRFB	Ribosomal DNA replication fork barrier
RTS1	Replication termination sequence 1
SD	Standard deviation
SEM	Standard error of the mean
SDS	Sodium dodecyl sulfate
SDSA	Synthesis dependent strand annealing
SSA	Single strand annealing
ssDNA	Single stranded deoxyribonucleic acid
SUMO	Small ubiquitin-like modifier
TLS	Translesion synthesis
UV	Ultraviolet light

Table of Contents

Chapter 1 – Introduction

1.1 Project Aims

Cell division is a key aspect to cellular life, whereby the whole of the genome needs to be accurately duplicated for inheritance into each new daughter cell. The process of genome duplication is termed DNA replication, and must be carried out accurately to avoid detrimental effects on the cell. Inaccurate DNA replication can result in incomplete genome duplication, gross chromosomal rearrangements, mutations, and cell death. There are several challenges to DNA replication that may result in these outcomes including, DNA base damage, DNA breaks, secondary structures, and protein-DNA barriers. Some of these can act as barriers to DNA replication fork progression and can result in replication fork stalling and collapse that need to be rescued to complete DNA synthesis of the entire genome. Inability to deal with challenges to DNA replication can contribute to cancer development and is a key area of interest for targets of cancer therapeutics.

In order to study overcoming replication fork stalling and collapse, the Carr lab and others have previously used the native *RTS1* replication fork barrier (RFB) found in *Schizosaccharomyces pombe* (*S. pombe*) to investigate site-directed replication fork restart. This restart is known to rely on homologous recombination (HR) and result in replication of both strands after restart by Polymerase δ. This is in contrast to the canonical division of labour of Polymerase ε/δ replicating the leading/lagging strands, respectively. Replication fork restart by HR is known to be error-prone but the exact mechanisms behind its error-proneness remain elusive.

This project aims to set up an optimised *RTS1* RFB system in *S. pombe* to allow investigation of the restarted replication fork without interference from convergent canonical replication forks. Utilizing the polymerase-usage sequencing method allows direct visualisation of the extent of Polymerase δ switch on the leading strand in several mutant backgrounds, as well as visualisation of the replication forks relative speed and termination with the convergent fork. Additionally, a replication fork slippage assay is

set up for use alongside as a direct readout for mutagenicity of the restarted replication fork. The optimised construct is used for two independent sub-projects: 1) Break Induced Replication (BIR); 2) the role of Rtf2. In the first project, mutants important for BIR in *S. cerevisiae* are used to distinguish key differences between BIR and HR-restart at *RTS1*. In the second sub-project, the role of Rtf2 on efficient replication fork stalling at *RTS1* is explored. Additionally, a mass spectrometry method is established for future use to assess the proteins Rtf2 interacts with to unravel its role at stalled replication forks. Altogether, this project exploits the *RTS1* RFB to investigate key aspects of HR-restart in *S. pombe.*

1.2 Fission Yeast Cell Cycle

The *Schizosaccharomyces pombe* (*S. pombe*) cell cycle consists of G1, S, G2, M phases (Figure 1.1). G1 phase contains a point at which the cell commits to the cell cycle, termed START, that is reminiscent of a similar point in other eukaryotes (Hartwell, 1974). S phase is the stage of DNA replication where the entire DNA content is copied once per cell cycle. This is followed by a gap phase, G2, before entering mitosis (M phase) to separate the sister chromatids into the two new daughter cells that are divided by cytokinesis. M phase is followed by an additional very short gap phase G1, before entering the next S phase. In *S. pombe* cytokinesis separates the two daughter cells by creating a septum and dividing the cell in two. However, the onset of S phase actually occurs prior to completion of cell division, coinciding with septum formation (Mitchison and Creanor, 1971).

Once cells enter the cell cycle, their progress is determined at two key points, the G1-S transition, and the G2-M transition. Activity of Cdc2, the *S. pombe* cyclin dependent kinase (CDK), is important for efficient progression at both of these stages (Nurse and Bissett, 1981). Cdc2 interacts and forms a complex with various cyclins, with Cdc13 being the only essential cyclin in fission yeast (Fisher and Nurse, 1996). Cdc2 activity is low in G1 and increases as cells enter S phase. A moderate level of Cdc2 activity is important for the onset of S phase as well as aiding inhibition of re-replication to ensure the correct

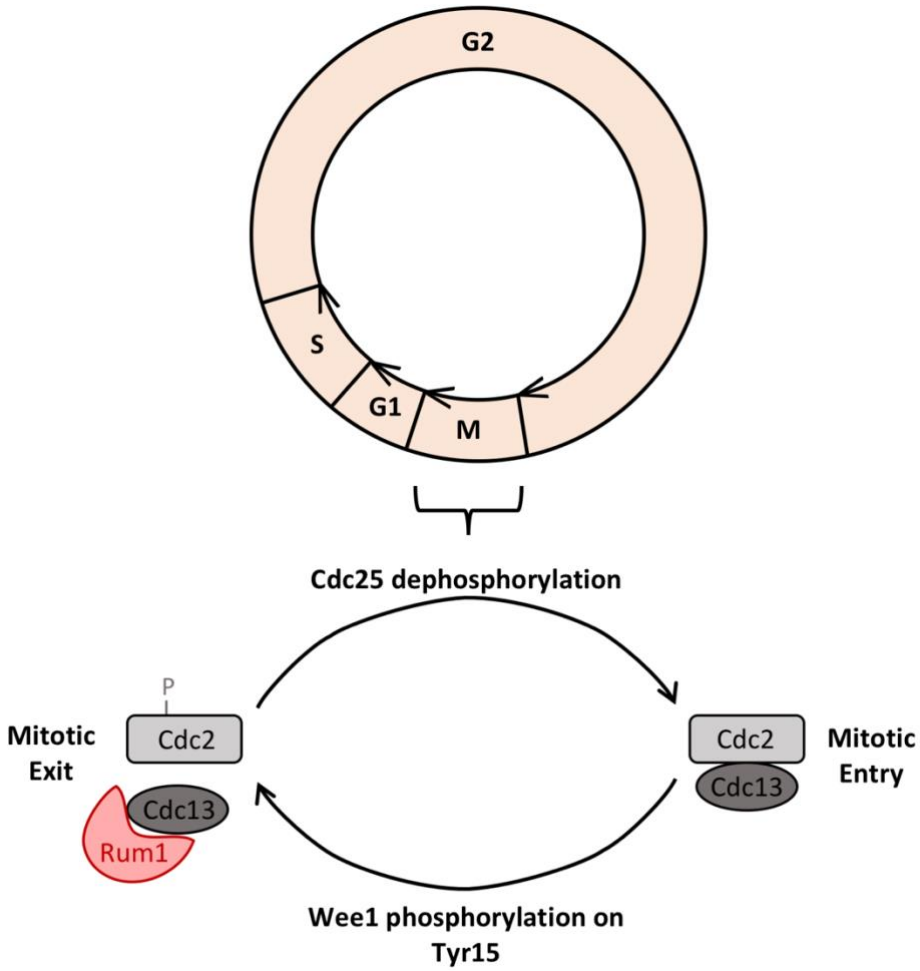

Figure 1.1. Fission Yeast Cell Cycle. The cell commits to the cell cycle at a point in G1 termed START. The cell then enters S phase during which the genome is duplicated before entering the long gap phase, G2. Entry into M phase (mitosis) allows separation of the sister chromatids for distribution into the two daughter cells and subsequent cytokinesis. Cdc2 (CDK) and the cyclin Cdc13 promote entry into mitosis. These proteins are inhibited by phosphorylation of Cdc2 on Tyr15 by Wee1 kinase and targeting of Cdc13 for proteolysis by Rum1 to allow mitotic exit. Cdc2 can be activated again by Cdc25 mediated dephosphorylation.

amount of duplicated DNA enters mitosis (Baum et al., 1998, Stern and Nurse, 1996, Vas et al., 2001). High Cdc2 activity is important for progression into mitosis (M phase). Inhibition of Cdc2 activity occurs by phosphorylation of Tyrosine 15 by the Wee1 and Mik1 tyrosine kinases (Gould and Nurse, 1989, Lundgren et al., 1991). Mik1's inhibitory action on Cdc2 appears to be most prominent during S phase where its protein levels are increased to prevent early entry into mitosis (Baber-Furnari et al., 2000, Christensen et al., 2000, Lundgren et al., 1991). Inhibition of Cdc2 is also important to allow subsequent mitotic exit and cytokinesis (Dischinger et al., 2008). The phosphatase Cdc25 counteracts the activity of Wee1, acting to dephosphorylate Cdc2 and allow its high level of activation to enable induction of mitosis (Russell and Nurse, 1986). Cdc2-Cdc13 levels are also kept low in G1 by the CDK inhibitor Rum1, which targets Cdc13 for proteolysis (Correa-Bordes et al., 1997, Correa-Bordes and Nurse, 1995). Altogether, these mechanisms ensure timely and efficient progression through the cell cycle.

1.3 Eukaryotic DNA Replication

1.3.1 Origins of DNA Replication

DNA replication initiates at multiple locations along the genome known as replication origins. In *S. cerevisiae* origins are defined by a specific consensus sequence where the origin recognition complex (ORC) binds, but only a subset are activated in any one S phase (Linskens and Huberman, 1988). In *S. pombe* there is no consensus sequence, instead origins are determined by AT rich sequences that have been associated with nucleosome free regions that define ORC binding sites (Dai et al., 2005, Hayashi et al., 2007, Segurado et al., 2003, Xu et al., 2012). Additionally, the origin firing pattern appears to be stochastic in fission yeast (Kaykov and Nurse, 2015, Patel et al., 2006).

1.3.1.1 Formation of Pre-Replicative Complex (Pre-RC)

Binding of ORC (Orp1-6) to sites in the genome is an important first step in DNA replication initiation occurring in G1/M phase of the cell cycle (Wu and Nurse, 2009).

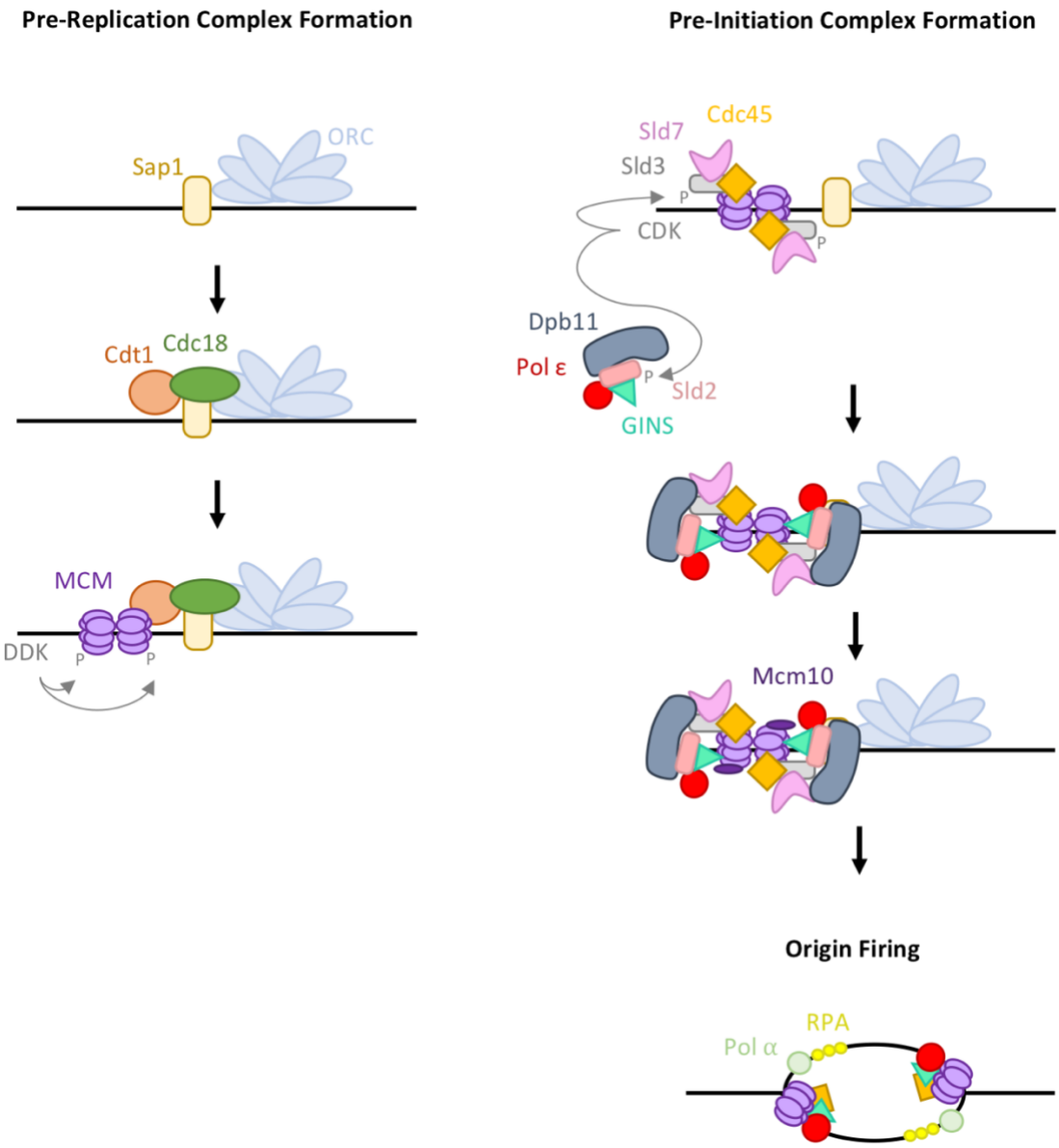

Figure 1.2. Replication Origin Formation. The first step in origin firing is the formation of the pre-replicative complex (Pre-RC) where ORC proteins bind and recruit Cdc18 and Cdt1 to enable the MCM's to be located to these regions. Next the Pre-Initiation complex is formed that includes recruitment of Cdc45 via Sld3 and Sld7, as well as recruitment of GINS and Polε via Dpb11 and Sld2. Finally, addition of Mcm10 allows origin firing. Recruitment of Cdc45 and GINS to MCM proteins allows formation of the active helicase CMG. Origin firing can then occur and recruitment of additional replisome factors to allow bidirectional replication.

The Orp4 subunit of the ORC complex in *S. pombe* has been found to contain nine AT-hook motifs that aid binding of ORC to AT-rich regions associated with origins (Lee et al., 2001). However, not all of the ORC bound sites will be used as origins of replication, only those that form the pre-recognition complex (pre-RC) in a process known as origin licensing (Figure 1.2, *left panel*). In fission yeast the Sap1 protein has been reported to bind ORC and allow formation of the pre-RC due to its role in recruiting Cdc18 (*Sc*Cdc6) to origins (Guan et al., 2017). Cdt1 also interacts with Cdc18 and these proteins work together to recruit the mini-chromosome maintenance (MCM) complex required for initiation of DNA replication (Nishitani et al., 2000). MCM is the catalytic core of the replicative helicase that forms a hexameric complex composed of Mcm2-7 loaded onto DNA as a double hexamer encircling the DNA in a head-to-head formation to enable bidirectional replication (Douglas et al., 2018, Evrin et al., 2009, Georgescu et al., 2017, Remus et al., 2009). This process forms the pre-RC, peaking during G1 phase of the cell cycle (Wu and Nurse, 2009).

The timing of this event is important for regulation of DNA synthesis at the correct phase of the cell cycle, and ensuring only single initiation of origins to inhibit multiple rounds of replication. Protein levels of both Cdt1 and Cdc18 peak at late G1 phase to ensure pre-RC formation only occurs before S phase (Muzi Falconi et al., 1996, Nishitani et al., 2000, Nishitani and Nurse, 1995). Cdc2 (*Sc*Cdc28), the cyclin dependent kinase (CDK), is responsible for controlling the levels of Cdc18. When levels of Cdc2 rise in S phase it results in phosphorylation of Cdc18 and targeting it for proteasomal degradation (Baum et al., 1998). Cdt1 is targeted for proteasomal degradation via Ddb1-Cdt2, subunits of the Cul4 E3 ubiquitin ligase complex (Ralph et al., 2006). Cdt2 is only present in S phase and also acts with Ddb1 to target Spd1, the ribonucleotide reductase (RNR) inhibitor, for degradation to ensure appropriate dNTP pools are available during replication (Liu et al., 2005). Additionally, Cdc2 also inhibits re-replication in S phase by phosphorylating Orp2 (Vas et al., 2001).

1.3.1.2 Formation of Pre-Initiation Complex (Pre-IC)

When cells enter S phase the pre-RC needs to be activated by a multitude of factors to allow DNA replication initiation, in a process that first forms the pre-initiation complex (Pre-IC) (Figure 1.2, *right panel*) that is subsequently activated by Mcm10. Each of the Mcm subunits loaded onto DNA are ATPases activated by the addition of Cdc45 and the GINS complex to form the active helicase CMG (Ilves et al., 2010, Moyer et al., 2006). Hsk1-Dfp1 (*Sc*Cdc7-Dbf4), the Dbf4-dependent kinase (DDK), activity is important for recruitment of Sld3 to the MCM complex in G1 and subsequent recruitment of Cdc45 (Nakajima and Masukata, 2002). Additionally, phosphorylation by CDK of Sld3 (*Sp*Sld3) and Sld2 (*Sp*Drc1) have been shown to be important for formation of a complex with Dpb11 (*Sp*Rad4/Cut5) to allow the downstream recruitment of both Cdc45 and GINS to replication origins (Fukuura et al., 2011, Noguchi et al., 2002). In fission yeast Sld3 recruitment to origins appears to occur upstream of Cdc45 recruitment (Yabuuchi et al., 2006). However, in budding yeast Sld3 forms a tight complex with Sld7 that associates with Cdc45 and is recruited to origins in a DDK dependent manner (Tanaka et al., 2011, Yeeles et al., 2015). There is no Sld7 orthologue in fission yeast, however, this factor is dispensable for Sld3-Cdc45 association to origins in budding yeast (Kamimura et al., 2001). Subsequent phosphorylation of Sld2 by CDK is important in recruiting GINS (tetrameric complex of Sld5, Psf1, Psf2, and Psf3) to origins in a complex composed of Sld2, GINS, Dpb11 and Pol ε termed the pre-loading complex (pre-LC) (Muramatsu et al., 2010). Without the addition of GINS, Polε (*Sc*Pol2) is unable to associate with origins and perform replication upon DNA unwinding (Pai et al., 2009). The final protein recruited to origins to allow DNA unwinding by active CMG is Mcm10 (Yeeles et al., 2015).

Hydrolysis of ATP by Mcm2-7 is also important for both helicase loading and activation of CMG (Coster et al., 2014, Kang et al., 2014). The active CMG is then able to unwind duplex DNA producing ssDNA that can be coated and protected by Replication Protein A (RPA) (Yeeles et al., 2015). Recently, the initial unwinding of DNA by the two CMG helicases has been shown to first occur by untwisting of the DNA separating the two CMG complexes prior to full activation (Douglas et al., 2018). Once Mcm10 has been recruited this allows further untwisting of the DNA and subsequent activation of the two

CMG helicases (Douglas et al., 2018). This results in their propagation along DNA by passing over each other at the site of the origin and travelling along the ssDNA of the leading strand. This unwinding event also enables the downstream recruitment of the other key replicative polymerases, Polα (*Sc*Pol1) and Polδ (*Sc*Pol3) (Heller et al., 2011).

1.3.2 DNA Replication Progression

Polα is required to initiate both leading and lagging strand replication by synthesising an RNA-DNA primer (Okazaki fragment) that is then elongated by one of the other main replicative polymerases (Okazaki et al., 1968). The CMG helicase translocates along leading strand ssDNA in a 3'-5' direction (Fu et al., 2011), with each of the newly replicated strands synthesised in a 5'-3' direction by its respective polymerase. Therefore, the leading strand is considered to be replicated in a continuous manner, whereas the lagging strand is replicated discontinuously as more DNA is unwound. Lagging strand synthesis requires multiple Okazaki fragments to be placed along DNA for the lagging strand polymerase to prime to in order to complete DNA replication of the entire strand. These Okazaki fragments are then displaced to produce a flap when the polymerase reaches the 5' end of the RNA-DNA primer (Bhagwat and Nossal, 2001, Stith et al., 2008). This flap is then nicked by Fen1 nuclease to remove the RNA, allowing subsequent ligation of the neighbouring newly synthesised DNA strands (Stodola and Burgers, 2016).

In fission yeast, Polδ is a four subunit complex composed of the catalytic subunit Pol3 and three other subunits Cdc1, Cdc27, and Cdm1. It is recruited to replication forks initially via replication factor C (RFC) interacting with the 3' end of the synthesised RNA-DNA primer by Polα. RFC loads PCNA at these primer-template junctions in an ATP driven reaction enabling opening of PCNA and subsequent closing after ATP hydrolysis, forming a ring shape round DNA (Chen et al., 2009). PCNA tethers Polδ to the replication fork for optimal processivity via several interaction points including the c-terminus of the Cdc27 (*Sc*Pol32) subunit (Chilkova et al., 2007, Reynolds et al., 2000). Cdc27 also interacts directly with Polα.

The widely accepted view of the division of labour between the two main replicative polymerases is that Polε is the predominant leading strand polymerase, and Polδ is the lagging strand polymerase. Sequencing experiments mapping mutational signatures of mutants of the main replicative polymerases (discussed below) in both budding yeast and fission yeast has confirmed this division of labour (Miyabe et al., 2011, Nick McElhinny et al., 2008, Pursell et al., 2007). However, an additional study in budding yeast has suggested the lack of mutational signatures on the leading strand in cells harbouring rNTP permissive Polδ mutants is due to removal by the proofreading capability of Polε (Johnson et al., 2015). This suggested Polδ is the primary polymerase of both leading and lagging strands. However, this has recently been challenged by use of a Polε mutant lacking its exonuclease proofreading capability still performing as the main leading strand polymerase (Garbacz et al., 2018).

The importance of Polδ replication also comes from studies on the cell viability of catalytic mutants of Polε lacking both exonuclease and polymerase activities, revealing it is dispensable for carrying out DNA replication (Dua et al., 1999, Feng and D'Urso, 2001, Kesti et al., 1999). Furthermore, recent next generation sequencing experiments using strains lacking Polε catalytic activity have revealed Polδ to replicate both DNA strands (Garbacz et al., 2018, Miyabe et al., 2015). However, in this context Polδ leading strand synthesis appears to occur at slower rates in comparison to wildtype Polε leading strand synthesis (Yeeles et al., 2017), and results in increased genome instability (Garbacz et al., 2018). However, some contribution of Polδ for leading strand synthesis cannot be ignored. Sequencing experiments have revealed a bias toward Polδ usage immediately proximal to origins (Daigaku et al., 2015, Garbacz et al., 2018). Mapping of Polα-primase replication suggests the lagging strand primer is placed to the side of the origin and extended by Polδ across the origin before switching to Polε for leading strand synthesis (Garbacz et al., 2018). This supports similar findings using an *in vitro* reconstituted replication system in *S. cerevisiae* (Aria and Yeeles, 2018). This suggests concerted action of all three polymerase to initiate DNA replication on the leading strand with Polε continuing replication of the downstream region.

1.3.3 DNA Replication Termination

Termination of DNA replication remains a fairly elusive process. Some studies mapping Polε usage suggest Polε from the leading strand of each converging replication fork pass over each other to complete replication (Daigaku et al., 2015). This is in line with the knowledge that the CMG helicase mainly interacts with and travels along the leading strand during DNA replication (Fu et al., 2011). Thus, as is shown in *Xenopus* egg extracts, the converging CMG complexes pass over one another on the leading strands during replication termination and is only removed once DNA synthesis and ligation has completed (Dewar et al., 2015). In both *Xenopus* egg extracts and *S. cerevisiae,* removal of CMG at the last stages of DNA replication has been shown to occur via ubiquitylation of Mcm7 (Dewar et al., 2017, Maric et al., 2014). However, other studies find a slight bias towards Polδ usage at termination zones in both budding and fission yeast suggesting Polδ takes over from Polε to complete DNA synthesis (Zhou et al., 2019). The authors propose this relieves topological stress that could arise if Polε completed replication due to its tight association with the CMG helicase (Langston et al., 2014). In line with this, Pif1-family DNA helicases have been shown to promote replication termination in *S. cerevisiae,* possibly by reducing torsional stress at the converging forks (Deegan et al., 2019). Even though Polε may not complete replication of the termination region, in *Xenopus* egg extracts, it remains associated to the DNA and is only removed when CMG is unloaded after synthesis completion (Dewar et al., 2017).

1.3.4 Fork Protection Complex

Additional factors also travel with the replication fork to ensure efficient replication and stabilisation. These were identified to include Ctf4 (*Sp*Mcl1), Mrc1 (*Sp*Mrc1), and Csm3/Tof1 (*Sp*Swi1/Swi3) in *S. cerevisiae* (Gambus et al., 2006). Together Mrc1, Csm3 and Tof1 form the fork protection complex that interact with each other to stabilise the replication fork and allow fork pausing upon encountering barriers to DNA replication (Bando et al., 2009, Katou et al., 2003). Cryo-EM structure of the fork protection complex at a replication fork have recently been resolved, showing Csm3/Tof1 binding to duplex DNA ahead of the replicative helicase CMG (Baretic et al., 2020). The inclusion of Ctf4

and the fork protection complex have also been shown to be essential for efficient replication rates (Yeeles et al., 2017). In *S. pombe* Swi1 and Swi3 together are termed the fork protection complex that have a role in co-ordinating leading and lagging strand synthesis, as well as replication fork stabilisation upon fork stalling (Noguchi et al., 2004). Swi1/Swi3 are important for replication fork pausing at a number of sites including ribosomal DNA (rDNA) barriers (Krings and Bastia, 2004). The complex also allows efficient mating type switching which relies on fork pausing at the *MPS1* element of *mat1* (Dalgaard and Klar, 2000). Additionally, the replication termination sequence 1 (*RTS1*) located at the mating type locus relies on Swi1/Swi3 to allow efficient replication fork stalling (Dalgaard and Klar, 2000). Sap1 is important for recruiting Swi1/Swi3 to chromatin and allowing efficient fork stalling and subsequent resumption of DNA replication (Noguchi and Noguchi, 2007). Swi1/Swi3 are also important for recruitment and binding of Mrc1 to DNA (Shimmoto et al., 2009, Tanaka et al., 2010). Not only do Swi1/Swi3 protect replication forks upon encountering barriers to DNA replication they also act to recruit repair mechanisms to the replication fork due to their role in the efficient activation of the S phase checkpoint kinase, Cds1 (Noguchi et al., 2003, Noguchi et al., 2004).

1.3.5 Polymerase Usage Sequencing (Pu-Seq)

Polymerase-Usage Sequencing (Pu-Seq) developed by the Carr lab allows allocation of strand-specific polymerase usage revealing detailed replication dynamics in *S. pombe* (Figure 1.3) (Keszthelyi et al., 2015). Genetic experiments in both *S. cerevisiae* and *S. pombe* have assigned the leading strand polymerase as Polε and the lagging strand polymerase as Polδ (Miyabe et al., 2011, Nick McElhinny et al., 2008). However, in *S. pombe,* defining the division of labour for Polε relied on polymerase mutants that resulted in an increased ribonucleotide (rNMP) incorporation, because the mutational spectra of *cdc20* alleles tested was insufficiently biased to assign strands on the mutations induced. The incorporation of excess rNMP allowed specific fragmentation at the site of rNTP incorporation while leaving deoxyribonucleotides (dNTPs) intact permitting identification of strand specific replication by Polymerase ε (Miyabe et al., 2011). Ribonucleotides incorporated in DNA are efficiently removed using

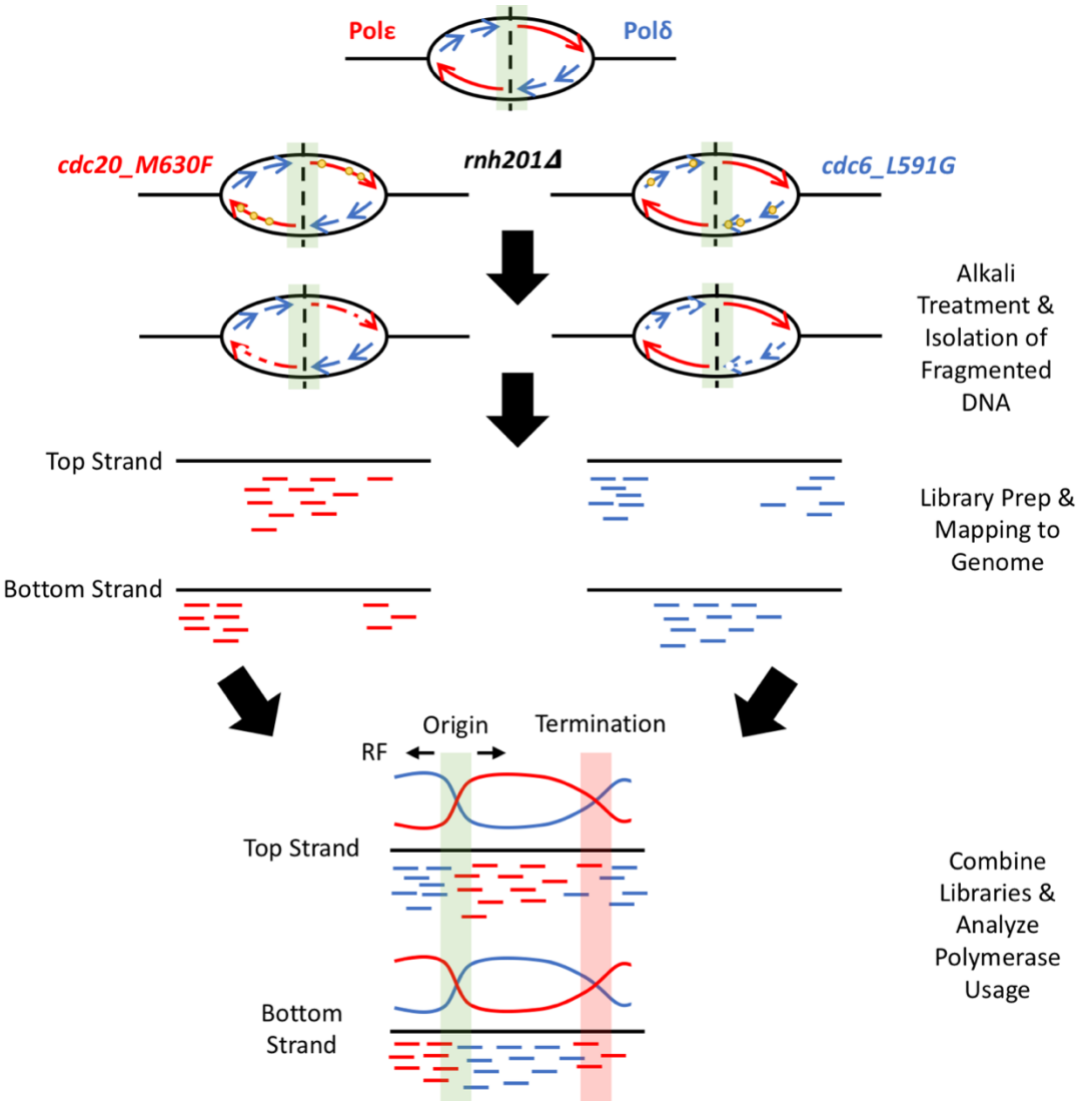

Figure 1.3. Schematic of the Polymerase-Usage Sequencing Method to Analyse Replication Dynamics in S. pombe. Separate strains containing either one of the rNTP permissive mutants of the main replicative polymerases *cdc6_L591G* (blue) or *cdc20_M630F* (red) are grown in a background deleted for *rnh201* to prevent removal of the incorporated rNTPs (yellow circles). Genomic DNA from each strain is extracted and treated with alkali to break the DNA at the site of rNTP incorporation. DNA libraries can then be made and sent for sequencing. Both libraries are then aligned to the genome and the data combined to extract the ratio of usage of each polymerase on each strand. From this other information can be inferred, including origin location, direction of replication fork movement and regions of termination.

ribonucleotide excision repair (RER) that is initiated by 5' incision of the rNTP by RNase H2 (Sparks et al., 2012). Deletion of *rnh201,* a subunit of RNase H2, allows the incorporated rNTPs to persist in the DNA and act as a marker for strand specific polymerase replication. Although, rNTP misincorporation represents DNA damage, replicative polymerases can replicate template DNA containing small numbers of rNTPs, albeit at a lower processivity (Watt et al., 2011). Therefore, cell synchronisation is not necessary to visualise polymerase usage due to the ability of the replicative polymerases to tolerate rNTPs incorporated in previous cell cycles. This enables the mutant polymerases to replicate the entire genome and allow a genome-wide view of rNTP incorporation and polymerase usage.

The initial analysis looked at only a defined locus by Southern blot hybridisation. Utilising two rNTP permissive mutant alleles of Polε (*cdc20_M630F*) and Polδ (*cdc6_L591G*), separate DNA libraries (one for each polymerase) can be made using Pu-Seq to analyse replication dynamics across the whole genome (Figure 1.3). DNA from cells containing either of these mutant polymerases is fragmented by Alkali treatment to allow specific fragmentation and isolation of rNTP incorporated DNA. These fragments represent regions of the genome that have been replicated by their respective polymerase and can be used to make DNA libraries for Next Generation Sequencing. Cleavage of DNA at the site of an rNTP leaves a non-ligatable 5' end due to the presence of an -OH group instead of a phosphate. The complementary strand is then synthesised using random primers and a dNTP mix containing uracil instead of thymidine to maintain strand specificity. DNA end repair is performed to allow ligation of hairpin adapters that contain uracil at the apex. Digestion of the complementary strand with uracil glycosylase and DNA lyase results in the original DNA fragment being specifically tagged at the 3' and 5' end. This allows for DNA library amplification using index primers for Next generation sequencing and subsequent strand specific mapping to the genome. Taking the two mutant polymerase libraries together a global pattern of division of labour between the two main replicative polymerases can be established.

Other replication dynamics can also be estimated including: origin firing efficiency, direction of replication, replication termination zones, and replication timing. Origins

can be identified due to knowledge of bidirectional replication initiating at origins that is conducted using the canonical division of labour between Polε (leading strand) and Polδ (lagging strand). Since origins initiate and produce bidirectional replication, reciprocal transitions between each polymerase to the opposite strand indicates origin location. The abruptness of the switch can be used to estimate the efficiency of the origin. Replication direction is calculated using the proportion of reads that map to each strand for either Polε or Polδ mutant Pu-seq libraries to provide a proportion of leftward or rightward moving replication forks across the genome. Using this fork directionality along with a fork speed of 1.5 Kb/min, replication timing profiles across the genome can also be calculated. Furthermore, this allows estimation of the frequency of termination events due to the knowledge of replication fork directionality and timing of replication providing information on the likelihood two forks will meet at certain locations. Other similar sequencing approaches have also been developed by labs to track rNTP incorporation at a genome wide scale (Clausen et al., 2015, Koh et al., 2015, Reijns et al., 2015).

1.4 Replication Stress

A key characteristic of replication stress is replication fork stalling or slow DNA synthesis that manifests in defective replication that can result in mutations, rearrangements, missegregation or breakage of the DNA. There are both endogenous and exogenous sources of replication stress. Endogenous sources of replication stress include DNA damage, replication-transcription collision, protein-DNA barriers, and inter-strand crosslinks. Exogenous sources include UV radiation which induces intrastrand crosslinks, hydroxyurea (HU) which depletes the dNTP pool, methyl methanesulfante (MMS) which alkylates DNA bases, and camptothecin (CPT) the Topoisomerase 1 inhibitor, among others. Outlined below are different consequences of replication stress and how the cell responds to them.

1.4.1 Replication Fork Stalling

Completion of DNA synthesis is crucial in maintaining genome stability and survival. Obstacles to DNA replication can result in replication fork stalling that can often be overcome by resuming DNA synthesis. If replication cannot be resumed and the replication fork becomes non-functional this can result in replication fork collapse. In the majority of cases these collapsed replication forks can be rescued by a convergent replication fork completing DNA synthesis of the intervening region. Not all licensed origins are used in the absence of replication stress, and are termed dormant origins. These dormant origins can fire in situations such as that of an arrested replication fork to allow completion of DNA replication of the downstream region (Ge et al., 2007, Woodward et al., 2006). However, in regions of the genome with a low level of origins capable of producing another replication fork, or when two convergent forks collapse without an intervening origin, replication fork restart is required (discussed in section 1.6).

Common fragile sites (CFS) are regions of the mammalian genome associated with a high degree of genomic instability. These sites have been associated with increased replication fork pausing and a decrease in the efficient activation of additional origins to complete replication (Ozeri-Galai et al., 2011, Palakodeti et al., 2010). This can result in un-replicated regions of the genome persisting into mitosis, resulting in the formation of ultra-fine bridges between the sister chromatids (Chan et al., 2009). During mitosis these UFBs can subsequently break introducing DNA lesions into the two daughter cells (Lukas et al., 2011, Moreno et al., 2016). Therefore, in order to maintain genome stability completion of DNA synthesis is critical.

Additionally, it has become clear that dNTP pools in the cell are a limiting factor for DNA replication, and tight regulation of their levels are important for maintaining efficient rates of replication and allowing origin firing under replication stress (Poli et al., 2012). Although regulation of dNTP levels varies slightly between budding and fission yeast, their dysregulation results in similar detrimental effects across eukaryotes. Overactivity of CDK can increase origin firing and deplete dNTP levels resulting in slow replication

fork progression and an accumulation of DNA double strand breaks (Beck et al., 2012). Additionally, inhibition of ribonucleotide reductase (RNR), responsible for catalysing the production of dNTP, results in increased spontaneous mutation rates (Holmberg et al., 2005). On the other hand, increased dNTP pools can increase rates of replication and mutagenesis, and appear to be a method employed as a means of overcoming replication stress (Chabes et al., 2003, Davidson et al., 2012, Poli et al., 2012). Increased dNTP pools by upregulating RNR activity increases the cells tolerance to continue replication in the presence of DNA lesions resulting in an accumulation of mutations. Moreover, dNTP pools and mutation rates are increased upon deletion of genome stability genes suggesting it is a method employed to overcome replication stress and avoid cell death. This is in line with findings that the RRM2 subunit of RNR when overexpressed can induce tumorigenesis in mice *in vivo* and has been found to be upregulated in several human cancers (Fujita et al., 2010, Jones et al., 2012, Kidd et al., 2005, Xu et al., 2008).

1.4.2 Checkpoint Response to Replication Stress

There are several checkpoints throughout the cell cycle to ensure correct and timely transitions between each phase of the cell cycle. The intra-S phase checkpoint is important for ensuring the correct completion of DNA replication before entry into mitosis. Upon replication stress this checkpoint is important for delaying the cell cycle to allow time for replication to overcome any obstacles and complete replication of the genome. Dysfunction of this checkpoint can lead to incomplete chromosome duplication and premature entry into mitosis resulting in the production of chromosome bridges and the mis-segregation of chromosomes (Eykelenboom et al., 2013). The intra-S phase checkpoint is also important for preventing replication errors by promoting the transcription of DNA replication and repair proteins to repair DNA damage and allow stalled replication forks to restart (Allen et al., 1994, de Bruin et al., 2008, Huang et al., 1998).

The importance of checkpoint signalling to maintain genome stability is evident in human cells whereby loss of the intra-S phase checkpoint kinase, ATR (ataxia

telangiectasia and Rad3 related), results in cell lethality (Cortez et al., 2001). Evidence suggests replication fork stalling can lead to uncoupling of the MCM helicase and replicative polymerases resulting in increased ssDNA and activation of the S phase checkpoint (Byun et al., 2005). Moderate replication stress that results in slow moving replication forks activates ATR in the DNA Replication Checkpoint (DRC) to prevent collapse of replication forks and accumulation of ssDNA (Koundrioukoff et al., 2013). Additionally, inactivation of ATR in S phase upon replication stress results in incomplete DNA replication, suggesting the checkpoint plays a key role in stabilising replication forks and preventing their collapse (Couch et al., 2013).

ATR and its partner ATRIP (ATR interacting protein) are integral to the S phase checkpoint (Figure 1.4). In *S. pombe* Rad3 (*Hs*ATR, *Sc*Mec1) and Rad26 (*Hs*ATRIP, *Sc*Ddc2) form a complex (Edwards et al., 1999) and is activated upon HU treatment which results in S phase inhibition (al-Khodairy and Carr, 1992, Enoch et al., 1992). Additionally, Rad9, Rad1 and Hus1 forms a ring-shaped complex termed the 9-1-1 complex that also interacts with Rad17 (Caspari et al., 2000). Rad17 is related to the replication factor C (RFC) proteins that form a complex known as the clamp loader responsible for loading PCNA onto DNA at the replication fork (Griffiths et al., 1995). Rad17 is important for the recruitment of the 9-1-1 complex to damaged DNA and its phosphorylation by Rad3 is dependent on Hus1 (Zou et al., 2002). The 9-1-1 complex forms a similar structure to the DNA binding clamp, PCNA (Dore et al., 2009) and is loaded at the 5' end of junctions between dsDNA and RPA-coated ssDNA by Rad17 (Majka et al., 2006, Zou et al., 2003). Subsequently, the 9-1-1 complex is phosphorylated by Hsk1 (DDK) to release the complex from DNA and allow downstream repair processes (Furuya et al., 2010, Lee et al., 2007). TopB1 has also been shown to bind to Rad9 as well as ATR and be important for its activation (Delacroix et al., 2007, Lee et al., 2007). Activation of Rad3 is important to activate downstream effector kinases in response to both DNA damage (Chk1) and replication inhibition (Cds1) (Martinho et al., 1998). Cds1 has been shown to be specifically phosphorylated and activated in S phase in the presence of DNA damage resulting in slowing of S phase progression (Lindsay et al., 1998).

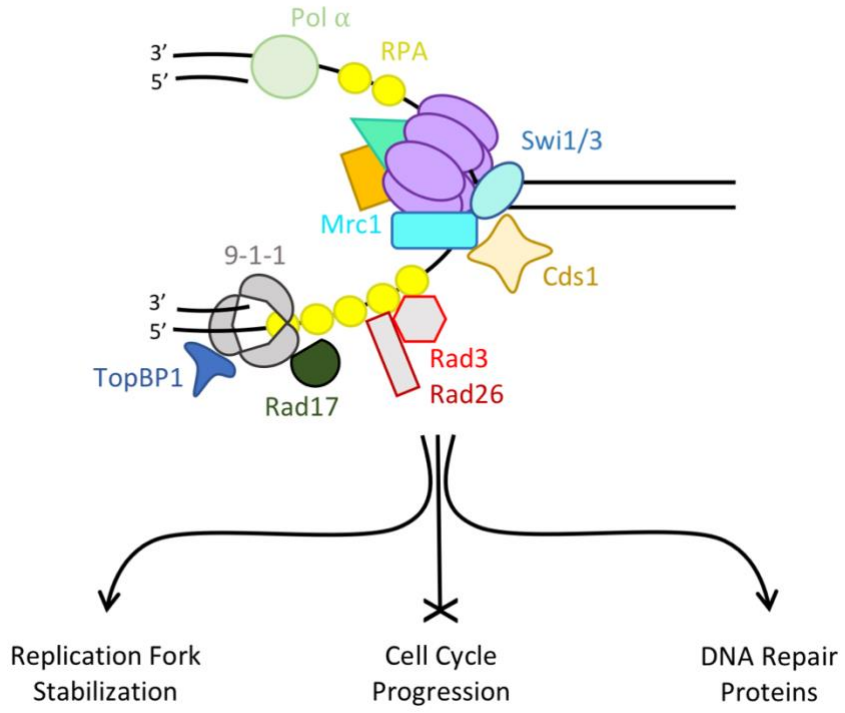

Figure 1.4. Intra-S Phase Checkpoint Response. Replication fork showing the key proteins involved in activating the checkpoint. In the event of uncoupling of polymerase and CMG helicase (Mcm2-7 = purple, Cdc45 = orange, GINS = green) activity extended regions of RPA-coated ssDNA (yellow circles) are produced. 9-1-1 complex is loaded at 5' dsDNA-ssDNA junctions by Rad17. TopBP1 is important for checkpoint activation and binds 9-1-1 and Rad3. Rad3 and Rad26 are a complex recruited downstream of 9-1-1 loading and result in activation of the Cds1 effector kinase that is recruited to the replication fork via its interaction with Mrc1 and the FPC (Swi1/Swi3). Pol α is also available to provide additional appropriate templates for 9-1-1 loading on the leading strand. Activation of the checkpoint results in replication fork stabilization, inhibition of cell cycle progression and induction of DNA repair proteins.

Stalled replication forks can result in increased ssDNA due to helicase polymerase uncoupling and activation of ATR. The nature of lagging strand synthesis provides the correct 5' ds-DNA-ssDNA primer template for 9-1-1 loading, but this is not the case for the leading strand. Therefore, it is not surprising that Polα was also found to be involved in this checkpoint response by synthesising the DNA primers on unwound leading strand DNA to provide the correct template for 9-1-1 loading (Yan and Michael, 2009). However, not all replication fork stalling results in uncoupling of polymerases and helicases, such as stalling at inter-strand crosslinks. Here, little ssDNA is produced to activate the intra-S phase checkpoint. However, processing of replication forks stalled at inter-strand crosslinks require further processing to produce RPA-coated ssDNA that can then activate the checkpoint (Ben-Yehoyada et al., 2009). It is also known that abrogation of the intra-S phase checkpoint can result in collapse of replication forks sometimes manifesting as reversed replication forks (Sogo et al., 2002). Recently, Dna2 nuclease has been found to be directed to stalled forks by Cds1 to stabilise replication forks and prevent fork reversal (Hu et al., 2012). However, Dna2 is also required to fully activate ATR (*Sc*Mec1) in budding yeast (Kumar and Burgers, 2013). This could suggest parallel roles of Dna2 in both being activated by the checkpoint and also in playing a role in its activation by providing the correct substrate for 9-1-1 loading at regressed replication forks.

Additionally, Mrc1, a replisome component implicated in replication fork protection, has been found to directly interact with Cds1 and be required for its activation by Rad3 (Tanaka and Russell, 2001). Similarly, Swi1/Swi3 the replication fork protection complex is also required for efficient activation of Cds1 (Noguchi et al., 2004). Full activation of Rad3 and its downstream effector kinase allows induction of phosphorylation of a vast array of proteins involved in cell division, origin firing, and DNA damage repair such as homologous recombination proteins (Willis et al., 2016). One of the proteins identified as a phosphorylation target is Cdc18 important for origin firing, which is in line with the fact the intra-S phase checkpoint slows S phase progression. Furthermore, Cdc25 a key protein for progression into S phase was previously identified to be inhibited by Cds1 (Kumar and Huberman, 2009). Additionally, repair proteins are also recruited to stalled

replication forks via phosphorylation of histone H2AX (γH2AX) by Rad3 (Rozenzhak et al., 2010).

1.5 Replication Fork Barriers

There are many barriers to DNA replication that result in replication fork stalling. Replication fork stalling is characterised by the ability of a replication fork to be stabilised and resume DNA replication. This stabilization can occur by activation of the intra-S phase checkpoint outlined above. However, failure of the checkpoint can result in collapsed replication forks that are unable to resume DNA synthesis. In these scenarios it has been shown that collapse of a replication fork does not mean the replisome falls apart, instead it appears to remain associated with the replication fork (De Piccoli et al., 2012). Some barriers to replication forks include: DNA damage to specific bases, repetitive sequences that form secondary structures, transcription, DNA:RNA barriers, and protein-DNA barriers. The effect this has on the replication fork and the methods used to overcome these barriers vary between each scenario and will be summarised below.

1.5.1 DNA Damage

DNA damage is a type of replication stress that manifests as a lesion in the DNA capable of stalling polymerases, such as cyclobutane pyrimidine dimers (CPD) that are produced from UV irradiation. After exposure to UV the resulting DNA has been observed to be replicated discontinuously in both leading and lagging strands, resulting in ssDNA gaps in the daughter DNA (Lehmann, 1972, Rupp and Howard-Flanders, 1968). If the lesion occurs on the lagging strand template the cells can continue replication in the canonical manner and re-prime and extend using Polδ as in unperturbed conditions. This has been evidenced by the replisome efficiently bypassing a lagging strand specific roadblock in *Xenopus* egg extracts (Fu et al., 2011). However, how a leading strand lesion is overcome is more problematic due to the continuous nature of replication of this strand. Recent experiments have confirmed re-priming can occur downstream of a leading strand

lesion to allow replication to continue (Taylor and Yeeles, 2018). However, Polα appears to be fairly inefficient at this process. Evidence suggests an additional primase existing in some eukaryotes, termed PrimPol, to be the primary method of re-priming to bypass DNA lesions (Bianchi et al., 2013). Re-priming past these types of lesions results in short ssDNA gaps in the DNA that are repaired by post replication repair (PRR) mechanisms outlined below.

1.5.2 Repetitive Sequences and Secondary Structures

There are many different circumstances that result in blocking of DNA replication. These can include repetitive sequences that form secondary structures such as guanine-rich regions that form G-quadruplexes (G4). These can perturb DNA replication particularly in the context of a leading strand G-quadruplexes (Lopes et al., 2011). Evidence from yeast models suggest G4 quadruplexes can be efficiently resolved using the Pif1 (*Sp*Pfh1) DNA helicase, due to Pif1 binding sites correlating with G4 sites and elevated levels of mutagenesis in cells lacking Pif1 (Paeschke et al., 2013, Paeschke et al., 2011, Wallgren et al., 2016). Other naturally forming secondary structures in DNA include inverted repeats that can fold to form DNA hairpins or cruciforms (Lilley, 1980, Panayotatos and Wells, 1981). These structures result in replication fork stalling (Voineagu et al., 2008) and DNA breaks that require recombination for repair (Lobachev et al., 2002).

1.5.3 Transcription-Replication Collisions

Additionally, collisions between replication and transcription machinery can block replication fork progression and result in recombination (Prado and Aguilera, 2005). These types of collisions are inevitable when considering the identification of human genes that take more than one cell cycle to be fully transcribed (Helmrich et al., 2011). Therefore, processes to deal with this kind of replication stress must have evolved. Topoisomerase I (TopI) is one such protein that relaxes DNA supercoiling to reduce topological stress, and appears to limit genomic instability that can arise from these types of collisions by suppressing R-loop formation (Tuduri et al., 2009). R-loops can

form during transcription when the transcript hybridises to the template strand forming an RNA:DNA hybrid, leaving the other strand as ssDNA. Other processes have evolved including RNA interference, which promotes heterochromatic silencing and release of RNA Pol II from the DNA to allow replication to continue without the need for recombination (Zaratiegui et al., 2011).

Transcription-replication collisions can occur in either a head-to-head orientation or a head-to-tail orientation, whereby they are travelling in the opposite or the same direction, respectively. There is much debate over which is more detrimental to the cell, however, a genome wide study in yeast identified equal levels of pausing at these locations regardless of the orientation of collision (Azvolinsky et al., 2009). However, an *in vivo* study using *S. cerevisiae* tRNA genes found fork pausing only when collision were head-to-head (Deshpande and Newlon, 1996). Conversely, R-loops formed during transcription have been found to be detrimental to replication and lead to genome instability and recombination specifically when replication and transcription are co-directional in both *E. coli* and human cells (Gan et al., 2011). This could be due to the RNA transcript being used as a primer for resuming replication upon collisions with transcription, specifically occurring when co-directionally orientated (Pomerantz and O'Donnell, 2008). The re-hybridized RNA transcript can be digested by RNAse H or unwound by the RNA-DNA helicase Senataxin to overcome these problems and prevent genome instability (Alzu et al., 2012, Huertas and Aguilera, 2003).

1.5.4 Protein-DNA RFBs

1.5.4.1 E. coli Tus/Ter RFB and rDNA

E. coli have evolved a natural polar protein-DNA replication fork barrier composed of the *Ter* sequence bound by the Tus protein, to organise replication termination to allow efficient chromosome segregation (Hill and Marians, 1990). Furthermore, use of the Tus/*Ter* RFB in mammalian cells supports HR initiation as the method of rescuing collapsed replication forks via fork reversal and template switch mechanisms of repair (Willis et al., 2018). However, when used in *S. cerevisiae* replication fork pausing at

Tus/*Ter* is independent of the replication fork protection complex protein Tof1 (*Sp*Swi1) in contrast to other polar protein-DNA RFB's outlined below (Larsen et al., 2014).

1.5.4.2 Ribosomal DNA (rDNA)

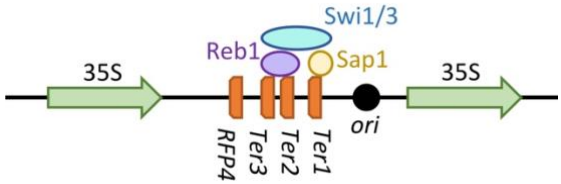

Figure 1.5. Ribosomal DNA Replication Fork Barrier (rRFB). Schematic of the *S. pombe* rDNA locus that acts as a polar replication fork barrier to prevent transcription-replication collisions. Position of the rRFB is located between 35S transcription units, comprising of 4 blocking motifs: RFP4, Ter1, Ter2, and Ter3. Ter1 is bound by Sap1 and Ter2-3 is bound by Reb1. Ter1-3 blocking activity is also stimulated by Swi1/3 fork protection complex. RFP4 does not intrinsically block replication forks, but may be a site of replication-transcription collisions when Ter1-3 fail.

If replication and transcription are not co-ordinated, collisions between the two machineries can happen as outlined above. Most eukaryotic cells contain replication barriers in the spacer regions of transcriptional units to co-ordinate orderly replication and transcription during S phase. In *S. pombe*, the ribosomal DNA (rDNA) contains four polar replication fork barriers (*Ter1*, *Ter2*, *Ter3* and *RFP4*) that block replication travelling in the opposite direction to transcription (Figure 1.5). The fork protection complex proteins Swi1 and Swi3 are required for replication fork pausing at *Ter1-3* (Krings and Bastia, 2004). Switch-activating protein 1 (Sap1) is an essential protein in *S. pombe* associated with mating-type switching and has been found to bind to and cause polar fork arrest at *Ter1* (Arcangioli et al., 1994, Krings and Bastia, 2005). Furthermore, the transcription termination factor Reb1 is responsible for polar barrier activity at *Ter2/3* (Sanchez-Gorostiaga et al., 2004). No trans-acting factor has been identified for RFP4, and it does not appear to block replication forks in a plasmid assay, thus pausing at this site may just be a result of failure of the *Ter1-3* blocking replication resulting in transcription-replication collisions (Krings and Bastia, 2005).

1.5.4.3 Replication Termination Sequence 1 (RTS1)

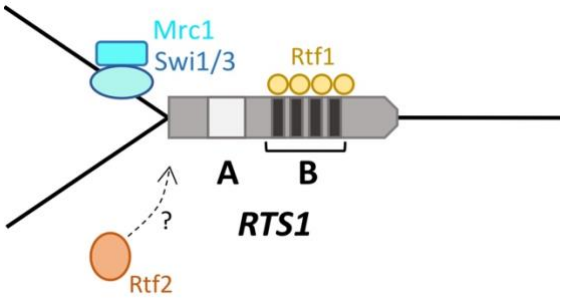

Figure 1.6. Replication Termination Sequence 1 (RTS1) Replication Fork Barrier. Schematic of the *S. pombe RTS1* RFB that acts as a polar replication fork barrier when bound by the protein Rtf1. *RTS1* consists of two key regions: A and B. Region B contains 4 blocking motifs that are bound by Rtf1 and are essential for barrier activity. Region A was originally proposed to enhance blocking capacity of *RTS1* and bind Rtf2, but has here been found to be dispensable for barrier activity. The fork protection complex proteins Mrc1, Swi1/3 are also important for efficient blocking of replication forks at *RTS1*.

Replication Termination Sequence 1 (*RTS1*) is located at the mating type locus of fission yeast to ensure replication of the locus occurs in the correct orientation to allow mating type switching to occur. The *RTS1* RFB is polar in nature, only blocking replication forks travelling from a single direction (Dalgaard and Klar, 2001). The *RTS1* sequence is bound by the *trans*-acting factor Rtf1 which mediates barrier activity (Figure 1.6). Fork protection complex (FPC) proteins Swi1 and Swi3 that travel with the replication fork are also essential for the RF blocking capacity of *RTS1* (Dalgaard and Klar, 2000). Additionally, the protein Mrc1 that interacts with both Swi1 and Swi3 has been shown to reduce but not completely eliminate the levels of pausing at *RTS1* (Zech et al., 2015). Another protein, Rtf2, originally suggested to bind the *RTS1* sequence, similarly enhances the blocking signal at *RTS1* (Inagawa et al., 2009). However, the precise mechanism behind how Rtf2 exerts this function is yet to be fully elucidated. Replication forks stalled at *RTS1* require homologous recombination for restart and is outlined below.

1.6 Overcoming Obstacles to Replication

There are several types of obstacles the cell needs to overcome in order to complete replication of the entire genome (described above). Some types of obstacles are removed or resolved prior to replication. If they are not removed before the replisome encounters them this can result in replication fork stalling or collapse. There are several mechanisms employed at the replication fork to overcome obstacles and ensure replication completion, including lesion bypass mechanisms and subsequent post-replicative repair. However, if stalled forks are not stabilised or rescued by a convergent replication fork, they can be prone to collapse and require homologous recombination restart mechanisms to complete replication of the downstream region. Outlined below are different mechanisms the cell can utilise in order to overcome these obstacles to replication.

1.6.1 Non-Homologous End-Joining (NHEJ)

Non-homologous end joining (NHEJ) is a method of DSB repair that ligates the two broken DNA ends together without the need for a homologous sequence to replicate across the region. This method of repair can lead to a few nucleotide deletions due to the DSB ends not being completely complimentary and requiring some processing before ligation. NHEJ is rarely used in *S. pombe* as a sister chromatid is present for the majority of the cell cycle due to a very short G1 phase and long G2 phase, making error-free HR (discussed below) the preferred method of repair. The Ku70/80 (*Sp*Pku70/80) heterodimer forms a ring structure and binds to the DSB ends (Walker et al., 2001). In human cells, recruitment of DNA-PKcs (DNA-dependent-protein kinase, catalytic subunit) to Ku bound dsDNA ends constitutes the DNA-PK complex that bridges the two DNA ends together (Gottlieb and Jackson, 1993, Yaneva et al., 1997). There is no DNA-PKcs in either budding or fission yeast. However, the MRN (Mre11-Rad50-Nbs1) (*Sc*MRX, Mre11-Rad50-Xrs2) complex in budding yeast has been implicated in bridging the two ends together instead of DNA-PKcs (Chen et al., 2001). In fission yeast, the MRN complex

has been shown to be dispensable for NHEJ due to deletions of the subunits having no impact on NHEJ proficiency in a plasmid-based assay (Manolis et al., 2001). The MRN complex has only been implicated in fission yeast in the context of capped DSB ends that form hairpin structures that require opening before ligation can occur (Runge and Li, 2018). In human cells, once the two DSB ends have been brought together they are ligated by the action of Ligase IV-XRCC4 complex to seal the break. There is no XRCC4 in fission yeast, but it does contain Xlf1, a protein with structural similarity to XRCC4, and both Xlf1 and Lig4 (*Hs*Ligase IV) are implicated in NHEJ (Hentges et al., 2014, Manolis et al., 2001). NHEJ is specifically suppressed in human cells at replication associated breaks to avoid toxic NHEJ which can result in incorrect ligation of broken ends producing aberrant chromosome fusions and cell death (Balmus et al., 2019).

1.6.2 Post Replicative Repair

Although DNA damage is an obstacle to replication, it does not necessarily result in stalling of the replication fork. Some forms of DNA damage can be repaired ahead of the replication fork by nucleotide excision repair (NER) or base excision repair (BER). If the damage is not repaired, some small DNA lesions can be bypassed by the replicative polymerases. These lesions are often repaired later by post replicative repair (PRR) mechanisms. This is due to the replicative polymerases inefficiently incorporating DNA bases opposite non-canonical bases. Although, Polδ has been shown to be able synthesise across some forms of DNA damage including abasic sites, as well as an increased ability to deal with UV damage when lacking its proofreading ability (Hirota et al., 2016). However, bulky lesions can block the advancing replication fork and result in the use of lesion tolerance mechanisms, including translesion synthesis (TLS) or HR-mechanisms to allow replication to continue and the damage is repaired later.

Sometimes the main replicative polymerases fail to synthesise past bulky DNA damage due to lesions or adducts on the DNA that are more efficiently bypassed by other polymerases with a larger active site. These include the TLS polymerases which are capable of incorporating bases opposite these sites. There are 5 main polymerases identified in eukaryotes that perform TLS: Polζ, Polη, Polι, Polκ, and REV1 (Prakash et al.,

2005). Regulation of these polymerases and their recruitment to the replication fork relies heavily on modifications to the PCNA sliding clamp. These modifications are also a key regulator in the decision of whether to commit to error-prone TLS or error-free HR-protein dependent template switch pathway. Mono-ubiquitination of PCNA at Lysine 164 by Rad6/Rad18 directs repair towards TLS in *S. cerevisiae* by providing the optimal binding site for these polymerases (Kannouche et al., 2004, Watanabe et al., 2004). However, poly-ubiquitination by the ubiquitin conjugating enzymes Rad6, Mms2 and Ubc13, induces the error free pathway of template switching which uses the sister chromatid to complete replication of the region (Hoege et al., 2002).

Conversely, in *S. pombe* polyubiquitination of PCNA has been shown to also promote TLS highlighting key differences between organisms in dealing with these types of lesions (Coulon et al., 2010). Additionally, a recent study in *S. cerevisiae* found ubiquitination of Lysine 63 to be important independently and in terms of its linkage to ubiquitinated Lysine 164 in promoting template switch pathway of repair (Takahashi et al., 2020). The pathway of how polyubiquitination drives the error-free pathway of repair is not completely clear. Evidence suggests inhibition of TLS polymerases such as has been seen for Polη may arise from polyubiquitination of PCNA trapping it in its inactive state so it is unable to perform TLS, thus favouring template switch mechanisms of repair (Yang et al., 2014). Additionally, TLS polymerases have recently been shown to be important for the correct chromosome segregation during meiosis (Mastro et al., 2020).

1.6.3 Homologous Recombination (HR)

Homologous recombination is a DNA repair method used on a variety of different DNA lesions. These include both DNA double strand breaks (DSBs) and single stranded DNA (ssDNA) gaps. Stalled or collapsed replication forks can result in ssDNA gaps that result in recombination for repair (Fabre et al., 2002). Additionally, homologous recombination proteins are important for maintaining efficient replication fork movement even in the absence of any blockade to their progression, as evidenced from a decreased velocity when HR is defective (Daboussi et al., 2008). HR mechanisms have

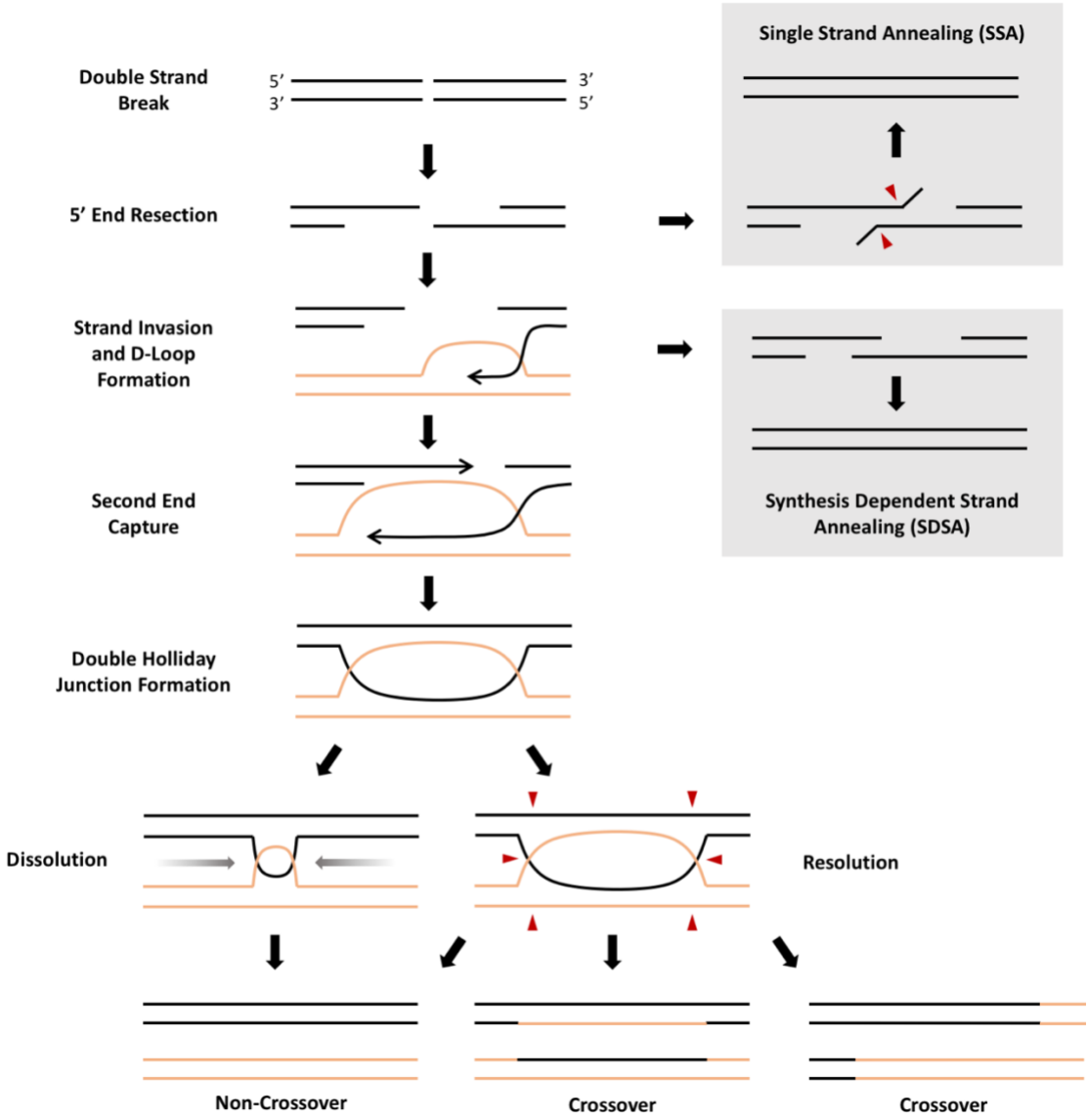

Figure 1.7. Overview of Homologous Recombination Methods of Repair of a DSB. A double strand break is first resected to create 3' overhangs. This can be directed towards the SSA pathway for annealing of homologous ssDNA overhangs and flap cleavage. Alternatively, the overhangs can be coated by Rad51 to create the presynaptic filament that performs strand invasion into a homologous template and D-loop formation. After elongation of the invaded strand it can release from the template DNA and reanneal with the second end of the break, termed SDSA. Alternatively, the second end is captured by the D-loop ssDNA and forms a double Holliday junction. This can be dissolved by Sgs1-Rmi1-Top3 by branch migration and decatenation to form a non-crossover product. Resolution of the double Holliday junction by either Mus81-Eme1 (cleaves at the crossover) or Yen1 (cleaves non-crossover template) can result in both crossover or non-crossover products.

been most extensively studied in the context of a DSB: resection of the DNA ends must first occur in order to produce a suitable 3' end for strand invasion. The key steps in homologous recombination outlined below include, presynaptic filament formation, strand invasion and production of a D-loop, followed by Holliday junction formation and resolution (Figure 1.7).

1.6.3.1 Presynaptic Filament Formation

Rad51 is a highly conserved protein that has the capacity to bind both dsDNA and ssDNA in an ATP-dependent manner, with ssDNA binding being the functionally relevant formation that allows strand invasion into a homologous template (Benson et al., 1994, Sauvageau et al., 2005, Sung and Robberson, 1995). Rad51 forms a helical filament on ssDNA often referred to as the presynaptic filament. However, RPA acts as an inhibitory factor for strand exchange of the presynaptic filament due to RPA and Rad51 both competing for binding to ssDNA. Although, RPA has also been found to promote the reaction, possibly by removing secondary structures on the ssDNA (Sugiyama et al., 1997). RPA generally outcompetes Rad51 for binding to ssDNA, and has been shown that the Rad52 protein is needed to promote exchange of Rad51 on ssDNA to enable strand invasion (Song and Sung, 2000).

Rad52 is known to directly bind and interact with Rad51, ssDNA and DNA bound RPA to facilitate presynaptic filament formation (Seong et al., 2008, Shinohara et al., 1992). In the context of DSB repair, Rad52 is also important in mediating capture of the second end to form a joint molecule (McIlwraith and West, 2008, Nimonkar et al., 2009). Additional Rad51 paralogues also aid in the nucleation of Rad51 onto RPA-coated single stranded DNA including Rad55 and Rad57 which form a stable heterodimer (Sung, 1997). These proteins have been shown to work together with the Shu complex, a complex of four proteins containing a further two Rad51 paralogues that promote HR (Shor et al., 2005), to facilitate presynaptic formation and strand invasion (Gaines et al., 2015). Rad55-Rad57 heterodimer also acts to oppose the antirecombinase activity of Srs2 that uses its translocase activity to disassemble Rad51 presynaptic filaments (Liu et al., 2011). Additionally, Swi5-Sfr1 complex has been identified as mediator proteins that

directly bind and stabilise Rad51-ssDNA presynaptic filaments and stimulate the strand exchange reaction (Haruta et al., 2006, Kurokawa et al., 2008).

1.6.3.2 Homology Search and Strand Exchange

Production of the presynaptic filament provides the correct substrate for invasion into a homologous template. When the sister chromatid is available, this provides the optimal template for homologous recombination. Evidence suggests that during homology search, chromosome mobility is increased within the nucleus allowing the DNA end to find an appropriate template to invade (Mine-Hattab and Rothstein, 2012). When searching for homology, the Rad51 presynaptic filament samples several sites in the genome until it finds regions with at least 8 nucleotides of microhomology, committing to strand invasion in 3 nucleotide steps once a 9^{th} nucleotide is matched (Qi et al., 2015). Once strand invasion has occurred, the non-template strand is displaced as a D-loop that is stabilised by coating with RPA to prevent secondary structure formation (Eggler et al., 2002).

Rad54 is another ATPase associated with recombinational repair processes that acts to displace Rad51 bound to template dsDNA (Solinger et al., 2002). The dsDNA translocase activity of Rad54 allows removal of Rad51 from dsDNA to simultaneously promote D-loop formation and allow strand exchange to occur (Wright and Heyer, 2014). In the context of double strand breaks, once the first end has successfully invaded the template strand, the second end of the break then needs to be captured. If this does not occur, synthesis dependent strand annealing can be used as outlined below. Rad52 has been shown to be important for directing the second end of the break to the RPA-coated ssDNA of the D-loop at the location where the first end has invaded (Nimonkar et al., 2009). Replication of the region is subsequently completed and DNA strands ligated, resulting in the formation of two four way DNA junctions termed a double Holliday Junction (Duckett et al., 1988).

1.6.3.3 Holliday Junction Resolution & Dissolution

It is imperative that the Holliday junctions are efficiently resolved before entry into mitosis, otherwise the joint molecules can result in aberrant separation of the sister chromatids and genome instability (Wechsler et al., 2011). Holliday junctions are processed in two different ways that has an impact on exchange of genetic material: dissolution resulting in non-crossover products, and resolution resulting in either crossover or non-crossover products. Dissolution in *S. cerevisiae* relies on the Sgs1-Top3-Rmi1 complex (Cejka et al., 2010). To dissolve the Holliday junction, the two branches must migrate toward each other. The unwinding of the two branched molecules towards each other by the helicase activity of Sgs1 (*Sp*Rqh1) relies on Top3-Rmi1 to remove torsional stress between the two junctions (Cejka et al., 2010, Cejka et al., 2012, Tang et al., 2015). These studies found Top3-Rmi1 to be important for the last steps of dissolution once the joint molecules have migrated to one another forming a hemicatenane, with RPA also stimulating dissolution. This method specifically results in non-crossover products resulting in genetic material from each chromatid not being exchanged.

Resolution of Holliday junctions relies on the action of structure specific nucleases to disentangle the DNA strands. One such nuclease complex is Mus81-Mms4 (*S. pombe* Mus81-Eme1), that preferentially cleaves 3' flaps and nicked Holliday junctions (Fricke et al., 2005). In *S. pombe* activation of Mus81-Eme1 occurs by phosphorylation of Eme1 by Cdc2 and Rad3 (Dehe et al., 2013). Another nuclease complex, Slx1-Slx4, cleaves branched DNA molecules, favouring Y-shaped structures and 5' flaps (Fricke and Brill, 2003). Additionally, a nuclease found in *S. cerevisiae* (Yen1) and humans (GEN1) but not *S. pombe*, favours cleavage of Holliday junctions on the non-crossover strand (Rass et al., 2010). The concerted action of these nucleases can result in either non-crossover products as with dissolution, or crossover products resulting in exchange of genetic material between the sister chromatids.

1.6.3.4 Single Strand Annealing (SSA)

Single-strand annealing pathway of repair is used when there are sites of homology on either side of the break and results in deletions of the intervening regions making this a highly mutagenic repair process. This process does not utilise a dsDNA template. Instead, after the broken arms have been resected, the 3' overhangs of each strand anneal together (Figure 1.7). Subsequently, the non-homologous overhangs are cleaved to allow replication of the ssDNA gaps and ligation to complete replication of the region. Cleavage of the overhangs is carried out by the structure specific endonuclease Rad1-Rad10 that is targeted to 3' dsDNA-ssDNA junctions (Bardwell et al., 1994). Converse to other HR methods, Rad51, Rad54, Rad55, and Rad57 are not needed for SSA, presumably due to the lack of need for presynaptic filament formation as there is no strand invasion step (Ivanov et al., 1996). Instead, Rad52 co-operates with RPA to allow efficient annealing of the complementary ssDNA overhangs (Shinohara et al., 1998).

1.6.3.5 Synthesis Dependent Strand Annealing (SDSA)

In the context of double strand breaks the second end is not always captured as described above. Instead, the invaded DNA strand can dissociate from the template DNA and anneals with the second end of the DNA break to complete DNA synthesis followed by ligation of the two ends (Figure 1.7). This method of repair results in non-crossover products. The cell may be directed to this method of repair via disruption of the D-loop which stops the second end from being captured. This can result from the action of helicases including *Sc*Srs2, *Sc*Mph1, *Sp*Fml1, and *Hs*BLM that promote non-crossover formation to avoid loss of heterozygosity characteristic of tumour cells (Ira et al., 2003, LaRocque et al., 2011, Lorenz et al., 2012, Prakash et al., 2009). Additionally, Top3 (Topoisomerase III), a protein capable of nicking ssDNA, has been found to also promote D-loop dissolution (Fasching et al., 2015).

1.6.4 Break Induced Replication (BIR)

Break induced replication (BIR) is used after production of a break whereby only one side of the break can find a homologous template for repair (Figure 1.8). Initiation of BIR occurs by 5'-3' resection of the double strand break (DSB) to produce an available 3' ssDNA end for homology search and strand invasion (Chung et al., 2010). Rad52 is required for all BIR events to allow the ssDNA end to invade the homologous template (Malkova et al., 1996). However, there are both Rad51-dependent and Rad51-independent BIR events, with the former being the more efficient method of repair (Malkova et al., 2005). Additionally, RPA has been found to be important for the initial steps of BIR presumably due to its role in aiding the loading of Rad51 onto ssDNA to allow strand invasion to occur (Ruff et al., 2016).

The mode of replication during BIR involves a migrating D-loop resulting in conservative replication, whereby the leading strand is synthesised first with subsequent lagging strand synthesis (Donnianni and Symington, 2013, Saini et al., 2013, Wilson et al., 2013). However, the usage of polymerases during this process is different from that of canonical replication. During BIR, Polε was shown to not be required for the replication of the initial kilobases of DNA, but it was thought to be important for longer range DNA synthesis (Lydeard et al., 2007). This study suggested that Polδ performs leading strand DNA synthesis after initiation of BIR with Polε having a more important role after replication has stabilised. However, a recent study suggests that both leading and lagging strands are replicated by Polδ during BIR, with little or no contribution from Polε over genomic regions of up to 60 Kb (Donnianni et al., 2019). Polδ has been implicated in being important for BIR in several studies. In particular, the non-essential subunit Pol32 has been shown to be essential for BIR (Lydeard et al., 2007). Pol32 is dispensable for S-phase synthesis but plays an important role in G2 when Polδ performs replication using strand displacement (Stith et al., 2008). Furthermore, the helicase Pif1 has been shown to be essential to allow D-loop migration and synthesis by Polδ after BIR initiation in *S. cerevisiae* (Wilson et al., 2013). Additionally, Polα-primase is essential for BIR (Lydeard et al., 2007). This is to be expected to allow completion of lagging strand synthesis, however, another study failed to detect strand invasion events when

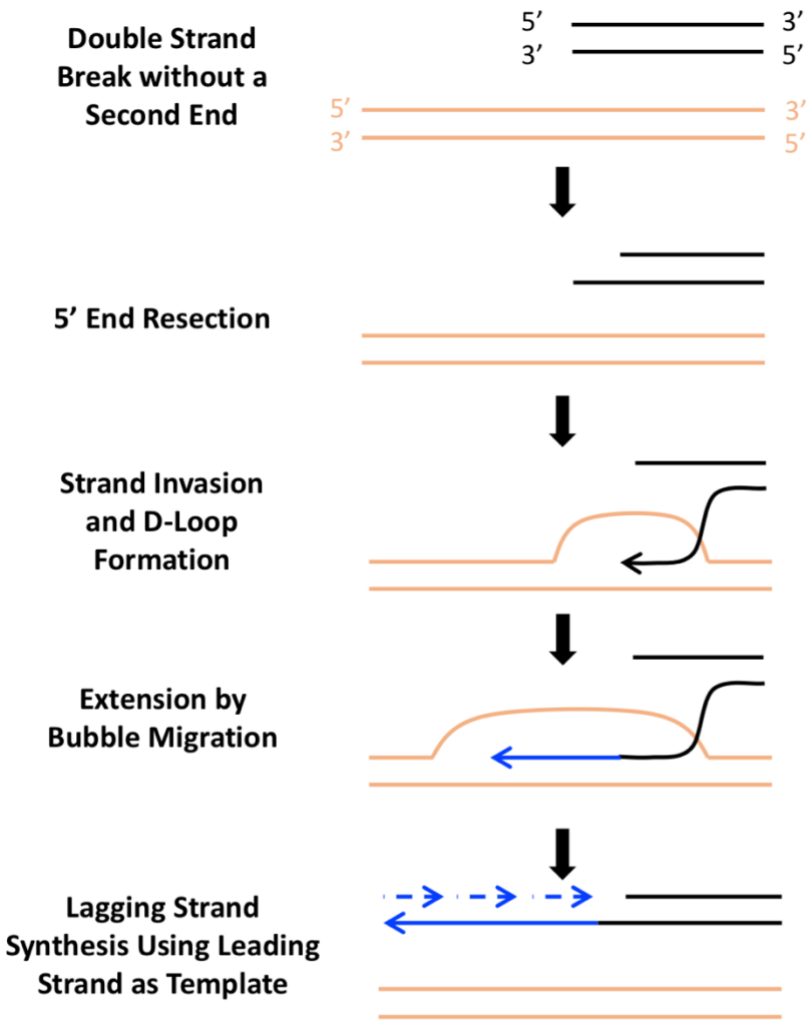

Figure 1.8. Break Induced Replication (BIR) Schematic. BIR occurs when only one end of a DSB is available for repair. First, 5′ end is resected to provide a 3′ ssDNA overhang for presynaptic filament formation and strand invasion into a homologous template and D-loop formation. Completion of DNA synthesis continues to the end of the template by bubble migration. The second strand of the break is then synthesised using the newly synthesised leading strand as a template to complete replication of the region. Both the leading and lagging strands are replicated using Pol δ (blue lines).

depleting Polα. This is surprising due to the invading strand providing the 3' DNA end sufficient for elongation. However, due to strand invasion producing ssDNA coated by RPA (Ruff et al., 2016) it is not surprising that Polα can be recruited to these intermediates. Additionally, recent evidence in *Xenopus laevis* has shown Polα to directly interact with Rad51 (Kolinjivadi et al., 2017) which could aid recruitment of HR proteins to the strand invasion event if this aspect is conserved in yeast.

Break induced replication has also been shown to be associated with an increased level of mutagenesis due to multiple rounds of strand invasion and dissociation from the template DNA, termed template switching (Smith et al., 2007). The Mus81 endonuclease is known to limit mutagenesis arising from template switching associated with BIR (Mayle et al., 2015). In this assay a single stranded DNA nick was introduced which can produce a single-ended DSB when the replication fork encounters it. Mus81 is proposed to prevent BIR continuation and allow resolution by termination with a convergent replication fork. Conversely, the FANCM-related DNA helicase Mph1 has been shown to promote template switching during BIR (Stafa et al., 2014). This could be due to the action of both Mph1 and Sgs1 helicases in driving repair away from BIR methods, favouring gene conversion methods of repair (Jain et al., 2016). Additionally, due to the asynchronous nature of BIR via bubble migration, whereby leading strand replication occurs first followed later by lagging strand synthesis, large amounts of ssDNA can be produced. Rad51 bound to this ssDNA would promote strand invasion that could produce toxic joint molecules for the cell. Srs2 helicase acts to suppress these events by dislodging Rad51 from ssDNA preventing its invasion into template DNA, thus limiting mutagenesis associated with BIR (Elango et al., 2017).

1.6.5 HR-Restart at *RTS1*

Replication fork stalling at *RTS1* does not result in the production of a DNA break (Ait Saada et al., 2017, Mizuno et al., 2009, Teixeira-Silva et al., 2017, Tsang et al., 2014). However, homologous recombination is crucial in allowing the restart of these replication forks (Figure 1.9). In terms of fork protection, Rad51 DNA-binding activity has been shown to be important in limiting excessive ssDNA production and allowing

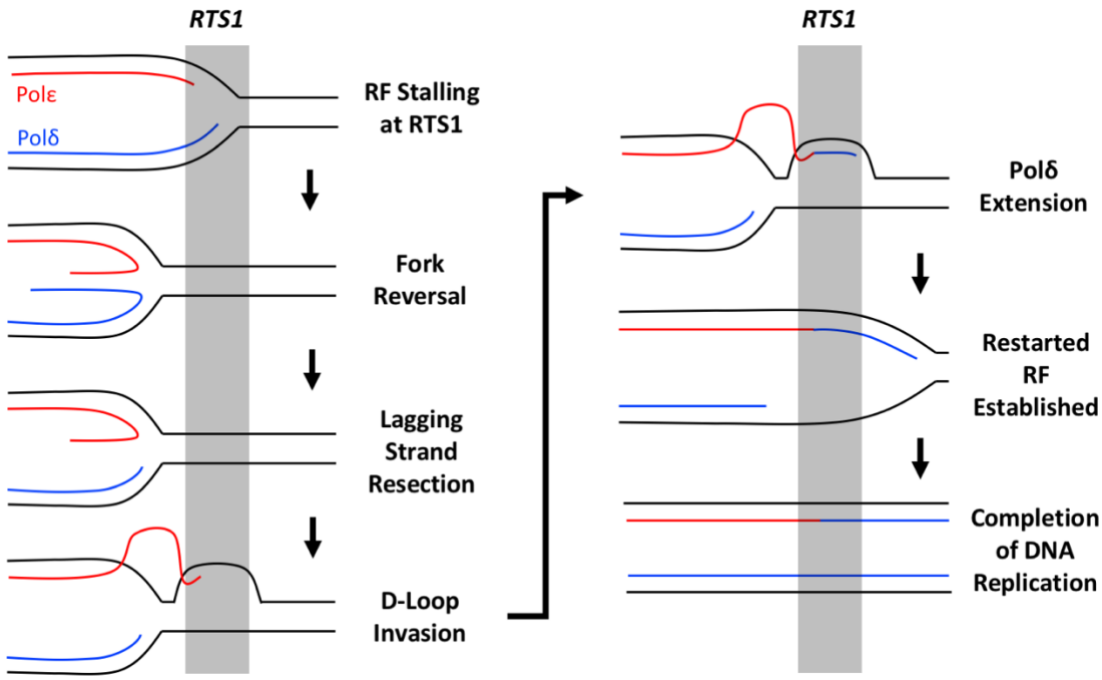

Figure 1.9. HR-Restart at RTS1 Replication Fork Barrier (RFB). Replication forks stall at the polar *RTS1* RFB and require HR for restart. First, replication fork reversal occurs producing a chicken foot structure that is subject to resection. The remaining 3' ssDNA of the leading strand can then invade the homologous DNA from which it was originally synthesised. Original synthesis of the leading strand by Pol ε (red lines) now switches to Pol δ (blue lines) to continue replication of the downstream region. This establishes the restarted replication fork with lagging strand replication subsequently completed using Pol δ.

efficient fork merging with a convergent replication fork (Ait Saada et al., 2017). Additionally, in terms of restart at *RTS1,* Rad51 strand exchange activity is important to allow presynaptic filament formation to enable restart (Ait Saada et al., 2017, Lambert et al., 2010). Rad52 is important for both merging of the arrested RF with a convergent RF, and allowing loading of Rad51 for the strand exchange reaction and RF restart (Ahn et al., 2005, Lambert et al., 2010). Retention of both Rad51 and Rad52 at the *RTS1* arrested RF has recently been shown to be dependent on the unloading of PCNA by Elg1, to counteract the antirecombinase effects of the helicases Srs2 and Fbh1 (Tamang et al., 2019).

However, due to the absence of a break at these stalled forks, fork reversal and regression can provide an appropriate substrate for presynaptic filament formation and strand invasion (Figure 1.9). Reversal of a replication fork would result in a "chicken foot" structure whereby the newly replicated strands anneal together behind the RF. Evidence suggests this structure is initially protected by the Ku protein which binds DNA DSB ends (Teixeira-Silva et al., 2017). Subsequent removal of Ku occurs via the MRN (Mre11-Rad50-Nbs1) complex and Ctp1 to allow the initial resection steps to produce a 3' ssDNA end for presynaptic filament formation (Teixeira-Silva et al., 2017). More extensive resection can then be carried out by the Exo1 nuclease to allow strand exchange, and is limited by both Rad51 and Rad52 which reduce the time available for resection to proceed (Ait Saada et al., 2017). However, even short tracts of resection by MRN have been shown to be sufficient to allow RF restart and strand invasion (Teixeira-Silva et al., 2017). Additionally, the chromatin remodeller, Fft3, has recently been shown to be important to allow DNA end resection and subsequent restart of *RTS1* arrested replication forks (Ait-Saada et al., 2019).

BIR in *S. cerevisiae* and HR-dependent restart in *S. pombe* are intrinsically different in several ways. Firstly, replication after HR-restart at *RTS1* occurs via semi-conservative replication and thus does not arise via a migrating D-loop (Miyabe et al., 2015). However, as with BIR, Polδ is used to replicate both the leading and lagging strand of the restarted replication fork, with no contribution from Polε (Miyabe et al., 2015).

Converse to BIR, the contribution of Polα to replication of the HR-restarted RFs at *RTS1* appears to be minimal in *S. pombe* (Miyabe et al., 2015, Naiman et al., 2020)

Furthermore, both BIR and HR-dependent replication after restart at *RTS1* are associated with increased levels of mutagenesis. Due to the formation of a presynaptic filament, the invading strand has been shown to be liable to invading the incorrect template when in the context of repetitive sequences, resulting in chromosomal rearrangements (Iraqui et al., 2012, Lambert et al., 2010, Mizuno et al., 2009, Mizuno et al., 2013). When replication fork restart occurs in the context of inverted repeats, Holliday junction structures are produced that require resolving by Mus81 nuclease (Lambert et al., 2010). Histone deposition by the Chromatin Assembly Factor-1 (CAF-1) can promote stabilization of the joint molecules by protecting them from disruption by the Rqh1 helicase (Hardy et al., 2019).

However, when the *RTS1* RFB was tested in the context of the invading strand of the restarted RF having the propensity to switch templates, both Mus81 and Fml1 (Mph1 homologue) had little to no impact on the levels of template switching (Jalan et al., 2019). However, the Whitby lab found deletion of *fml1* to specifically reduce gene conversion events at the site of RF stalling at *RTS1*, indicative of more rounds of strand invasion than deletion events (Jalan et al., 2019). This is consistent with *S. cerevisiae* studies identifying Mph1 as being important for promoting multiple strand invasion events during BIR (Stafa et al., 2014). Additionally, all template switching events 12.4 Kb away from the site of *RTS1* arrest were comparable to WT when either *fml1* or *mus81* were deleted (Jalan et al., 2019). This is similar to the replication produced from BIR stabilizing after roughly 10 Kb (Smith et al., 2007). Similarly, Pfh1 (*Sc*Pif1) and Srs2 are also important for efficient restart at *RTS1* in *S. pombe* while also suppressing template switching associated with the restarted replication fork (Inagawa et al., 2009, Jalan et al., 2019, Lambert et al., 2010). The helicases Rqh1 and Fbh1 are not required for HR-restart at *RTS1*, but have been shown to be important for limiting template switching, as well as ectopic recombination associated with the restart (Ahn et al., 2005, Jalan et al., 2019, Lambert et al., 2010, Lorenz et al., 2009).

1.7 Summary

This project aims to utilise the *RTS1* RFB to further investigate the mechanisms behind the error-prone nature of the HR-restarted replication fork. An optimised *RTS1* system is produced to allow investigation into the restarted replication fork with little interference from canonical convergent replication forks. Polymerase-Usage sequencing of the optimised *RTS1* system demonstrates the restarted replication fork uses Polymerase δ to replicate both leading and lagging strands for regions of up to at least 10 Kb downstream of restart. Using this optimised system the results presented here also provide further insight into the key similarities and differences between BIR and HR-restart at *RTS1*. Cdc27 and PCNA mutants shown to be important for BIR in *S. cerevisiae* are used to analyse their impact on HR-restart at *RTS1*. Additionally, the importance of the Rtf2 protein for efficient replication fork barrier activity of *RTS1* is demonstrated. Its mechanism of action is shown to not be through Region A of *RTS1* as previously suggested. Furthermore, implementation of a proximity-based labelling mass sprectrometry method will allow future investigation into the role of Rtf2.

Chapter 2 – Materials & Methods

2.1 Growth Media

2.1.1 Yeast Growth Media

2.1.1.1 Yeast Extract (YE) – Rich Media

5.0 g/l	Yeast Extract
30 g/l	Glucose
0.2 g/l	Uracil
0.1 g/l	Leucine
0.1 g/l	Adenine
0.1 g/l	Histidine
0.1 g/l	Arginine

2.1.1.3 Yeast Agar Plates

YE media or Yeast Nitrogen Base (YNB) with added:

12.5 g/l	Difco Bacto Agar

2.1.2 Bacterial Growth Media

2.1.2.1 Luria-Bertani (LB)

10.0 g/l	Tryptone
5.0 g/l	Yeast Extract
5.0 g/l	Sodium Chloride

2.1.2.2 LB Agar (LA) Plates

LB with added:

12.0 g/l Difco Bacto Agar

2.1.3 Drugs & Genotoxic Agents

2.1.3.1 Drugs for Genetic Selection

Name	**Concentration**
Nourseothricin (NAT)	100 µg/ml
Geneticin disulphite (G-418)	200 µg/ml
Phleomycin	200 µg/ml
5-Fluoroorotic acid (5-FOA)	1 mg/ml
Ampicillin sodium salt (AMP)	100 µg/ml

Table 2.1 Drugs Used for Genetic Selection

2.1.3.2 Genotoxic Agents

Name
Hydroxyurea (HU)
Methyl Methansulfonate (MMS)
Camptothecin (CPT)

Table 2.2 Genotoxic Agents

2.2 Molecular Cloning Techniques

2.2.1 Restriction Digest

Restriction digests were carried out using enzymes purchased from New England Biolabs (NEB). Manufacturer's Instructions were followed unless otherwise stated.

2.2.2 DNA Ligation

Restriction digested PCR products and restriction digested plasmid DNA were ligated using T4 DNA Ligase (NEB) in a 1:3 ratio. Manufacturer Instructions were followed and incubated overnight at 16 °C.

2.2.3 *E. coli* Transformation

Competent DH5α cells were thawed on ice and incubated on ice for 30 mins in Eppendorf tubes containing the DNA mixture. Cells were heat-shocked at 42 °C for 60 secs and immediately placed on ice for 5 mins. 500 µl LB was added and reactions incubated at 37 °C for 30 mins. Cells were then plated onto LB plates with added Ampicillin and grown at 37 °C overnight.

2.2.4 *E. coli* Plasmid DNA Extraction (Miniprep)

Individual *E. coli* cells were inoculated in 5 ml LB with supplemented ampicillin (10 µg/ml) and grown at 37 °C overnight. Cultures were pelleted at 4000 x g for 10 mins and resuspended in 200 µl Qiagen Buffer P1 (50 mM Tris.Cl, pH 8.0; 10 mM EDTA; 100 µg/ml RNase A). 200 µl Qiagen Buffer P2 (200 mM NaOH, 1% SDS (w/v)) was added and incubated for 5 mins followed by addition of Qiagen Buffer P3 (3.0 M potassium acetate, pH 5.5). Samples were pelleted (16,000 x g, 1 min) and supernatant transferred into a 1:1 volume of isopropanol. Mixture was inverted 6-8 times, pelleted (16,000 x g, 1 min), and washed with 70% (w/v) ethanol. DNA pellet was then dried in a SpeedVac for 10 min and resuspended in 200 µl ddH_2O with added RNase A (0.5 mg/ml).

2.3 General *S. pombe* Techniques

2.3.1 *S. pombe* Genetic Crosses & Random Spore Analysis

Cells from *S. pombe* strains of opposite mating types were mixed together in 10 µl ddH_2O and incubated on ELN (Extremely Low Nitrogen) plates at 25 °C for 2-3 days. Samples that formed tetrads were then incubated O/N in 500 µl ddH_2O plus 1 µl ß-Galactosidase. Roughly 500 spores were then plated onto YEA plus any relevant selection.

2.3.2 *S. pombe* Transformation

10 ml of cells grown O/N in YE to a density of 1 x 10^7 cells/ ml were used for each transformation. Cultures were pelleted at 4000 x g for 4 mins and washed with 1 ml LiAc-TE (10 mM lithium acetate, 1 mM Tris-EDTA, pH 7.5). Pelleted cells were then resuspended in 100 µl LiAc-TE. 2 µl salmon sperm DNA (10 mg/ml) and plasmid (1 µg) or linear fragment DNA (up to 10 µg) was added to each sample and incubated at RT for 10 mins. 260 µl of 40% (w/v) PEG/LiAc-TE was added and incubated at 30 °C for 1 hr. 43 µl DMSO was added and samples were heat shocked at 42 °C for 1 min. Samples were then pelleted and washed with 1 ml ddH_2O. Cells were resuspended in 500 µl ddH_2O and spread onto two plates per sample with the relevant selection.

2.3.3 Recombination Mediated Cassette Exchange

Individual colonies of *S. pombe* cells transformed with a plasmid containing the Cre-Lox recombination mediated cassette exchange constructs (pAW8 origin) were grown O/N in 10 ml YE at 30 °C. Cultures were then pelleted and 10^4 cells were plated onto YE plates supplemented with 5-FOA and grown at 30 °C for 3-5 days. Colony formation indicates loss of *ura4* and successful incorporation of plasmid DNA into the correct location in the genome. Loss of plasmid DNA was confirmed by replica plating onto YNBA plates lacking leucine (supplemented with uracil and adenine).

2.3.4 Standard *S. pombe* Genomic Extraction

S. pombe cultures were grown to exponential phase and 1 ml of cells pelleted and resuspended in NIB Buffer (13 mg/ml MOPS, 18 mg/ml KAc, 20% Glycerol, 2.5 mM $MgCl_2$, pH 7.2) plus 1 mg/ml 20T Zymolyase and incubated at 37 °C for 30 min. Cells were pelleted and re-suspended in 450 µl 5xTE (Tris-EDTA, pH 7.5) with 50 µl 10% SDS (v/v) added and incubated at RT for 5 mins. 150 µl 5M potassium acetate was added and incubated on ice for a further 5 mins. Samples were pelleted at 16,000 x g for 10 mins at 4 °C. Supernatant was added to isopropanol (1:1 volume) and DNA precipitated by inversion and centrifugation at 16,000 x g for a further 10 mins at 4 °C. Pelleted DNA was washed with 500 µl 70% ethanol, supernatant discarded and pellet dried in a SpeedyVac. Dried pellet was then re-suspended in 200 µl ddH_2O plus 5 µl RNase A (10 mg/ml) and stored at -20 °C.

2.3.5 Whole Cell Protein Extract (TCA Extraction)

S. pombe strains grown to logarithmic phase were collected and 5 x 10^7 cells pelleted (3,000 x g for 5 mins). Pelleted cells were re-suspended in 1 ml 20% trichloroacetic acid (TCA) and centrifuged for 2,000 x g for 2 mins. Supernatant was removed and pellet re-suspended in 200 µl 20% TCA and transferred into ribolyser tubes. A cap full of acid washed glass beads were added to each sample before 3 rounds of ribolysing (Fast Prep Hybaid, FP120) at 6.5 m/s for 30 seconds with a 5 min rest on ice between each cycle. Samples were separated from the glass beads by puncturing the ribolyser tubes and centrifuging into fresh Eppendorf tubes (4,000 x g for 2 mins at 4 °C). Separated samples were then pelleted at 16,000 x g for 10 mins at 4 °C and supernatant removed. Pellet was then re-suspended in 200 µl 1X Protein Loading Buffer (250 mM Tris pH 6.8, 8% SDS, 20% glycerol, 20% β-mercaptoethanol, and 0.4% bromophenol blue) and boiled at 95 °C for 10 mins. Samples were stored at -20 °C.

2.3.6 Western Blot (SDS PAGE & Immunostaining)

Proteins were separated using Sodium dodecyl sulphate polyacrylamide gel electrophoresis (SDS PAGE). Gels consisted of a stacking gel (5% acrylamide, 0.125 M TrispH 6.8, 0.1% (w/v) SDS, 0.1% (w/v) ammonium persulphate, and 0.1% (v/v) TEMED) and resolving gel (10% or 12% acrylamide, 0.375 M Tris pH 8.8, 0.1% (w/v) SDS, 0.1% (w/v) ammonium persulphate, and 0.04% (v/v) TEMED) ran in 1x SDS running buffer (0.025 M Tris Base, 0.25 M Glycine, 0.1% SDS). Samples were loaded into gels alongside PageRuler prestained protein ladder (Thermo Scientific, 26616) and run at 80V through the stacking gel and at 180V through the resolving gel. Gels were then washed with ddH_2O and transferred onto a nitrocellulose membrane (Amersham, 45004003) using the Invitrogen XCell II Blot Module. The module was filled with 1x transfer buffer and run at 30V for 90 mins. Membranes were then blocked in 5% Milk (dissolved in PBST (PBS + 0.1% (v/v) Tween)) for 1 hr with gentle rocking. Membranes were incubated with the relevant primary antibody (Table 2.3) dissolved in 5% Milk PBST overnight at 4 °C with gentle rocking. Membranes were then washed three times in PBST for 5 mins each at room temperature with gentle rocking. Membranes were then incubated with an HRP-conjugated (horse radish peroxidase-conjugated) secondary antibody at room temperature for 1 hr with gentle rocking followed by a further 3 washes with PBST as before. Addition of ECL chemiluminescent reagents allowed detection of proteins using autoradiograph film and developed in an X-ray film developer.

Name	Type	Dilution	Source
GFP	Mouse	1:1000	Roche
HA	Mouse	1:1000	Santa Cruz (SC-739)
Myc	Mouse	1:1000	Cell Signalling (9811)
PCNA (PC10)	Mouse	1:1000	Santa Cruz (SC-56)
Streptavidin	Rabbit	1:10,000	Anthony Oliver
Tubulin	Mouse	1:20,000	Sigma (T5168)

Table 2.3 Antibodies Used for Immunostaining

2.3.6.1 Silver Staining

Gels containing proteins separated by SDS-PAGE were prepared for silver staining using the Silver Stain Plus kit (BioRad, 1610449) according to manufacturer's instructions.

2.3.7 FACS Analysis

5 ml of cells grown to 5-10 x 10^6 cells/ml were fixed by resuspending in 500 µl 70% ethanol and stored at -20 °C. Cells were washed with 500 µl 50 mM sodium citrate (pH 7.0) and resuspended in 500 µl 50 mM sodium citrate plus 50 µl 10 mg/ml RNase A and incubated at 37 °C for at least 3 hours. 500 µl 50 mM sodium citrate plus 0.2 µl Sytox Green was added to each sample followed by sonication using a tip sonicator (10 secs, 20%). Samples were loaded into the BD Accuri C6 Flow Cytometer and analysed using BD CSampler Software and FCS Express Flow 4.

2.3.8 Microscopy

Logarithmically grown cells fixed in 70% (v/v) ethanol were spread onto a glass slide and air dried. 5 µl of a mixture of DAPI (1 µg/ml) and Calcofluor (50 µg/ml) was added to each slide before adding the coverslip and analysis under a fluorescence microscope.

2.4 *S. pombe* Strain Construction

2.4.1 *S. pombe* Strain List

Strain	Genotype
BAY1	*I-3220::KAN*
BAY2	*II-8535::3xrRFB, rnh201Δ::KAN*
BAY4	*I-3220::10xrRFB, rnh201Δ::KAN, rtf1Δ::NAT*
BAY6	*I-3220::3xrRFB, rnh201Δ::KAN, rtf1Δ::NAT*
BAY8	*I-3220::3xrRFB, rnh201Δ::KAN, cdc6-L591G*
BAY12	*I-3220::10xrRFB, rnh201Δ::KAN, cdc20-M630F*
BAY16	*I-3220::10xrRFB, rnh201Δ::KAN, cdc6-L591G*
BAY21	*I-3220::3xrRFB, rnh201Δ::KAN, cdc20-M630F*
BAY24	*II-8535::3xrRFB, rnh201Δ::KAN, cdc20-M630F*
BAY29	*II-8535::3xrRFB, rnh201Δ::KAN, cdc6-L591G*
BAY33	*I-3220::KAN-10xrRFB*
BAY37	*I-3220::Rura-10xrRFB*
BAY43	*I-3320::Rura-10xrRFB, rnh201Δ::KAN, cdc6-L591G*
BAY44	*I-3320::Rura-10xrRFB, rnh201Δ::KAN, cdc20-M630F*
BAY45	*I-3320::Rura-10xrRFB, rnh201Δ::KAN, rtf1Δ::NAT, cdc6-L591G*
BAY46	*I-3320::Rura-10xrRFB, rnh201Δ::KAN, rtf1Δ::NAT, cdc20-M630F*
BAY60	*II::Rura-10xrRFB, RTS1Δ::Phleo, rtf1Δ::NAT*
BAY71	*II::Rura-10xrRFB, pcn1_R80A, RTS1Δ::Phleo, rnh201Δ::KAN, cdc20_M630F*
BAY72	*II::Rura-10xrRFB, pcn1_R80A, RTS1Δ::Phleo, rtf1Δ::NAT, rnh201Δ::KAN, cdc20_M630F*
BAY73	*II::Rura-10xrRFB, pcn1_R80A, RTS1Δ::Phleo, rnh201Δ::KAN, cdc6_L591G*
BAY74	*II::Rura-10xrRFB, pcn1_R80A, RTS1Δ::Phleo, rtf1Δ::NAT, rnh201Δ::KAN, cdc6_L591G*
BAY75	*II::Rura-10xrRFB, pcn1_F248A, RTS1Δ::Phleo, rnh201Δ::KAN, cdc20_M630F*
BAY76	*II::Rura-10xrRFB, pcn1_F248A, RTS1Δ::Phleo, rtf1Δ::NAT, rnh201Δ::KAN, cdc20_M630F*
BAY77	*II::Rura-10xrRFB, pcn1_F248A, RTS1Δ::Phleo, rnh201Δ::KAN, cdc6_L591G*
BAY78	*II::Rura-10xrRFB, pcn1_F248A, RTS1Δ::Phleo, rtf1Δ::NAT, rnh201Δ::KAN, cdc6_L591G*
BAY81	*II::Rura-10xrRFB, RTS1Δ::Phleo, rtf1Δ::HYG*
BAY87	*II::Rura-10xrRFB, rad52-GFP::KAN, cdc2asM17*
BAY88	*II::Rura-10xrRFB, rad52-GFP::KAN, cdc2asM17, rtf1Δ::NAT*
BAY111	*II::Rura-10xrRFB, rpa3-GFP::KAN, cdc2asM17*
BAY112	*II::Rura-10xrRFB, rpa3-GFP::KAN, cdc2asM17, rtf1Δ::NAT*
BAY119	*II::Rura-10xrRFB, RTS1Δ::Phleo, rnh201Δ::KAN, rtf2Δ::NAT, cdc6L591G*

BAY120	*II::Rura-10xrRFB, RTS1Δ::Phleo, rnh201Δ::KAN, rtf2Δ::NAT, rtf1Δ::HYG, cdc6L591G*
BAY121	*II::Rura-10xrRFB, RTS1Δ::Phleo, rnh201Δ::KAN, rtf2Δ::NAT, cdc20_M630F*
BAY122	*II::Rura-10xrRFB, RTS1Δ::Phleo, rnh201Δ::KAN, rtf2Δ::NAT, rtf1Δ::HYG, cdc20_M630F*
BAY123	*II::Rura-10xrRFB, RTS1Δ::Phleo, rnh201Δ::KAN, rtf1Δ::HYG, cdc20M630F*
BAY124	*II::Rura-10xrRFB, RTS1Δ::Phleo, rnh201Δ::KAN, cdc20M630F*
BAY125	*II::Rura-10xrRFB, RTS1Δ::Phleo, rnh201Δ::KAN, rtf1Δ::HYG, cdc6L591G*
BAY126	*II::Rura-10xrRFB, RTS1Δ::Phleo, rnh201Δ::KAN, cdc6L591G*
BAY127	*II::Rura-10xrRFB, cdc27_D1, RTS1Δ::Phleo, rnh201Δ::KAN, cdc6_L591M*
BAY128	*II::Rura-10xrRFB, cdc27_D1, RTS1Δ::Phleo, rnh201Δ::KAN, rtf1Δ::NAT, cdc6_L591M*
BAY129	*II::Rura-10xrRFB, cdc27_D1, RTS1Δ::Phleo, rnh201Δ::KAN, rtf1Δ::NAT, cdc20_M630F*
BAY130	*II::Rura-10xrRFB, cdc27_D1, RTS1Δ::Phleo, rnh201Δ::KAN, cdc20_M630F*
BAY140	*pcn1_F248A,Y249A*
BAY144	*II::Rura4sd20-10xrRFB, RTS1Δ::Phleo, rtf1Δ::NAT*
BAY146	*II::Rura4sd20-10xrRFB, RTS1Δ::Phleo*
BAY153	*II::Rura4sd20-10xrRFB, pcn1_F248A, RTS1Δ::Phleo*
BAY154	*II::Rura4sd20-10xrRFB, pcn1_F248A, RTS1Δ::Phleo, rtf1Δ::NAT*
BAY162	*II::Rura4sd20-10xrRFB, cdc27_D1, RTS1Δ::Phleo*
BAY163	*II::Rura4sd20-10xrRFB, cdc27_D1, RTS1Δ::Phleo, rtf1Δ::NAT*
BAY166	*II::Rura4sd20-10xrRFB, pcn1_R80A, RTS1Δ::Phleo*
BAY167	*II::Rura4sd20-10xrRFB, pcn1_R80A, RTS1Δ::Phleo, rtf1Δ::NAT*
BAY176	*II::Rura4sd20-10xrRFB, RTS1Δ::Phleo, rtf2Δ::NAT*
BAY178	*II::Rura4sd20-10xrRFB, cdc27-D3, RTS1Δ::Phleo, rtf1+*
BAY179	*II::Rura4sd20-10xrRFB, cdc27-D3, RTS1Δ::Phleo, rtf1Δ::NAT*
BAY180	*rtf2-GFP:KAN*
BAY181	*rtf2-13Myc:KAN*
BAY182	*rtf2-3HA:KAN*
BAY186	*II::Rura4sd20-10xrRFB, RTS1Δ::Phleo, rtf2-GFP:KAN*
BAY187	*II::Rura4sd20-10xrRFB, RTS1Δ::Phleo, rtf2-13Myc:KAN*
BAY188	*II::Rura4sd20-10xrRFB, RTS1Δ::Phleo, rtf2-3HA:KAN*
BAY190	*II::Rura-10xrRFB, rtf1+, cdc2asM17, rtf2-GFP:KAN*
BAY206	*II::Rura-10xrRFB, cdc27_D3, RTS1Δ::Phleo, rnh201Δ::KAN, cdc20_M630F*
BAY207	*II::Rura-10xrRFB, cdc27_D3, RTS1Δ::Phleo, rnh201Δ::KAN, rtf1Δ::NAT, cdc20_M630F*
BAY210	*rtf2-mEOS:KAN*
BAY211	*II::Rura-10xrRFB, RTS1Δ::Phleo, rtf2-mEOS:KAN*
BAY223	*II::Rura-10xrRFB, cdc27_D3, RTS1Δ::Phleo, rnh201Δ::KAN, cdc6_L591M*
BAY224	*II::Rura-10xrRFB, cdc27_D3, RTS1Δ::Phleo, rnh201Δ::KAN, rtf1Δ::NAT, cdc6_L591M*
BAY230	*II::Rura-10xrRFB, rtf1+, cdc2asM17, rtf2-13Myc:KAN, mcm4-GFP:KAN*
BAY232	*cdc27-GFP:KAN*
BAY233	*II::R:AΔura-10xrRFB, rtf1Δ::NAT*

BAY234	*II::Rura-10xrRFB, RTS1Δ::Phleo, rnh201Δ::KAN, cdc6L591M*
BAY235	*II::Rura-10xrRFB, RTS1Δ::Phleo, rnh201Δ::KAN, rtf1Δ::NAT, cdc6L591M*
BAY236	*II::R:AΔura-10xrRFB, RTS1Δ::Phleo, rnh201Δ::KAN, rtf2Δ::NAT, rtf1Δ::HYG*
BAY237	*II::R:AΔura-10xrRFB, RTS1Δ::Phleo, rnh201Δ::KAN, cdc6L591G*
BAY238	*II::R:AΔura-10xrRFB, RTS1Δ::Phleo, rnh201Δ::KAN, cdc20M630F*
BAY239	*II::R:AΔura-10xrRFB, RTS1Δ::Phleo, rnh201Δ::KAN, rtf1Δ::HYG, cdc6L591G*
BAY240	*II::R:AΔura-10xrRFB, RTS1Δ::Phleo, rnh201Δ::KAN, rtf1Δ::HYG, cdc20M630F*
BAY241	*II::R:AΔura-10xrRFB, RTS1Δ::Phleo, rnh201Δ::KAN, rtf2Δ::NAT, cdc20_M630F*
BAY242	*II::R:AΔura-10xrRFB, RTS1Δ::Phleo, rnh201Δ::KAN, rtf2Δ::NAT, cdc6L591G*
BAY243	*II::R:AΔura-10xrRFB, RTS1Δ::Phleo, rnh201Δ::KAN, rtf2Δ::NAT, rtf1Δ::HYG, cdc6L591G*
BAY244	*II::R:AΔura-10xrRFB, RTS1Δ::Phleo, rnh201Δ::KAN, rtf2Δ::NAT, rtf1Δ::HYG, cdc20_M630F*
BAY246	*rtf2-3HA:TurboID:KAN*
BAY248	*II::Rura-10xrRFB, rtf2-3HA:KAN, mcm4-GFP:KAN*
BAY249	*II::R:AΔura4sd20-10xrRFB, RTS1Δ::Phleo, rtf1Δ::HYG*
BAY250	*II::Rura-10xrRFB, cdc27-GFP:KAN, pcn1_R80A*
BAY251	*II::R:AΔura4sd20-10xrRFB, RTS1Δ::Phleo*
BAY252	*II::R:AΔura4sd20-10xrRFB, RTS1Δ::Phleo, rtf2Δ:NAT*
BAY253	*II::R:AΔura4sd20-10xrRFB, RTS1Δ::Phleo, rtf2Δ:NAT, rtf1Δ:HYG*
BAY254	*II::Rura-10xrRFB, cdc27-GFP:KAN, pcn1_F248A*
BAY266	*II::Rura-10xrRFB, cdc2asM17, rtf2-3HA:KAN, mcm4-GFP:KAN*
503	*ade6-704, leu1-32, ura4-d18*
995	*cdc6-L591G*
997	*cdc20-M630F*
1144	*I-3220:KAN, rtf1Δ::NAT*
KA2	*II-8535:KAN, rtf1Δ::NAT*
KA58	*II::Rura-10xrRFB, rtf1Δ::NAT*
1170	*II::TuraR, rtf1Δ::NAT, rnh201Δ::KAN*
KA39	*II-8535:KAN-ura4, rtf1Δ::NAT*
KA56	*II-8535:KAN-10xrRFB, rtf1Δ::NAT*

Table 2.4 List of strains used in this project.

All strains are in a 503 genetic background unless otherwise stated.

2.4.2 Primer List

Name	Sequence
A30	GGAGGTTGAGTGTGGGACGTTTCTGCCATACCCTTTTTAAGT
A31	GGTATGGCAGAAACGTCCCACACTCAACCTCCCAAT
F29	GCATTTAAGTGTAATACGAAATCTGTAGAATTTGTGGCCAAGAACCGCTACAAA TCCCACTGGCTA
R30	GCACTAAAGAGAAAGTCCCGTTCCTTTTATTCAGTACGTTATGGGTAATACTAAT AATTGCGAGAGGTTGTACAATTCTCTTTTAGTTTTTAAGAAAACTTGTGATATTG ACGAAACTTT
F41	AATTATCATTGCTTGAATTATACAATTAATACATTTTGCATTCATGTGCAATTCGC ATTTAAGTGTAATACGAAATCTGTAGAATTTGTGGCCAAGAACCAGCTCATGAT AATCTATTAA
R42	GCACTAAAGAGAAAGTCCCGTTCCTTTTATTCAGTACGTTATGGGTAATACTAAT AATTGCGAGAGGTTGTACAATTCTCTTTTAGTTTTTAAGAAAACTCTATTAGTCA GCACAGTATA
A5	GAATAAGTTGAATTAATTTCGTAAAATCAAATTTTTTAAACGGGAGATTATGTGT AAGGATTCATTTTTTATTAGAATGGAATGGTAATAATATTCTACAATATTTAATGA TTTAAAAGT
A6	TAAATAGTGGAAACAAGTAAGCAATTAGTTCGGCTGAAAGTTGCATACCTCAGT ATATAATAATCACATTGGCTTGTGATATTGACGAAACTTTTTGACATCTAATTTAT TCTGTTCCAA
A13	GAATAAGTTGAATTAATTTCGTAAAATCAAATTTTTTAAACGGGAGATTATGTGT AAGGATTCATTTTTTATTAGAATGGAATGGTAATAATATTCTACAAGCTCATGAT AATCTATTAA
A14	TAAATAGTGGAAACAAGTAAGCAATTAGTTCGGCTGAAAGTTGCATACCTCAGT ATATAATAATCACATTGGCTTAAATTACTTTTAAATCATTAAATATCTATTAGTCA GCACAGTATA

Table 2.5 List of Primers used in this Project

2.4.3 Creating rRFB Control Strains

Yeast strains containing LoxP-*ura4*-LoxM at either the ChrI (1170) or ChrII (KA15) locus were transformed with pAW8-3xrRFB or pAW8-10xrRFB using the RMCE method to create the strains BAY6 (ChrI::3xrRFB), BAY4 (ChrI::10xrRFB), and BAY2 (ChrII::3xrRFB).

2.4.4 Creating Optimised *RTS1*-10xrRFB Construct Strains

Yeast strains containing LoxP-KanMX-LoxM at the ChrI (1144) and ChrII (KA2) locus used were transformed with a *ura4* fragment using primers containing homologous overhangs to a region 10 Kb downstream of each locus (primers A5/A6 and F29/R30, respectively) to create strains BAY1 and KA39, respectively. Transformants were selected for on YNBA +*leu* +*ade* plates to select for gain of uracil prototrophy and correct site of integration by colony PCR. The 10xrRFB sequence was amplified from pAW8-10xrRFB (primers A13/A14 and F41/R42), and subsequently transformed to replace the inserted *ura4* and create the strains BAY33 and KA56 on ChrI and ChrII, respectively. Transformants were selected for loss of uracil proficiency on YE+5-FOA plates and correct sequence insertion by PCR amplification and sequencing. Subsequent transformation of each of these strains with the pAW8-*RTS1-ura4* using the RMCE method to insert *RTS1-ura4* between the LoxP/LoxM sites were selected for on YNBA+*leu*+*ade* and checked for loss of Kanamycin resistance by replica plating onto YE+G4-18. This created the strains BAY37 (ChrI::*RTS1-ura4*-10xrRFB) and KA58 (ChrII::*RTS1-ura4*-10xrRFB).

2.4.5 Creating *RTS1_A*Δ-10xrRFB Construct Strains

Deletion of region A of *RTS1* was conducted using overlapping primers lacking region A (A30/A31) to amplify the pAW8-*RTS1-ura4* plasmid to create pAW8-*RTS1_A*Δ-*ura4*. Transformation of KA58 with this plasmid created the strain BAY233.

2.4.6 Creating *RTS1* Slippage Assay Strains

A fragment containing a region of *ura4* containing the 20 bp tandem repeat was synthesised by Eurofins and digested with StuI and DraIII. The pAW8-*RTS1-ura4* or pAW8-*RTS1_A*Δ-*ura4* plasmids were digested with the same enzymes and both digestions ran on a 2% Agarose gel and insert and vector gel extracted. Subsequent ligation of the insert and vector followed by *E. coli* transformation created the plasmid

pAW8-*RTS1-ura4sd20* or pAW8-*RTS1_AΔ-ura4sd20.* These plasmids were then transformed using the RMCE method into BAY60 to create the strain BAY144 and BAY249. Transformants were selected for by loss of uracil proficiency on YE+5-FOA and the sequence checked by PCR amplification and sequencing.

2.5 Cell synchronisation

2.5.1 *cdc25_22* Synchronisation

S. pombe strains containing the *cdc25_22* temperature sensitive allele were grown O/N at 25 °C. Once cell density reached 2.5 x 10^6 cells/ml, cultures were incubated at the restrictive temperature of 36 °C for 4 hrs to synchronise in G2. Flasks were then cooled on ice until a temperature of 25 °C was reached and placed into a shaking 25 °C water bath for sample collection every 15 mins.

2.5.2 *cdc2asM17* Synchronisation

S. pombe strains containing the *cdc2asM17* ATP-analogue sensitive allele were grown O/N at 28 °C. Once cell density reached 2.5 x 10^6 cells/ml, 1:1000 volume of 3BrPP1 (2 mM) was added to the culture and incubated at 28 °C for a further 3 hrs to synchronise in G2. Cultures were then filtered using a vacuum flask filter unit. Cells collected on the filter paper (0.22 µm, Millipore N8645) were then washed 3 times by addition of fresh YE media and filtration. The cell coated filter paper was then placed into pre-warmed fresh YE media before resuspension by shaking. Cells were grown at 28 °C for sample collection every 7.5 mins.

2.6 Chromatin Immunoprecipitation (ChIP)

Collected cells were formaldehyde crosslinked by addition of 37% (w/v) formaldehyde (Sigma F-8775) to 20 ml of cells at a final concentration of 1% for 15 mins with gentle

shaking. Crosslinking reaction was quenched by addition of 2.5 ml of 2.5 M Glycine and incubated for 5 mins with gentle shaking. Cells were then pelleted (4,000 x g for 10 mins at 4 °C) and washed with 10 ml PBS before snap freezing in liquid nitrogen and storage at -80 °C until ready for processing.

Cell pellet was re-suspended in 400 µl ChIP Lysis Buffer and placed into a ribolyser tube containing an eppendorf cap of glass beads. Samples were ribolysed (Fast Prep Hybaid, FP120) twice at 6.5 m/s for 15 seconds with a 5 min rest on ice between each cycle. The bottom of each tube was pierced with a sterile needle before placing in another tube and centrifuging for 2 mins at 4,000 x g (at 4 °C) to remove glass beads from sample. The samples in the collection tubes were then spun for a further 10 mins at 16,000 x g at 4 °C before removing the supernatant and washing the pellet in 1 ml ChIP Lysis Buffer. Samples were pelleted again as in the previous step to obtain the nuclear fraction and re-suspended 400 µl ChIP Lysis Buffer. Samples were placed in sonication tubes and sonicated (QSonica Q800R) for 12 mins (20 secs ON, 40 secs OFF) at 70% Amplitude. Sonicated samples were spun for 10 mins at 16,000 x g at 4 °C and 5 µl of supernatant was added to 95 µl Elution buffer for use as input sample. 300 µl of supernatant was then placed into a fresh Eppendorf tube and 1 µl of GFP antibody (Invitrogen A11122) was added and incubated for 1 hr at 4 °C with rotation. During antibody incubation Protein G coated dynabeads (Invitrogen 100.04) were blocked by incubation with 0.3 mg/ml Salmon Sperm DNA (10 mg/ml, Invitrogen AM9680) for 1 hr followed by 3 washes with ChIP Lysis Buffer. 20 µl of beads were then added to each sample and incubated overnight at 4 °C with rotation. Beads were washed for 5 mins with rotation at 4 °C and separated from supernatant by gentle spinning and use of a magnetic stand in the following buffers: Twice with 1 ml ChIP Lysis Buffer, twice with 1 ml ChIP Lysis Buffer (high salt), twice with ChIP wash buffer, and once with 1 ml TE. Immunoprecipitation bound beads were then RNase treated by addition of 130 µl Elution buffer + 2 µl RNase A (10 mg/ml) at 37 °C for 30 mins, before addition of 6 µl 5M NaCl and 2 µl Proteinase K (20 mg/ml) and incubated at 65 °C for 2 hrs. The sample was then separated from the beads using a magnetic rack and 100 µl supernatant containing eluted IP transferred to a new tube. DNA from the IP and input samples were then purified using the Qiagen PCR purification kit and eluted into 200 µl ddH_2O and stored at -20 °C.

2.7 Quantitative PCR Analysis

qPCR reactions were aliquoted using sterile filter tips and qPCR strip tubes with each step performed on ice. A master mix was created containing (per reaction): 10 µl Luna Universal qPCR Master Mix, 0.5 µl forward primer (10 µM), 0.5 µl reverse primer (10 µM), and 4 µl nuclease free water. 15 µl of the master mix was then added to each tube plus 5 µl DNA sample. Each sample was aliquoted in duplicate before mixing by gentle flicking and spinning tubes briefly. Samples were run in an AriaMX Real-time PCR System using the conditions outlined in Table 2.6.

Step	Temperature (°C)	Time	Cycles
Initial Denaturation	95	60 secs	1
Denaturation	95	15 secs	40
Extension	60	30 secs	
Melt Curve	95	60 secs	1
	65	30 secs	
	95	30 secs	

Table 2.6 qPCR Thermocycler Conditions

2.8 Co-Immunoprecipitation

S. pombe cells grown to logarithmic phase in liquid YE media were collected to obtain 5 x 10^8 cells. Cells were pelleted (4,000 x g for 5 mins at 4 °C) and washed with 10 ml PBS before snap freezing in liquid nitrogen and storage at -80 °C until ready for processing. Pellet was re-suspended in 400 µl Lysis Buffer (50 mM HEPES, 1% Triton x100, 0.1% NaDeoxycholate, 2 mM $MgCl_2$, 40 mM NaCl) and split equally into two ribolyser tubes containing an Eppendorf cap of glass beads. Samples were ribolysed (Fast Prep Hybaid, FP120) three times at 6.5 m/s for 15 seconds with a 5 min rest on ice between each cycle. The bottom of each tube was pierced with a sterile needle before placing in another tube and centrifuging for 2 mins at 4,000 x g (at 4 °C) to remove glass beads from sample. Ribolysed samples originating from the same pellet were then recombined

and DNA digested by addition of 1 µl Benzonase for 30 mins on ice. Tubes were then centrifuged at 16,000 x g for 10 mins at 4 °C. 30 µl of the supernatant was then added to 10 µl 4x SDS Sample buffer (final concentration 1x) and saved as input sample. GFP-Trap beads (Chromotek gta-20) were washed three times in lysis buffer before adding 10 µl per sample to 300 µl of supernatant. Salt concentration of the IP sample containing beads was then increased to 140 mM by addition of 9 µl 5M NaCl and incubated for 1 hr at 4 °C with rotation. Beads were then washed 5 times in 500 µl Lysis Buffer with gentle centrifugation (2,000 x g for 2 mins at 4 °C) between each wash to separate beads from supernatant. Beads were then eluted into 2x SDS Sample buffer and boiled at 95 °C for 15 mins. Samples were stored at -20 °C until ready to perform western blot analysis.

2.8 Replication Fork Slippage Assay

S. pombe strains containing the *RTS1-ura4sd20* construct were grown in 10 ml YE containing 1 mg/ml 5-FOA overnight at 30 °C. Cells were washed in 1 ml 5-FOA free YE and resuspended into 10 ml fresh YE at a density of 2 x 10^6 cells/ml. Cells were grown for 2 cell cycles before pelleting and re-suspending in 1 ml ddH_2O. 100 µl of cells were then plated in appropriate dilutions onto 2 YEA plates and 2 YNBA plates containing appropriate amino acids minus uracil. Plates were then incubated at 30 °C for 3-5 days. Number of colonies were counted and the mean average was taken between each of the two plates. Reversion frequency of Ura^+ colonies was then calculated taking into consideration the dilutions plated between YEA plates and YNBA plates lacking uracil.

2.9 Polymerase Usage Sequencing

800 ml of asynchronous *S. pombe* cultures were grown to a density of 3-5 x 10^6 cell/ml and collected by centrifugation (6,000 x g for 10 mins at 4 °C). Cell pellets were washed with 40 ml ice cold ddH_2O and snap frozen in liquid nitrogen for storage at -80 °C.

2.9.1 Genomic Extraction

Cell pellets were thawed at room temperature before resuspension in 2 ml of NIB buffer plus 5 mg/ml 100T Zymolyase and incubated at 37 °C for 15-30 mins until cells were sufficiently lysed. Cells were washed with 20 ml of ice cold ddH_2O (4,000 x g for 10 mins at 4 °C) before resuspending in 2 ml of Qiagen Buffer G2 plus 100 µl 10 mg/ml RNase A and incubated at 37 °C for 30 mins. 100 µl 30% (w/v) N-lauroyl sarcosine and 100 µl 20 mg/ml proteinase K was added and incubated at 55 °C for 60 mins. Cells were pelleted (4,000 x g for 15 mins at 4 °C) and supernatant transferred to a new tube. Cell pellet was resuspended in 1 ml Qiagen buffer G2 plus 50 µl 30% (w/v) N-lauroyl sarcosine and 50 µl 20 mg/ml proteinase K and incubated at 55 °C for a further 30 mins. Cells were pelleted as in the previous step and supernatant transferred to the tube containing the supernatant already collected.

Qiagen 100/G Genomic Tips were incubated with 4 ml Qiagen Buffer QBT before addition of the collected supernatant. Wash the tips with 2x 7.5 ml Qiagen Buffer QC and elute using 5 ml Qiagen Buffer QF. Eluted DNA was precipitated by adding 3.5 ml isopropanol and centrifuged at 4,000 x g for 20 mins at 4 °C. Pelleted DNA was resuspended in 100 µl TE.

2.9.2 Alkali Treatment & Size Selection

20 µg DNA was added to 30 µl 1M NaOH and made up to a final volume of 100 µl by addition of ddH_2O and incubated at 55 °C for 2 hours. 50 µl of the alkali treated DNA was run on a 2% (w/v) TBE agarose gel in 0.5x TBE buffer for 2 hours at 100 V. Gels were stained in 0.5 µg/ml acridine orange solution at room temperature on a shaker for 2 hours. Gels were destained overnight in ddH_2O before visualisation of DNA under a longwave UV lamp. Fragments of 300-500 bp were isolated and extracted using the Macherey-Nagel Gel Extraction kit according to manufacturer's instructions. ssDNA was eluted into 20 µl TE.

2.9.3 Second Strand Synthesis & Adapter Ligation

100 ng ssDNA was made up to 30 µl with ddH_2O. DNA was placed in a PCR tube with 5 µl 10x 8N random primers (3 mg/ml) and 5 µl 10x NEB 2.1 buffer and boiled at 95 °C for 5 min followed by incubation on ice for 5 min. 5 µl 10x dNTP mix (with dTTP substituted for dUTP, 2 mM each), 4 µl ddH_2O, and 1 µl T4 polymerase and incubated at 37 °C for 20 mins. Reaction was stopped by addition of 5 µl 0.5 M EDTA (pH 8.0).

Samples were added to a 1.5 ml Eppendorf tube and resuspended in 99 µl AMPure XP beads and incubated at room temperature for 5 mins. Beads were separated from supernatant by placing tubes on a magnetic rack, and supernatant discarded. Beads were washed twice with 200 µl 80% (v/v) ethanol and air dried for 10 mins. DNA was eluted by addition of 60 µl ddH_2O and beads separated using magnetic rack before collection of the size selected dsDNA.

55.5 µl of the size selected dsDNA was added to 6.5 µl 10x NEBNext end repair reaction buffer and 3 µl NEBNext end prep enzyme mix. Reaction was incubated in a thermocycler at 20 °C for 30 mins followed by 30 mins at 65 °C. Adapters were then ligated by addition of 15 µl Blunt/TA ligation master mix, 1 µl 10x diluted (1.5 µM) NEBNext adapter, and 2.5 µl ddH_2O and incubated at 20 °C for 15 mins.

100 µl sample (volume adjusted by addition of ddH_2O) was mixed with 35 µl AMPure XP beads and incubated at room temperature for 5 mins. Each sample was placed onto a magnetic rack until the beads separate from solution and transfer the supernatant to a new tube. Another 35 µl AMPure XP beads was added to the supernatant and incubated as before. Beads were separated from solution using a magnetic rack before discarding the supernatant. Beads were then washed three times with 200 µl 80% (v/v) ethanol before air drying for 10 mins. DNA was eluted from the beads by addition of 25 µl TE (pH 8.0). Beads were separated on a magnetic rack and 23 µl of sample containing target DNA was transferred to a new tube.

2.9.4 Final Library Amplification & Purification

In a PCR tube components added were: 20 µl DNA, 3 µl NEBNext USER enzyme, 25 µl 2x NEBNext high-fidelity PCR master mix, 1 µl Universal PCR primer (25 µM), and 1 µl index primer (25 µM). PCR was carried out using the conditions in Table 2.3 with number of cycles adjusted according to manufacturer's guidance on starting DNA concentration.

Step	Temperature (°C)	Time	Cycles
USER Digestion	37	15 min	1
Initial Denaturation	98	30 secs	1
Denaturation	98	10 secs	8-15
Annealing	65	30 secs	
Extension	72	30 secs	
Final Extension	72	5 min	1
Hold	4	∞	1

Table 2.7 Thermocycler Conditions Used for Final Pu-Seq Library Amplification

Equal volume of AMPure XP beads were mixed with the PCR reaction (50 µl) and incubated at room temperature for 5 mins. Supernatant was removed and discarded by separation on a magnetic rack before washing beads twice with 200 µl 80% (v/v) ethanol. Beads were air dried for 10 mins before elution into 51 µl ddH_2O. 50 µl of supernatant was transferred to a new tube using a magnetic rack and 25 µl AMPure XP beads was added to each supernatant. Beads were purified as before and eluted into 23 µl ddH_2O. 20 µl of the final purified library was transferred to a new tube before quality checking on a Bioanalyzer.

2.9.5 Sequencing & Data Processing

Libraries were sent for Next Generation Sequencing and raw reads from each set of *cdc6* and *cdc20* mutant strains were used to calculate polymerase usage ratios as previously published (Keszthelyi et al., 2015). The sequenced libraries produce 4 FASTQ files (2 for

3’ ends, and 2 for 5’ ends). These files are compiled together and the 5’ end of the reads are trimmed by 1 nucleotide, and the 3’ is trimmed by 30 nucleotides. The paired-end reads are then aligned to an indexed *S. pombe* reference genome using Bowtie2 to produce an aligned SAM file. The aligned reads are then sorted into bins of 300 bp using a perl script to produce two files, one for each DNA strand (forward and reverse). The number of reads in each bin are then counted to produce a csv file organised by chromosome that can be further analysed using IGV and RStudio. Full details of the scripts used can be found in the previously published manuscript (Keszthelyi et al., 2015). Below is a summary of the Pu-seq libraries presented in this thesis. All libraries in the table are one representative independent repeat. Additional repeats were conducted on some of the libraries as indicated on the following page.

Name	Strain	Polymerase Mutation	Total Reads	Alignment Rate	Repeats
ChrI_3xrRFB	BAY8	*cdc6_L591G*	20,025,693	95.14%	1
ChrI_3xrRFB	BAY21	*cdc20_M630F*	12,236,468	92.41%	1
ChrI_10xrRFB	BAY16	*cdc6_L591G*	10,360,005	94.76%	1
ChrI_10xrRFB	BAY12	*cdc20_M630F*	90,280,601	94.74%	1
ChrII_3xrRFB	BAY29	*cdc6_L591G*	11,718,899	92.54%	1
ChrII_3xrRFB	BAY24	*cdc20_M630F*	25,233,740	93.94%	1
ChrI_RTS1_ON	BAY43	*cdc6_L591G*	29,087,203	93.97%	1
ChrI_RTS1_ON	BAY44	*cdc20_M630F*	39,480,705	94.86%	1
ChrI_RTS1_OFF	BAY45	*cdc6_L591G*	35,501,178	95.63%	1
ChrI_RTS1_OFF	BAY46	*cdc20_M630F*	40,196,998	90.01%	1
ChrII_RTS1_ON	BAY126	*cdc6_L591G*	22,445,972	81.61%	2
ChrII_RTS1_ON	BAY124	*cdc20_M630F*	14,525,765	94.53%	2
ChrII_RTS1_OFF	BAY125	*cdc6_L591G*	30,325,307	92.47%	2
ChrII_RTS1_OFF	BAY123	*cdc20_M630F*	11,837,636	92.69%	2
Cdc6_L591M ON	BAY234	*cdc6_L591M*	23,815,943	79.12%	1
Cdc6_L591M OFF	BAY235	*cdc6_L591M*	3,448,693	73.46%	1
Pcn1_R80A ON	BAY73	*cdc6_L591G*	23,185,220	93.79%	1
Pcn1_R80A ON	BAY71	*cdc20_M630F*	16,801,712	95.59%	1
Pcn1_R80A OFF	BAY74	*cdc6_L591G*	28,197,174	94.26%	1
Pcn1_R80A OFF	BAY72	*cdc20_M630F*	20,059,908	95.44%	1
Pcn1_F248A ON	BAY77	*cdc6_L591G*	17,578,088	94.08%	1
Pcn1_F248A ON	BAY75	*cdc20_M630F*	14,960,667	96.58%	1
Pcn1_F248A OFF	BAY78	*cdc6_L591G*	44,903,990	91.95%	1
Pcn1_F248A OFF	BAY76	*cdc20_M630F*	17,359,497	96.35%	1
Cdc27_D1 ON	BAY127	*cdc6_L591M*	21,465,902	82.43%	2
Cdc27_D1 ON	BAY130	*cdc20_M630F*	4,495,045	76.33%	2
Cdc27_D1 OFF	BAY128	*cdc6_L591M*	7,311,864	80.04%	2
Cdc27_D1 OFF	BAY129	*cdc20_M630F*	8,036,379	80.49%	2
Cdc27_D3 ON	BAY223	*cdc6_L591M*	18,307,311	77.61%	1
Cdc27_D3 ON	BAY206	*cdc20_M630F*	19,003,118	88.97%	1
Cdc27_D3 OFF	BAY224	*cdc6_L591M*	15,108,300	82.01%	1
Cdc27_D3 OFF	BAY207	*cdc20_M630F*	21,261,607	90.10%	1
Rtf2**Δ** ON	BAY119	*cdc6_L591G*	39,869,610	94.80%	3
Rtf2**Δ** ON	BAY121	*cdc20_M630F*	28,752,227	92.90%	3
Rtf2**Δ** OFF	BAY120	*cdc6_L591G*	10,149,735	93.54%	1
Rtf2**Δ** OFF	BAY122	*cdc20_M630F*	9,054,312	93.50%	1
Rtf2-GFP ON	BAY228	*cdc6_L591G*	15,595,806	95.52%	1
Rtf2-GFP ON	BAY227	*cdc20_M630F*	15,983,210	96.70%	1
ChrII_RTS1_A**Δ**_ON	BAY237	*cdc6_L591G*	11,979,785	95.09%	1
ChrII_RTS1_A**Δ**_ON	BAY238	*cdc20_M630F*	13,409,409	96.16%	1
ChrII_RTS1_A**Δ**_ON Rtf2**Δ**	BAY242	*cdc6_L591G*	11,213,937	96.63%	1
ChrII_RTS1_A**Δ**_ON Rtf2**Δ**	BAY241	*cdc20_M630F*	9,071,370	95.48%	1
ChrII_RTS1_A**Δ**_OFF	BAY239	*cdc6_L591G*	13,837,819	85.92%	1
ChrII_RTS1_A**Δ**_OFF	BAY240	*cdc20_M630F*	9,717,956	96.09%	1

Table 2.8 Polymerase Usage Sequencing Libraries

2.10 Mass Spectrometry

2.10.1 Buffer Preparation

Buffer	Components
FASP Urea Solution	8 M Urea 0.1 M Tris/HCl, pH 8.5
FASP IAA	8 M Urea 50 mM iodoacetamide (IAA)
ABC Buffer	50 mM Ammonium Bicarbonate
Trypsin Stock	1 mM Hydrochloric acid (HCl) 0.2 µg/µl Trypsin (Promega, V511A)
Digestion Solution	Trypsin Stock (2.5 µl) 50 mM ABC buffer (37.5 µl)
Buffer A	5% Acetonitrile 0.1% Formic Acid
Buffer A*	5% Acetonitrile 3% Trifluoroacetic Acid
Buffer B	80% Acetonitrile 0.1% Formic Acid
Buffer C	5% Acetonitrile 0.1% Trifluoracetic Acid

Table 2.9 Buffers Used for Mass Spectrometry Sample Preparation

All buffers were prepared using HPLC grade H_2O. To Prepare the FASP Urea solution, 12.114g Trizma Base was dissolved in 80 ml HPLC grade H_2O and pH adjusted to 8.5 using HCl. Total volume was increased to 100 ml before incubated with 0.5 g AmberLite MB20 H/OH Mixed Bed Ion Exchange Resin with a magnetic stirrer for 15 min at RT. Solution was then filtered through a filter unit and stored as 1 ml aliquots at -20 °C.

2.10.2 Biotin Pull Down

250 ml *S. pombe* cells were grown in either YE or EMM (plus 50 µM biotin for 3 hrs) to a density of 5 x 10^6cells/ml. Cells were collected and washed once in 10 ml PBS before snap freezing and storing at -80 °C until ready for processing. Pelleted cells were then thawed at RT and re-suspended in 250 µl cold RIPA buffer. Samples were split into two tubes before being ribolysed… Glass beads were removed by centrifugation into a fresh Eppendorf tube and sample volume increased to 500 µl. Each sample was then sonicated using a stick sonicator three times for 10 secs at 20% with a 30 secs rest on ice between each round. 1 µl of benzonase was added to each sample and incubated on ice for 1 hr before centrifugation at 16,000 x g for 10 mins at 4 °C. Supernatant was transferred into a fresh Protein LoBind Eppendorf tube and Bradford was conducted to determine protein concentration of each sample. Samples were pre-cleared by incubation with sepharose beads for 2 hours prior to binding. 3 mg of total protein was then incubated with 50 µl Streptavidin sepharose beads (pre-washed 3x in cold RIPA buffer) in a final volume of 1 ml RIPA buffer (SDS concentration increased to 0.4%). Beads were then washed for 5 mins at RT with gentle rotation and beads separated from supernatant by centrifugation at 800 x g for 3 mins in the following buffers: 1x wash buffer; 3x RIPA buffer + DTT; 5x 20 mM ammonium bicarbonate. 50 µl SDS protein loading buffer (with added *d*-Desthiobiotin to a final concentration of 2.5 mM) was added to the beads and boiled at 95 °C for 10 mins before cooling at RT for 10 mins.

2.10.3 FASP Protocol

Beads were separated from supernatant as before and 50 µl of the eluate was added to 333 µl of FASP Urea Solution (plus DTT, 30 mM) and transferred to a Microcon Y M-30 (Millipore, 42410) filter unit. Filter units were centrifuged at 14,000 x g for 15 min followed by addition of another 200 µl FASP Urea solution (plus DTT, 30 mM) and centrifuged again. Flow through was discarded before addition of 100 µl FASP IAA solution to each filter unit and incubation at RT for 20 mins followed by centrifugation as before. Filter units then received 100 µl FASP Urea solution (plus DTT, 30 mM) before centrifuging as before (this step is repeated twice for a total of three times). Flow

through was discarded and 100 µl ABC buffer was added to each filter unit before centrifuging at 14,000 x g for 10 mins (this step is repeated twice for a total of three times). Flow through was discarded and 40 µl digestion solution was added to each filter unit and incubated overnight in a wet chamber. Filter units were transferred to fresh collection tubes and centrifuged at 14,000 x g for 10 mins. Following this 40 µl ABC buffer was added and centrifuged again in the same conditions.

2.10.4 Desalting of Peptides with Stage Tips

Acidify the filtrate from the FASP digestion by addition of 100 µl Buffer A*. Spin columns containing 8 mg C-18 resin (Pierce, 89870) were activated by addition of 100 µl 50% methanol and centrifuged at 1,500 x g for 1 min, and flow through discarded (repeat once for a total of two times). Spin columns were then equilibrated twice by addition of 200 µl Buffer A and centrifuged as before discarding the supernatant after each spin. Each samples was then added to a spin column and centrifuged as before. 200 µl Buffer A was then added to each filter unit to wash and desalt the peptides and centrifuged again at 1,500 x g for 1 min (repeat once for a total of two washes).

2.10.5 LC-MS/MS Run & Analysis

LC-MS/MS was conducted by Benno Kuropka at the Freie Universität Berlin briefly as follows. Peptides were eluted by addition of Buffer B into a fresh Protein LoBind Eppendorf tube by centrifuging for 10 min at 1,500 x g. Samples were then concentrated to 1-2 µl in a vacuum concentrator before reconstitution by addition of 15 µl Buffer C and strong vortexing for >30 sec. Peptides were sorted using the Ultimate 3000 NCS-3500RS NanoLC (Thermo Scientific). 7 µl of a 1:10 dilution of each sample was injected for each LC-MS/MS run onto Acclaim PepMap100 C-18 trap columns (75 µm i.d. x 20 mm, 100Å nanoViper, Thermo Scientific 164535). Peptides were eluted on Acclaim PepMap RSL C-18 analytic columns (75 µm i.d. x 500 mm, 100Å nanoViper, Thermo Scientific 164942) before analysis using an Orbitrap Velos (Thermo Scientific) mass spectrometer. Raw data files were then processed by Murat Eravci using the MaxQuant software package.

Chapter 3 – System to Investigate Homologous Recombination Restarted Replication Forks

3.1 Introduction

The *RTS1* (Replication Termination Sequence 1) replication fork barrier (RFB) is polar in nature, only blocking replication forks travelling from a single direction (Dalgaard and Klar, 2001). The *RTS1* sequence contains binding sites for the trans-acting factor Rtf1, whose binding is necessary for barrier activity and fork arrest (Eydmann et al., 2008). When forks stall at *RTS1*, single stranded DNA (ssDNA) is produced which is rapidly coated by RPA. Rad52 can then stimulate Rad51 to replace RPA to form a Rad51-nucleofilment which is able to perform homology search and strand invasion (Lambert et al., 2010). Replication forks stalled at *RTS1* have been shown to be resolved independently of break induced replication (BIR) in a recombination-dependent manner using template exchange mechanisms of repair (Lambert et al., 2010, Mizuno et al., 2009). Lambert, et al., (2010) also implicated the homologous recombination (HR) restart of replication forks in the absence of a DSB to lead to gross chromosomal modifications due to template exchange. Although Rad51 is essential for restart of replication forks by HR it was non-essential when template exchange is used for restart (Ahn et al., 2005, Lambert et al., 2010). However, resolution of *RTS1* by both HR-restart and template exchange are dependent on Rad52. The HR-restarted RF also leads to replication slippage in the DNA (Iraqui et al., 2012) and results in gross chromosomal rearrangements when forks stall in the context of inverted repeats (Mizuno et al., 2009, Mizuno et al., 2013).

During canonical DNA replication, the leading strand is replicated by Polymerase ε (Polε) and the lagging strand is replicated by Polymerase δ (Polδ) (Miyabe et al., 2011). Conversely, the Carr lab has recently shown that forks restarted at *RTS1* replicate both the leading and lagging strand using Polδ (Miyabe et al., 2015). However, the precise mechanisms of restart as well as the dynamics of the restarted replication fork are still unknown. Here, I describe a system optimised to study specifically the restarted

replication fork to allow investigation of the components that contribute to its dysfunction.

3.2 Results

3.2.1 Ribosomal Replication Fork Barriers Delay Replication Fork Progression Without δ/δ Restart

The ability to investigate HR-restarted replication forks (RFs) at the *RTS1* RFB is hindered by canonical replication forks travelling from the opposite direction. Our previous system to study restarted RFs had a clear drawback due to the restarted RF terminating shortly after restart at *RTS1*. This hindered the ability to clearly distinguish the ratio of convergent canonical RF and restarted RF in the region downstream of the *RTS1* barrier. In order to allow investigation of the restarted replication fork with minimal interference from the oncoming canonical replication fork, more time is needed to allow forks to restart. Several genomic loci were selected from Pu-Seq data as regions of unidirectional replication due to them being a transition zone between an early and late replicating region (Figure 3.1). To delay the oncoming convergent RF and create a region replicated by only the *RTS1* restarted RF, we used repetitions of the ribosomal replication fork barrier (rRFB) sequence, *TER2/3*. Similar to *RTS1*, rRFBs are uni-directional, only blocking RFs travelling in one direction. However, fork arrest at rRFBs are Rtf1 independent and do not result in gross chromosomal rearrangements or require HR to restart in δ/δ dependent manner as at *RTS1* (Krings and Bastia, 2004, Mizuno et al., 2013, Sanchez-Gorostiaga et al., 2004).

First, in order to establish the extent of delay rRFBs have on replication forks, Polymerase-Usage Sequencing (Pu-Seq) was conducted on constructs containing differing numbers of repeats of the rRFB sequence. Either 3x rRFB or 10x rRFB, were inserted at two of the loci identified as being a transition zone between early and late replicating regions on different chromosomes (Chr I and II) near the efficient early firing

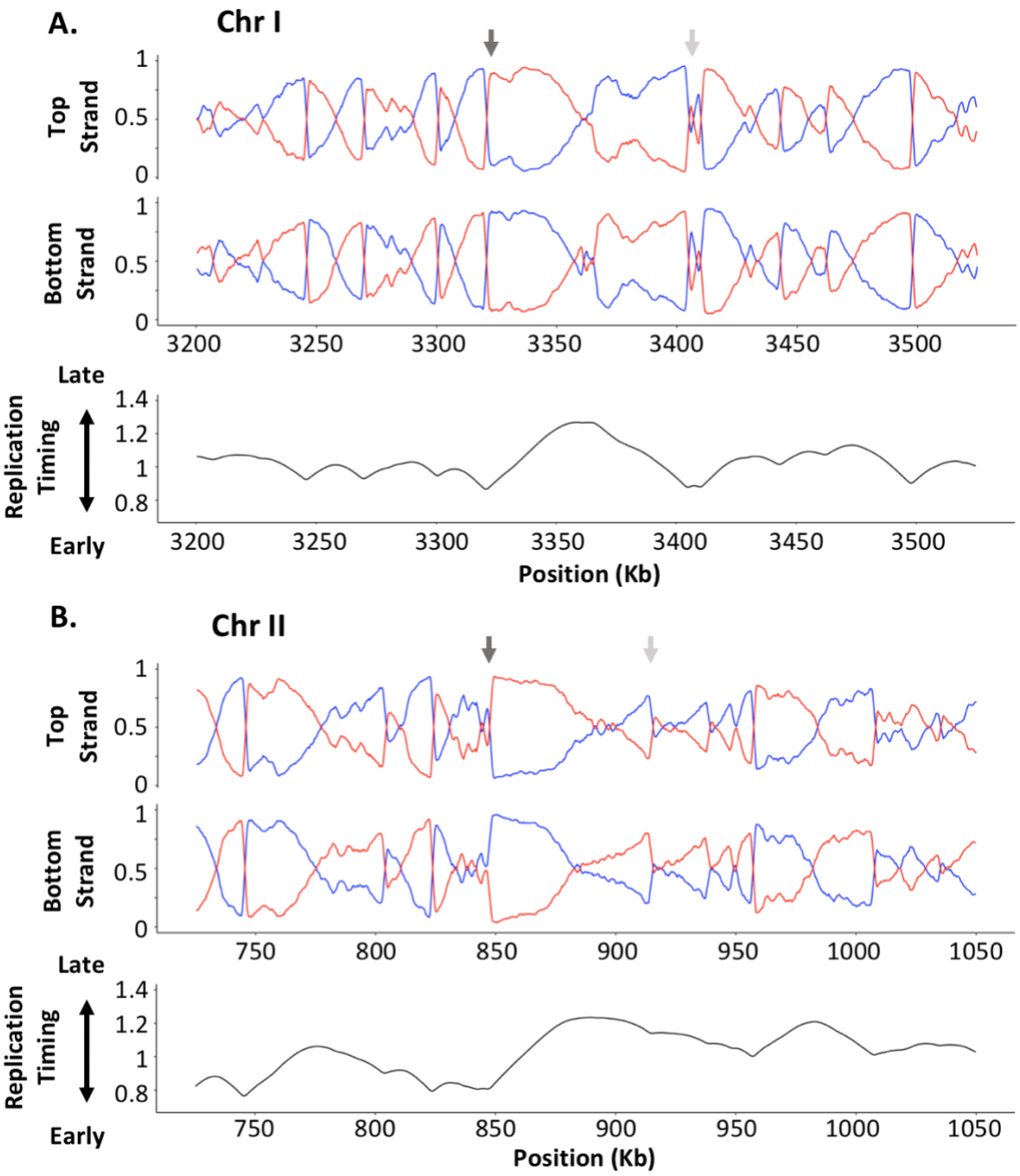

Figure 3.1. Genomic Loci Selected for Insertion of the *RTS1* RFB. Polymerase usage across regions on **A.** Chr I and **B.** Chr II. Location of the early efficient origin (dark grey) and the downstream distal origin (light grey) are indicated. Ratio of Polymerase usage for both the top and bottom strand is shown: The red trace represents Polymerase ε usage and the blue trace represents Polymerase δ usage. The lower black trace represents estimates of the replication timing profiles across the regions obtained using a uniform fork velocity and fork directionality calculated using the Pu-Seq data (*see Section 1.3.5*). Low values indicate early replicating regions, and high values indicate late replicating regions.

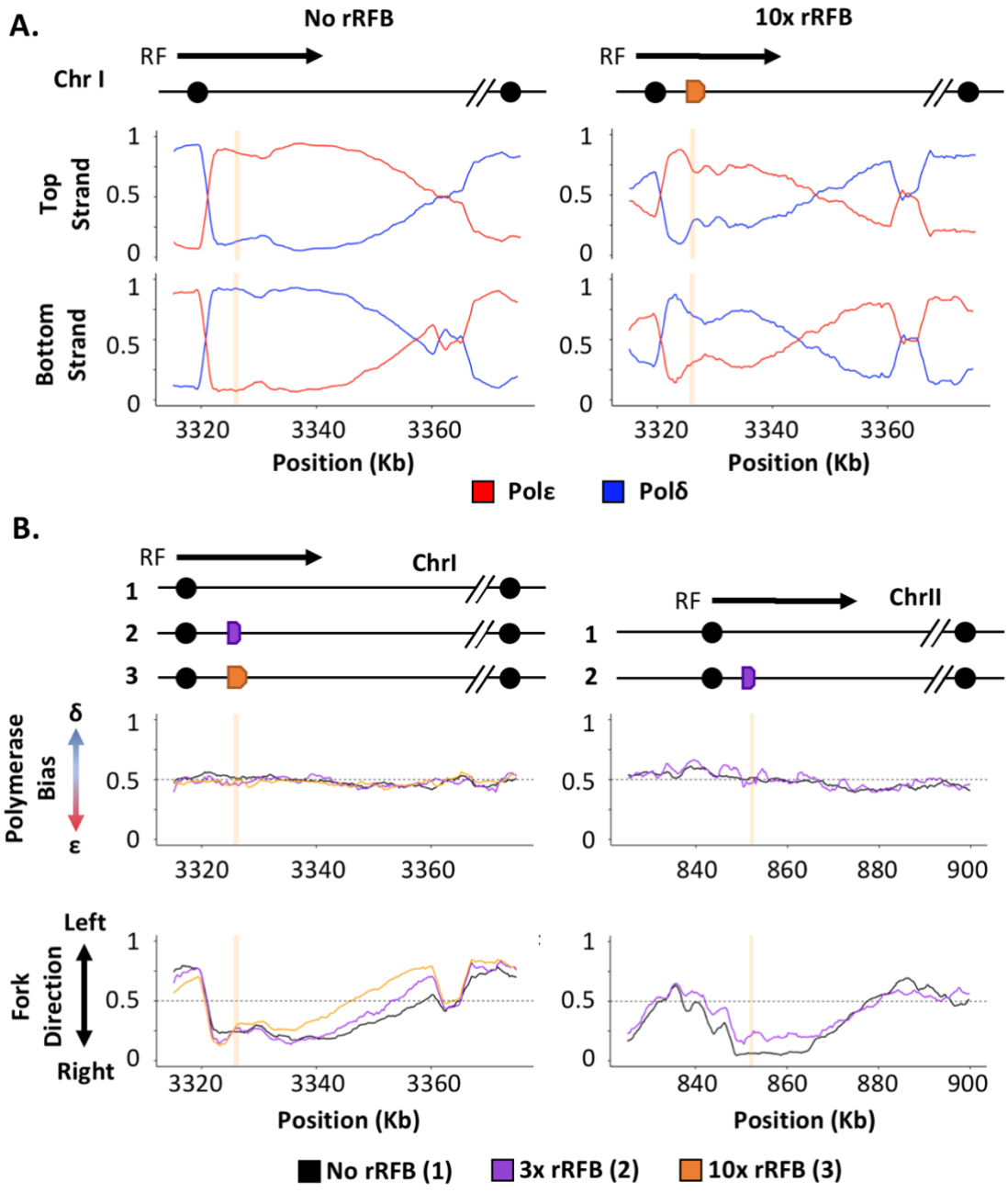

Figure 3.2. Ribosomal Replication Fork Barriers Delay Replication Fork Progression Without δ/δ Restart. A. Polymerase usage across a region on Chr I with and without 10x rRFB's inserted. Ratio of Polymerase ε (red) and Polymerase δ (blue) for both the top and bottom strand is shown. **B.** No (black), 3 (purple), or 10 (orange) rRFB's placed next an early firing origin on different chromosomes, Chr I (*left panel*) and Chr II (*right panel*). Top graphs: polymerase bias across the regions (ratio of polymerase usage across both DNA strands). Bottom graphs: direction of replication fork movement calculated from the Pu-Seq data.

origin. The barriers were placed in the orientation blocking forks travelling from the origin (rightward travelling RFs) (Figure 3.2). In our control (no rRFB), RF is fired from the strong early firing origin (left black circle on the schematic) and DNA is replicated by Polε in the leading strand (top strand) and Polδ in the lagging strand (bottom strand) (Figure 3.2A, *left panel*). Assuming canonical replication this indicates a predominantly rightward moving replication fork. Addition of rRFBs slows this rightward moving replication fork allowing convergent replication forks to travel further in a leftward direction, thus increasing the ratio of δ/ε on the top strand and equivalently decreasing it on the bottom strand downstream of the rRFB's (Figure 3.2A, *right panel*). Fork direction can be calculated using this rational and depicted in a graph whereby a high value (low Polε on top strand – lagging strand replication) indicates a leftward moving replication fork, and a low value (high Polε on top strand – leading strand replication) indicates a rightward moving replication fork (Figure 3.1B, *bottom panel*). Insertion of rRFBs (3x and 10x) at both genomic loci increase the amount of leftward moving forks downstream of the rRFBs in comparison to no rRFB. This increase is larger for 10x rRFB than 3x rRFB on Chromosome I indicating a delay in replication fork movement from the efficient early firing origin with increasing numbers of rRFB's (Figure 3.2B).

Taking total polymerase usage together for each construct, the ratio of polymerase usage between the two DNA strands produced no polymerase bias downstream of the region (Figure 3.2B, *top panel*). This confirms that these barriers do not produce the same δ/δ restart that has been reported for restart at the *RTS1* RFB. Thus, these barriers are efficient for delaying replication forks while maintaining canonical division of labour between Polymerase ε/δ during replication.

3.2.2 Replication Fork Restart at RTS1 Results in δ/δ Replication

In order to study the HR-restarted replication fork without interference from converging canonical replication forks, previously published *RTS1* system has been placed in a region of the genome next to an early firing origin with a distant late firing origin downstream (Figure 3.3A). Thus, the predominant orientation of replication in this region is in a rightward direction, as the exact same locus has been used as with the rRFB

constructs (Figure 3.2). The *RTS1* sequence has been inserted in the orientation blocking RFs originating from the early firing origin, but permissive to those originating from the late firing origin. Additionally, having established the use of rRFBs as a suitable means to delay replication fork progression, 10x rRFB sequence were placed ~10 Kb downstream, in the orientation blocking RFs originating from the late firing origin. Previous work conducted by the Carr lab established positioning of the rRFBs 3 Kb downstream of *RTS1* to be suboptimal for creating a region replicated by only the restarted replication fork. Additionally, positioning of the rRFBs further downstream (10+ Kb) increases the chance for additional origins to be fired between the rRFBs and *RTS1*, thus hindering the analysis of the restarted replication fork. Altogether, this system increases the time available for replication forks blocked at *RTS1* to restart and replicate the DNA downstream. In this system, the *RTS1* barrier activity is controlled by the presence/absence of Rtf1 (*rtf1*$^{+}$ = ON, *rtf1***Δ** = OFF) with the differences in RF movement depicted in the schematic (Figure 3.3B).

Regions replicated downstream of replication fork stalling and restart at *RTS1* have previously been shown to switch from Polymerase ε to Polymerase δ usage for leading strand replication (Miyabe et al., 2015). To confirm this observation, Polymerase Usage Sequencing (Pu-Seq) was carried out in strains containing the *RTS1* construct, both with (RFB ON) and without *rtf1* (RFB OFF) (Figure 3.4A). When *RTS1* is OFF (*rtf1***Δ**) the region to the right of the early firing origin is replicated by Polε on the top strand and by Polδ on the bottom strand. Taking into consideration Polε is the leading strand polymerase of canonical replication forks, this confirms the predominant direction of replication to be carried out by a rightward moving fork, as is the case when no RFB is present (Figure 3.2). When *RTS1* is ON (*rtf1+*) there is an abrupt switch to Polδ usage on the top strand at the point at which *RTS1* has been inserted. I observed this switch at two distinct genomic loci on two separate chromosomes (Chr I and II) where we inserted the *RTS1* barrier. Small dips in the Pu-Seq profiles of Chr I at *RTS1* are due to the native *RTS1* sequence still being present in these strains, resulting in mis-mapping of some reads in this short region. Additionally, analysis of the raw Pu-Seq reads confirmed the Polδ usage calculated on each strand after restart at *RTS1* was not solely due to loss of Polε usage, but indeed gain of Polδ reads mapping to the top strand. These results confirm

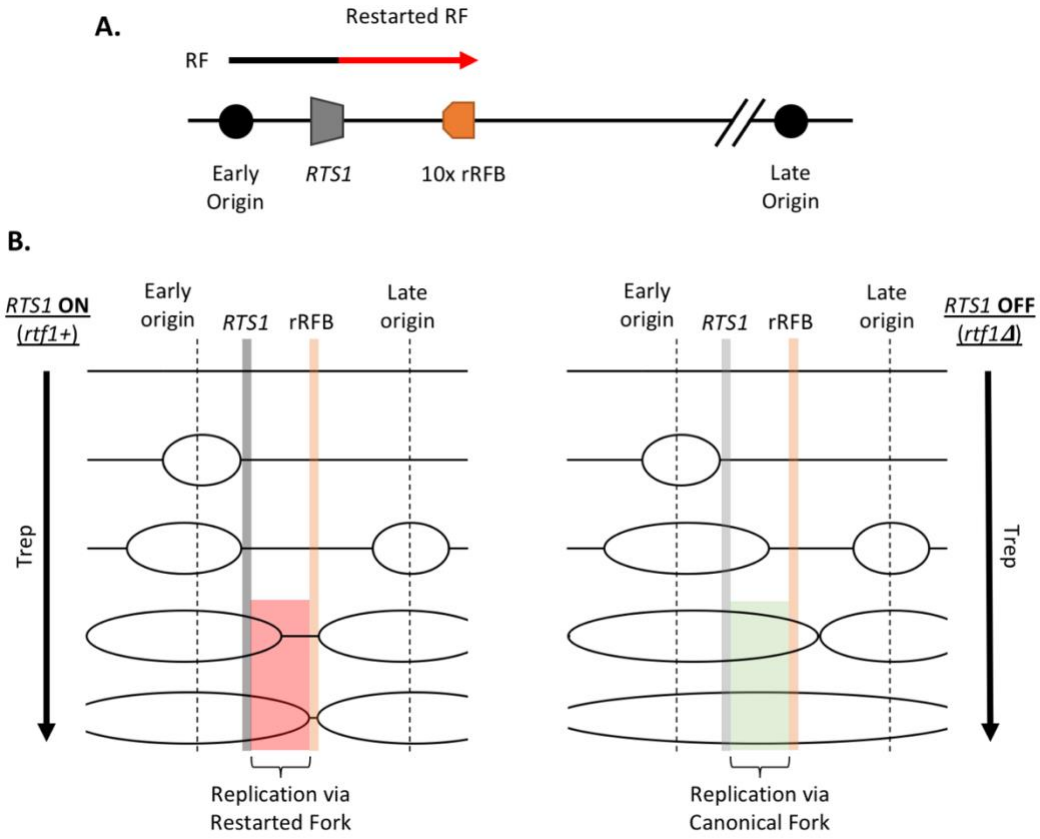

Figure 3.3. RTS1 System to Investigate Replication Fork Restart Using Homologous Recombination. A. The *RTS1* sequence (grey box) inserted between an early and a late firing origin of replication with 10 ribosomal replication fork barriers (10x rRFB, orange box) 10 Kb downstream. Predominant direction of replication is shown with canonical (black) and restarted replication forks (red) indicated. **B.** Graphical visualisation of the movement of replication forks radiating from the early and late firing origins flanking the *RTS1* construct. Direction of replication timing (Trep) is indicated by the black arrows. Left panel: When *RTS1* is active (ON) by binding of the Rtf1 protein, the early firing origin fires first getting blocked by the *RTS1* RFB. Subsequent firing of the late firing origin gets blocked by the 10x rRFB allowing enough time for *RTS1* blocked forks to restart and replicate the downstream region without interference from the canonical RF. Right panel: When *RTS1* is inactive by absence of Rtf1 (*rtf1***Δ**), the RF from the early firing origin does not block at *RTS1* and replicates the downstream region with a canonical RF.

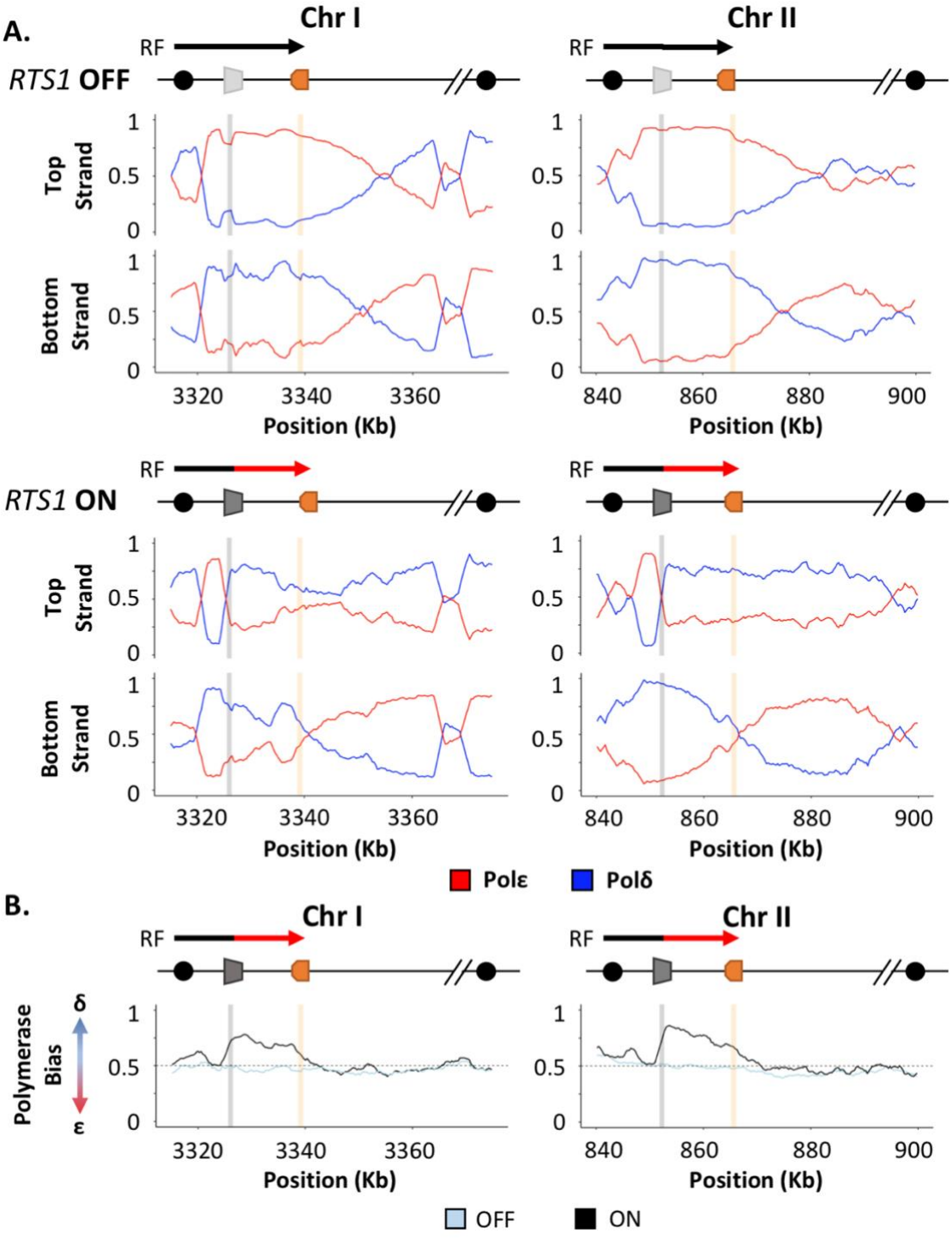

Figure 3.4. Replication Fork Restart at RTS1 RFB Results in δ/δ Replication. A. Polymerase usage at *RTS1* RFB on Chr I (left panel) & II (right panel); *RTS1* OFF (top panel) and ON (bottom panel). Ratio of Polymerase ε (red) and Polymerase δ (blue) for both the top and bottom strand is shown. **B.** Polymerase bias graph calculated using the ratio of polymerase usage across both strands at the *RTS1* RFB; *RTS1* ON (black) and OFF (light blue).

previous evidence that Polε is no longer used in replication forks restarted at *RTS1*. This is further supported by calculation of the ratio of polymerase usage across both strands showing a clear Polymerase δ bias downstream of active *RTS1* (Figure 3.4B). This provides a distinct genomic region where the majority of replication is carried out by a HR-restarted replication fork.

3.2.3 System to Investigate Protein Involvement in the Restarted Replication Fork

Establishment of a system to study HR-restarted replication forks with little interference from canonical replication forks allows to clearly distinguish between the restarted and canonical RF. In contrast to the canonical RF, the restarted replication fork is more error-prone and conducts replication of the leading and lagging strand using Polymerase δ. Previously, it has been shown that the error-prone nature of the restarted replication fork was not due solely to the use of Polymerase δ replicating both strands (Miyabe et al., 2015). This suggests other aspects of the restart or the restarted RF contribute to its error-prone nature. To investigate proteins associated with the replication fork, Chromatin Immunoprecipitation (ChIP) followed by quantitative PCR (qPCR) can be conducted. To be able to follow recruitment of proteins in the cell cycle, cells are synchronised in G2 using the *cdc25_22* loss of function temperature sensitive allele that inhibits entry into mitosis (Figure 3.5A) (Russell and Nurse, 1986). Cells are synchronised by a temperature shift to the restrictive temperature (36 °C) for 4 hrs, followed by release into the permissive temperature (25 °C) for sample collection every 15 mins. Cells start to go through S phase from 75 mins after release as evident from the appearance of septum's which correlates to the onset of S phase (Figure 3.5B). Additionally, FACS profiles show an equivalent shift toward 2X 2C DNA content indicating onset of S phase (Figure 3.5C). This is due to the *S. pombe* cell cycle involving a short G1 phase resulting in S phase starting before cell division has completed and manifesting in FACS profiles indicating 2X 2C DNA content rather than the expected 1X 2C. Bulk S phase is completed by 120 mins, with all cells finished by 135 mins. FACS profiles were taken for each repeat with Figure 3.5C showing a representative profile.

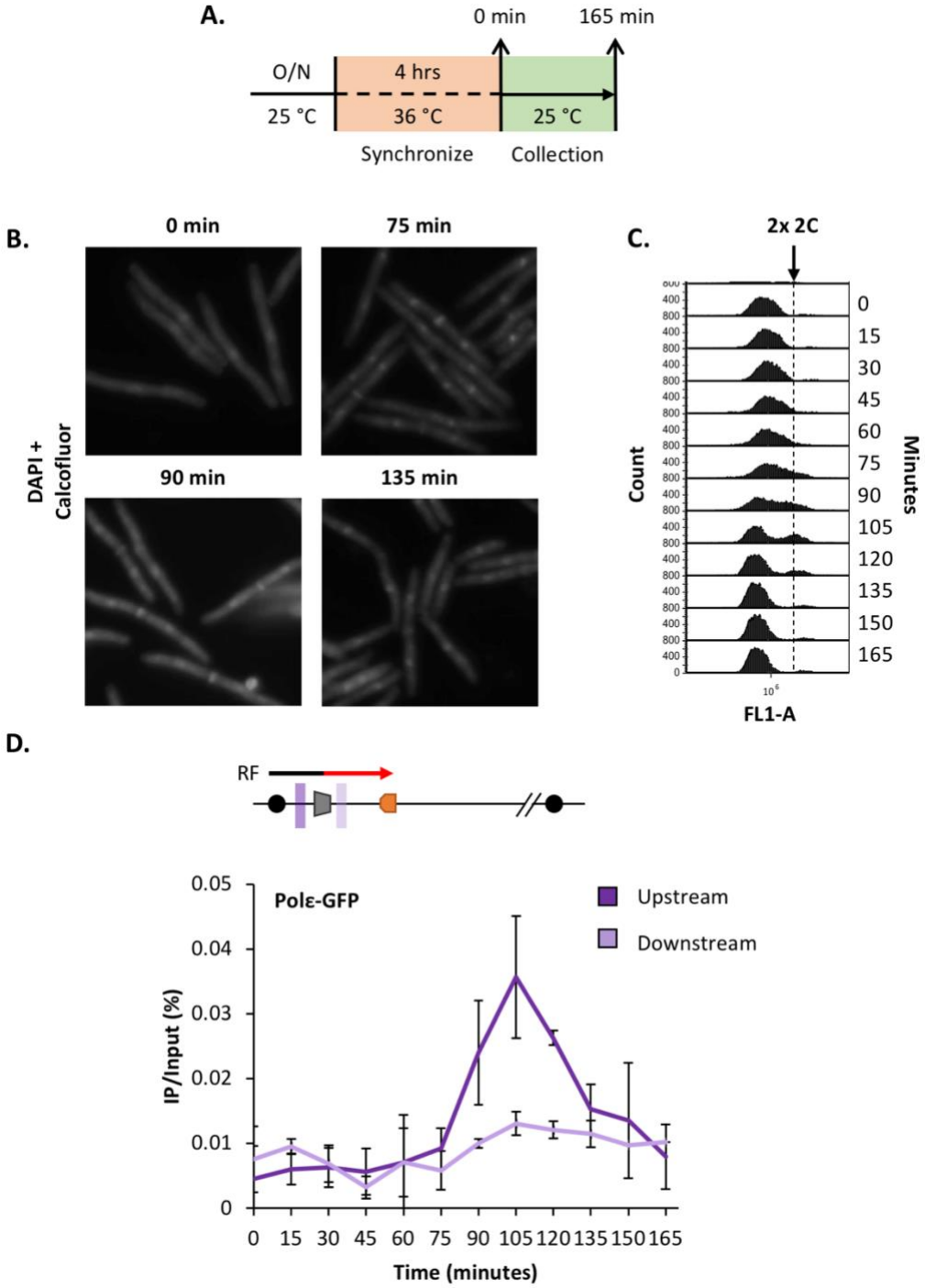

Figure 3.5. Loss of Polymerase ε enrichment Downstream of Active RTS1. A. Cells containing the temperature sensitive *cdc25_22* allele were grown overnight at the permissive temperature 25 °C, blocked in G2 at the restrictive temperature 36 °C, then released into 25 °C and samples collected every 15 mins. **B.** Cell images of Polε-GFP containing cells synchronised using *cdc25_22* stained with DAPI (DNA) & calcofluor (septum) at indicated times after release from G2. **C.** FACS profile of cells collected at indicated times after release from G2. **D.** Enrichment of Polε-GFP 100 bp upstream and downstream of active *RTS1* using Chromatin Immunoprecipitation (ChIP) followed by quantitative PCR (qPCR). Data from three independent experiments ± SEM.

Where necessary, time points were adjusted to align according to S phase entry to allow visualisation of ChIP-qPCR analysis in cells synchronously progressing through S phase.

Polymerase δ is used to replicate both DNA strands downstream of active *RTS1*. This suggests Polymerase ε is no longer associated with the restarted replication fork. Direct comparison in protein enrichment between the canonical vs. HR-restarted replication fork can be tested using primer sets that anneal 100 bp upstream or downstream of the *RTS1* sequence, respectively. ChIP-qPCR analysis of GFP-tagged Polymerase ε show accumulation upstream (canonical RF) of the *RTS1* RFB as the cells enter S phase (Figure 3.5D). This enrichment is detectable for ~30 mins, supporting data that replication forks take between ~15-20 mins to restart at *RTS1* (Miyabe et al., 2015, Mohebi et al., 2015). The signal is detectable for slightly longer than this time due to slower cell growth at 25 °C than at 30 °C (the temperature used to grow cells in the published experiments) and synchrony not being 100% when using the *cdc25_22* allele. Additionally, enrichment of Polymerase ε 100 bp downstream of *RTS1* (restarted RF) is completely lost to background levels. This suggests, that not only does Polymerase ε not conduct leading strand replication in the restarted replication fork, it may also be lost from the reconstituted replisome. Although, further experiments would be needed to confirm this observation. Comparison of these results to those obtained from cells lacking *RTS1* barrier activity would highlight the differences in polymerase enrichment when *RTS1* is on. Additionally, the use of a no antibody control or probing with qPCR primers for another distal locus not associated with *RTS1* would enable better quantification of the reduction in Polε enrichment downstream of *RTS1* when the barrier is on.

To improve cell synchrony, the *cdc2as_M17* ATP-analogue sensitive allele can be used to synchronise cells in G2 (Aoi et al., 2014). Cells grown in media containing the ATP-analogue 3BrPP1 for 3 hrs arrest in G2, and are released upon filtration, washing, and release into 3BrPP1 free media (Figure 3.6A). In comparison to *cdc25_22* allele, this method of synchronisation results in less elongation of cells and better cell synchrony upon release as evident from images of cells stained with DAPI (visualise DNA) and calcofluor (visualise septum), as well as tighter FACS profiles. Additionally, cells are able to grow at 28 °C, thus progress through the cell cycle at a rate comparable to WT cells.

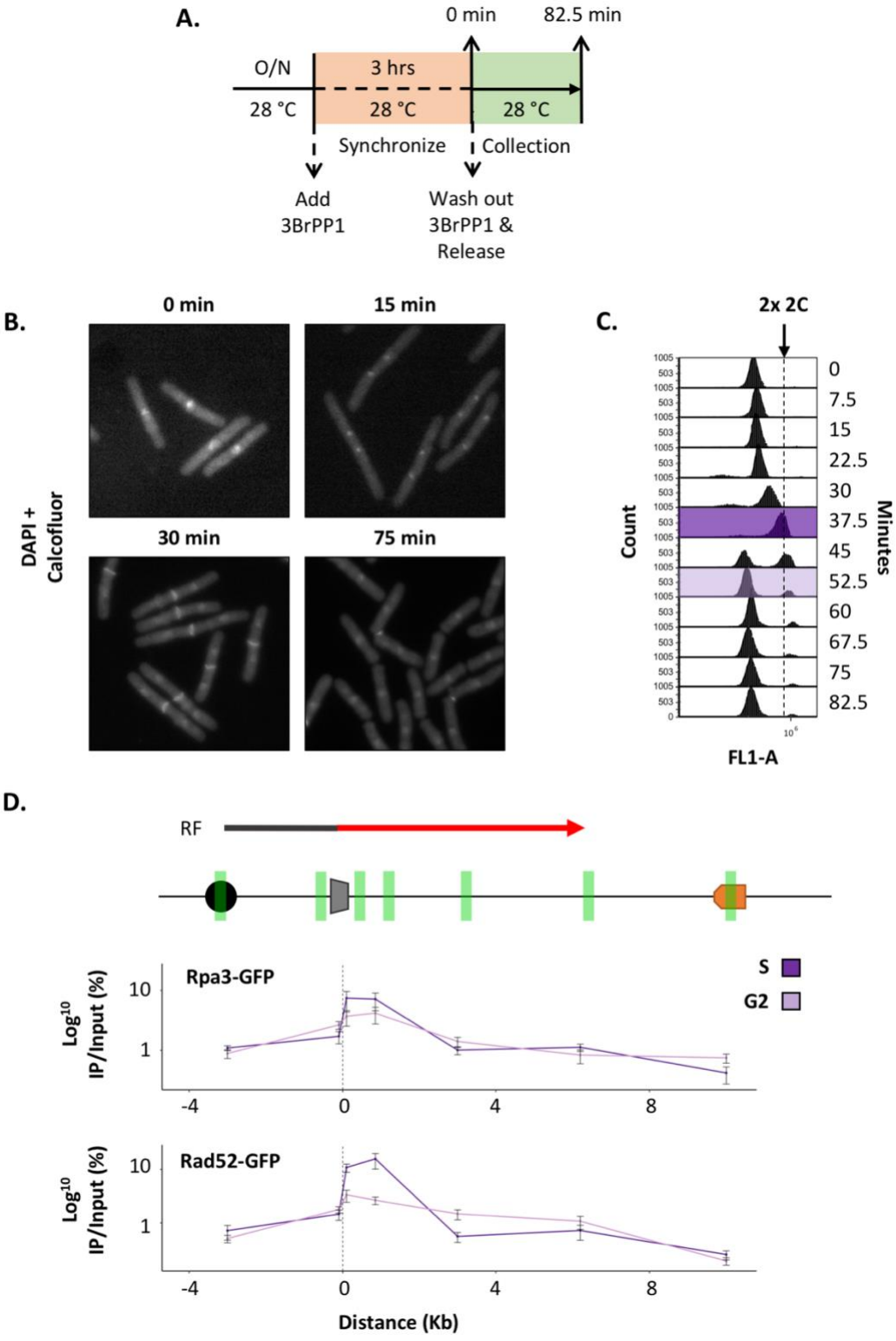
A.
0 min
82.5 min
O/N
3 hrs
28 °C
28 °C
28 °C
Synchronize
Collection
Add
3BrPP1
Wash out
3BrPP1 &
Release
B.
0 min
15 min
30 min
75 min
DAPI +
Calcofluor
C.
2x 2C
Count
Minutes
0
7.5
15
22.5
30
37.5
45
52.5
60
67.5
75
82.5
FL1-A
D.
RF
Rpa3-GFP
S
G2
Log10
IP/Input (%)
10
1
-4
0
4
8
Rad52-GFP
Distance (Kb)

Figure 3.6. (previous page) ssDNA Binding Proteins are Enriched Downstream of Active RTS1 During S Phase. A. Cells containing the ATP sensitive allele *cdc2as_M17* are grown overnight at 28 °C and synchronised for 3 hrs in G2 by addition of the ATP analogue 3BrPP1. Cells are washed by filtration, released into fresh media and samples collected every 7.5 mins. **B.** Cell images of *cdc2as_M17* synchronised cells stained with DAPI (DNA) and calcofluor (septum) at indicated times after release from G2. **C.** FACS profile of cells collected at indicated times after release from G2. S (dark purple) and G2 (light purple) phase samples used for ChIP-qPCR analysis are indicated. **D.** Enrichment of Rpa3-GFP (*top graph*) and Rad52-GFP (*bottom graph*) across the region containing active *RTS1* on Chr II using ChIP-qPCR. Numbers indicate the distance from *RTS1* of the primer sets used, with approximate positions represented on the schematic by green boxes. Data from three independent experiments ± SEM.

This is evident by peak of septation (30 mins after release) correlating with the FACS profile moving towards 2x 2C and the bulk DNA synthesis being completed in ~15 mins (Figure 3.6B-C).

As it has been shown before the replication fork restart generates single stranded DNA (ssDNA) in order to facilitate homologous recombination (HR). To follow ssDNA formation in the *RTS1* RFB system set up on Chromosome II, GFP tagged versions of the ssDNA binding proteins, Rpa3 (RPA subunit) and Rad52, were analysed by ChIP-qPCR. In order to investigate changes in ssDNA accumulation, both temporally and spatially across the *RTS1* region, an S and G2 phase time points were subjected to qPCR analysis using a variety of primer pairs placed upstream and downstream of the RFB (Figure 3.6D). Rad52-GFP and Rpa3-GFP become enriched up to ~1 Kb downstream of *RTS1* in S phase. This enrichment is reduced after 30 mins when the majority of cells have entered G2. This is in agreement with previous studies showing Rad52 recruitment to *RTS1* to occur within minutes of replication fork stalling (Nguyen et al., 2015). This is also in support of recombination intermediates remaining visible for up to 45 mins after RF stalling at *RTS1* (Mohebi et al., 2015).

3.3 Discussion

An optimised system to study HR-restarted replication forks by utilising the *RTS1* RFB has been constructed (Figure 3.2). Positioning of *RTS1* near an early firing origin with downstream rRFBs and a distant late firing origin form a region of over 10 Kb that is replicated by the restarted replication fork with little interference from convergent canonical replication forks. The use of 10 repeats of the rRFB sequence provides adequate delay to the convergent replication fork without producing a HR-restarted RF (Figure 3.1). Mathematical modelling of this data suggests the 10x rRFBs to delay replication fork progression by ~6 min (Eduard Campillo-Funollet, unpublished data) providing the additional time needed for use in the *RTS1* RFB system. Polymerase-Usage Sequencing of the optimised *RTS1* system shows a clear switch to Polymerase δ replication in leading strand replication (on the top DNA strand), providing a ~10 Kb region downstream of the *RTS1* RFB that is replicated almost completely by the restarted replication fork, as evident from the large Polymerase δ bias when the *RTS1* RFB is ON (Figure 3.3). Moreover, we can see that the restarted RF does not switch back to δ/ε configuration of RF and terminates with the convergent canonical RF.

Establishment of a system containing a region that is specifically replicated by HR-restarted RFs, allowed further investigation into the dynamics of both the restart and the restarted RF. In order to study the dynamics of different protein factors at *RTS1* both spatially and temporally, cells were synchronised in G2 using two different alleles (*cdc25_22* or *cdc2as_M17*). Both alleles were adequate in studying protein enrichment in this system. The *cdc2as_M17* allele appeared optimal due to the increased synchrony of cells, and cell size and growth rate being closer to WT (Figure 3.5BA-C). ChIP-qPCR of Polε-GFP revealed enrichment upstream of active *RTS1* when the replication fork is canonical but not downstream in the restarted replication fork (Figure 3.4D). This is consistent with the Pu-Seq analysis of the *RTS1* region showing a loss of Pol ε usage once the RF stalled at *RTS1* has restarted. Having demonstrated the developed system to work, this can now be exploited in more detail and pave the path to study recruitment of other molecular factors involved in the restarted/canonical RFs, such as helicases (CMG, Psf1, Fml1, Mgs1).

The same *RTS1* construct allowed us to investigate the recruitment of ssDNA binding proteins, RPA and Rad52, during restart. Time points enriched for S phase cells were chosen for in depth analysis at different distances upstream and downstream of *RTS1* using qPCR primers that target these regions (Figure 3.5). Large increases in enrichment of both ssDNA binding proteins, RPA and Rad52, is observed up to 1Kb downstream of *RTS1* when the barrier is ON. Both also show only slight enrichment immediately upstream of *RTS1* in S phase (compared to 3kb upstream), suggesting little fork reversal during *RTS1* restart in this system. However, this is contradictory to reports using a similar system at a different genomic locus that observes resection upstream of the *RTS1* site (Tsang et al., 2014). This could be due to fork reversal occurring prior to downstream unwinding of DNA. Therefore, analysis of an earlier time point (containing early S phase cells) may reveal increased ssDNA accumulation upstream of *RTS1*. Alternatively, in the previous *RTS1* system, convergent forks arrive nearer to the barrier and may cause increased steric torsion pushing the restarting RF into reversal and resulting in more robust resection. Additionally, no enrichment of ssDNA is observed at the rRFB's. This is unexpected due to the Pu-Seq analysis suggesting termination of replication in this region (Figure 3.3A). Either, the levels of termination occurring in this region are below detectable levels, or the termination of a non-canonical and canonical replication fork does not produce large amounts of ssDNA. Nevertheless, it has been shown that Rad51 participates in the termination of restarted and canonical RFs (Lambert et al., 2005).

Comparison of S phase cells with a later time point containing mainly cells that have completed S phase and entered G2 phase (Figure 3.5), reveals a decrease in both ssDNA binding protein enrichment downstream of *RTS1*. However, G2 cells appear to have slightly increased Rad52 enrichment further downstream of *RTS1* (~3Kb) compared to S phase cells that is not observed with RPA. This Rad52 enrichment may reflect few late S phase cells persisting in this population that still contain unresolved ssDNA. Pu-Seq on Polymerase α (Polα) usage at *RTS1* in this system shows a clear reduction in usage for replication priming on the lagging strand when *RTS1* is ON (Naiman et al., 2020). This suggests persistence of ssDNA on the bottom strand that is later replicated in a continuous manner. Thus, the late Rad52 enrichment may reflect ssDNA on the bottom

strand (lagging strand) that is initially protected by RNA:DNA hybrids and later replaced by RPA and Rad51.

Taken together, the construction of this novel *RTS1* system provides a universal tool for studying restarted replication forks. This has shown a long-range recruitment of Rpa3 and Rad52 downstream of the *RTS1* barrier. On top of this, it will solve the question concerning the presence/absence of helicases or other molecular factors possibly involved in the restarted replication machinery. Thus, this approach can reveal factors underpinning the error-prone nature of the restarted replisome.

Chapter 4 – Interaction of PCNA and Cdc27^{Pol32} During Replication Fork Restart

4.1 Introduction

Break-induced replication (BIR) is a process that has been suggested to be used as the repair of single-ended DSBs (seDSBs) using strand invasion mechanisms to copy a homologous template in order to restart stalled or collapsed replication forks (McEachern and Haber, 2006). In contrast to HR-dependent restart at *RTS1*, BIR occurs outside of S phase and is not terminated by an incoming fork. In addition, BIR progresses via a D-loop and is therefore conservative, whereas HR-dependent restart at *RTS1* is semiconservative, implying the D-loop is rapidly resolved. Induction of BIR can lead to multiple cycles of detachment and reattachment of the nascent strand that result in chromosome rearrangements when this occurs between repetitive sequences (Smith et al., 2007). Furthermore, BIR has been shown to induce high levels of mutations along the entire length of the DNA that the restarted fork replicates (Deem et al., 2011). BIR has been shown to require the Pol32 subunit of Polδ (homologue of Cdc27 in fission yeast) which is dispensable when the break is a deDSB and uses homologous recombination for repair (Lydeard et al., 2007). Given the distinctions between BIR and HR-dependent restart at *RTS1*, we wished to examine the role of Cdc27 at *RTS1*.

Pol32 is non-essential in *S. cerevisiae* (Gerik et al., 1998), but the *S. pombe* homologue is essential (Bermudez et al., 2002) making function of this protein difficult to test in fission yeast. In budding yeast Pol32 directly binds to PCNA and stabilises the Polδ multi-subunit complex. Previously, two PCNA mutants have been identified which exhibit BIR deficiency even in the presence of WT Pol32 (Lydeard et al., 2010) and which are epistatic to loss of Pol32. The original point mutants in *S. cerevisiae* were R80A and F248A F249A. R80A resides on the α-helices lining the hole of PCNA, where the molecule interacts with DNA (McNally et al., 2010). F248 and F249 are highly conserved residues among PCNAs, and reside as sidechains on the interdomain connector loop buried inside the structure of PCNA (Eissenberg et al., 1997). F249 is partially exposed in a pocket where PIP-box containing proteins interact with PCNA. In *S. pombe*, the Carr lab have

successfully created the R80A mutant, and a single point mutant F248A (Thomas Etheridge). I subsequently constructed the double point mutant F248A Y249A which resulted in a large decrease in cell viability. The interaction between PCNA and Pol32 can also be studied in fission yeast using truncated versions of Cdc27 (*cdc27_D1* & *cdc27_D3*) that lack the PCNA binding motif at the C terminus of the protein (Tanaka et al., 2004). Although deletion of Cdc27 (*S. cerevisiae* Pol32 homologue) is lethal in *S. pombe*, the truncated Cdc27 alleles and PCNA mutants can be used to investigate the role of this protein and its interaction with PCNA in RF restart at *RTS1*.

4.2 Results

4.2.1 Characterising Interaction Between Cdc27 and PCNA Mutants Deficient in Binding Pol32 (in *S. cerevisiae*)

Spot tests indicated no sensitivity of the single PCNA point mutants to either hydroxyurea (HU) or camptothecin (CPT) in comparison to WT (Figure. 4.1A). The double PCNA point mutant (*pcn1_F248A,Y249A*) and both of the Cdc27 truncations (*cdc27_D1* and *cdc27_D3*) however are sensitive and exhibit slight slow growth phenotypes even in the absence of any replication stress inducing drug. However, these are not as sensitive as the HR deficient Rad51 allele (*rad51-3A*) that can form nucleoprotein filaments on ssDNA but cannot perform the strand exchange reaction (Cloud et al., 2012). Although, the slow growth of the *cdc27* mutants on YE media makes it difficult to interpret whether the reduced growth upon replication stress is due to increased sensitivity or their inherent slow growth. Nevertheless, the difference in sensitivity to these replication stress inducing agents suggests that the Pcn1 single point mutations may not be phenocopying the Cdc27 mutations.

The PCNA point mutants deficient for BIR and to binding Pol32 (Cdc27) were identified in *S. cerevisiae*. Mapping of these mutations onto *S. pombe* PCNA (Pcn1) has enabled equivalent mutants to be produced. However, the impact these mutations have on the ability of Pcn1 to bind Cdc27 has yet to be characterised. Co-precipitation of Cdc27 and

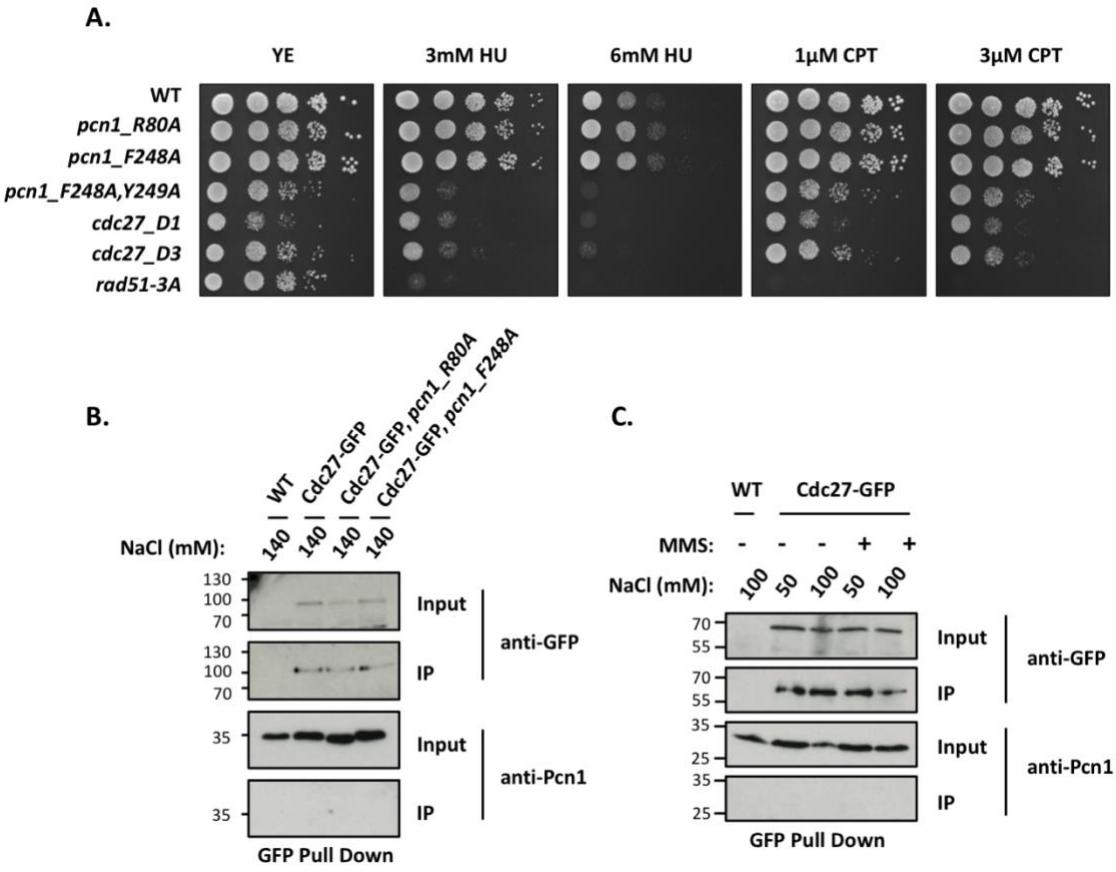

Figure 4.1. Characterisation of PCNA and Cdc27 Mutants Deficient for Binding Each Other. A. Serial dilution viability assay in the presence of replication stressing agents. Plates were incubated with the indicated concentration of each genotoxic agent (CPT or MMS) for 3-5 days at 30 °C. **B.** Cdc27 pull down using GFP-Trap beads to detect an interaction with PCNA. WT untagged control was used alongside strains containing cdc27-GFP with either: WT *pcn1*; *pcn1_R80A*; or *pcn1_F248A*. **C.** Low salt Cdc27 pull down using GFP-Trap beads to detect interaction with WT PCNA. Either 50 mM or 100 mM NaCl was used as indicated on untreated cells and cells incubated with 0.03% MMS for 5 hours. Untreated WT untagged Cdc27 was used as a control.

Pcn1 has only previously been reported *in vivo* in *S. pombe* when expressed from a plasmid under the control of a high expression promotor (*nmt1*) (Reynolds et al., 2000). Unfortunately, this interaction was undetectable when expressed under the control of their native promoter in the genome (Figure 4.1B). To try and increase the detectable signal, replication stressing agents were used to increase the likelihood of their interaction. High levels of MMS which alkylates DNA and can block the progression of replication, failed to result in visualisation of their interaction by western blot (Figure 4.1C). Additionally, lowering the salt concentration to increase signal from transient and less tightly bound proteins resulted in no detectable signal. Therefore, characterisation of each of the PCNA point mutants has proved difficult and it is not yet possible to say if the Pcn1 mutations affect the binding of Cdc27 in the same way as has been reported for Pol32 in *S. cerevisiae*. In the future, two-hybrid analysis can be tested as well as yeast transformation with high expression plasmids containing the PCNA point mutants and Cdc27-GFP.

4.2.2 Confirming Two Different rNTP Permissive *Cdc6* Alleles Can Be Used to Investigate Contribution of BIR Mutants in Restart at *RTS1* By Pu-Seq

The standard Pu-Seq protocol uses the rNTP permissive Cdc6 allele, *cdc6_L591G*, to track Polδ replication. Unfortunately, I was unable to construct the *cdc6_L591G cdc27_D1* or *cdc6_L591G cdc27_D3* double mutant. This was not entirely unexpected as this allele has proved problematic when combining with a selection of other mutations. Some other gene deletions that have been unable to be produced in a Pu-seq background include *mus81*, *rad50*, *rad52*, *rad3* and *mrc1*. It is likely that the intrinsic polymerase ability of this Polδ mutation, as opposed to the incorporation of rNMPs, causes replication problems that result in the activation of checkpoints (unpublished observations from the lab) and the deployment of HR. This can affect some mutants that render cells sick in an otherwise wildtype background. Therefore, construction of the Cdc27 truncated mutants in a standard Pu-Seq background was impossible. However, another rNTP permissive Polδ allele can be used instead, *cdc6_L591M*. This Cdc6 allele incorporates rNTPs at a lower rate than *cdc6_L591G* and retains a closer to WT

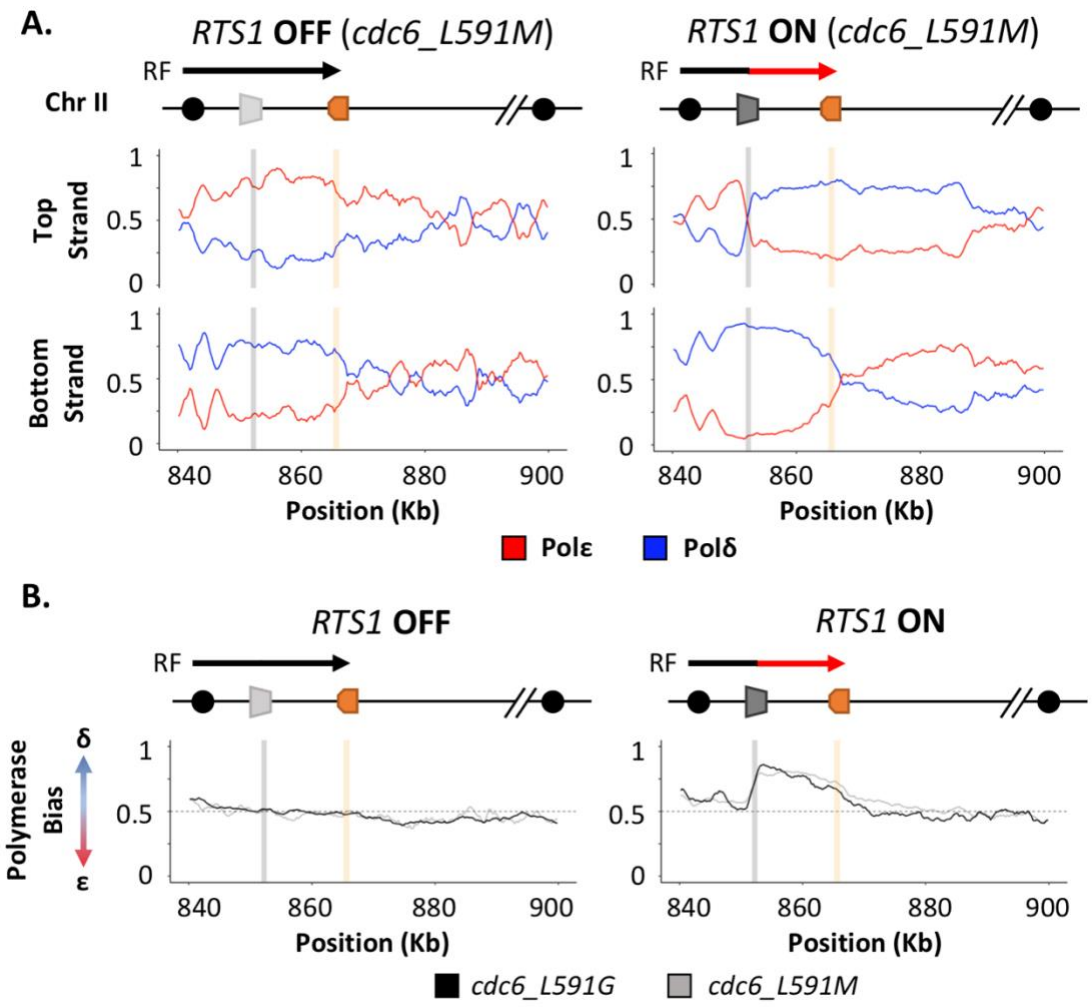

Figure 4.2. Low rNTP Incorporation Cdc6 Mutant (cdc6_L591M) Produces Same Replication Fork Restart as High rNTP Incorporation Mutant (cdc6_L591G). A. Polymerase usage at *RTS1* RFB on Chr II using Polδ Mutant, *cdc6_L591M*; *RTS1* ON (right panel) and OFF (left panel). Ratio of Polymerase ε (red) and Polymerase δ (blue) for both the top and bottom strand is shown. **B.** Polymerase bias graph calculated using the ratio of polymerase usage across both strands at the *RTS1* RFB using Polε rNTP mutant and each of the Polδ rNTP mutants; *cdc6_L591G* (black) and *cdc6_L591M* (grey).

phenotype. Using *cdc6_L591M,* Pu-Seq strains harbouring the Cdc27 truncations were successfully constructed.

Recently, equivalent rNTP permissive Polδ mutants in *S. cerevisiae* have been established. Two mutants that similarly incorporate rNTPs at higher (*pol3_L612G*) and lower levels (*pol3_L612M*) were tested in a BIR assay (Donnianni et al., 2019). This study found the rNTP incorporation rates of *pol3_L612G* and *pol3_L612M* correlated with a reduced ability to perform BIR. Thus, we wanted to establish if there was any change to the ability of *cdc6_L591M* to replicate the *RTS1* locus after replication restart when compared to the standard protocol using *cdc6_L591G*. This would allow us to determine if any change to polymerase usage we may see with the Cdc27 truncated mutants is related to the Cdc27 allele, rather than the polymerase allele used. To this end, Pu-Seq was first carried out on the WT *RTS1* RFB system using our low rNTP incorporation mutant, *cdc6_L591M*. Polymerase Usage profiles confirm the same switch to Polδ replication on the top strand as with *cdc6_L591G*. Direct comparison of the levels of Polymerase δ bias after restart at *RTS1* confirms virtually identical levels of replication fork restart with the restarted fork replicating a similar distance downstream of *RTS1*. Slight differences in the shape of the Polδ bias curve could indicate the restarted RF replicating a slightly longer region downstream of *RTS1*, possibly due to faster kinetics of the restarted RF. However, these differences are minimal allowing direct comparisons to be made between mutants constructed in either *cdc6* allele background for analysis of restart at *RTS1*.

4.2.3 PCNA Point Mutants Reduce Replication Fork Slippage Downstream of Active *RTS1* Without Reducing Progression of Restarted Replication Fork

The two PCNA point mutants identified in *S. cerevisiae* to inhibit BIR regardless of Pol32 presence are F248A F249A and R80A (Lydeard et al., 2010). We tested *pcn1_R80A* and *pcn1_F248A* in the *RTS1* RFB system to investigate their contribution to replication fork restart. The double point mutant (F248A,Y249A) was not possible to analyse due to its poor viability. Our first assay was to determine the impact they may have on the error-prone nature of the restarted replication fork using a mutation assay. Mutation assays

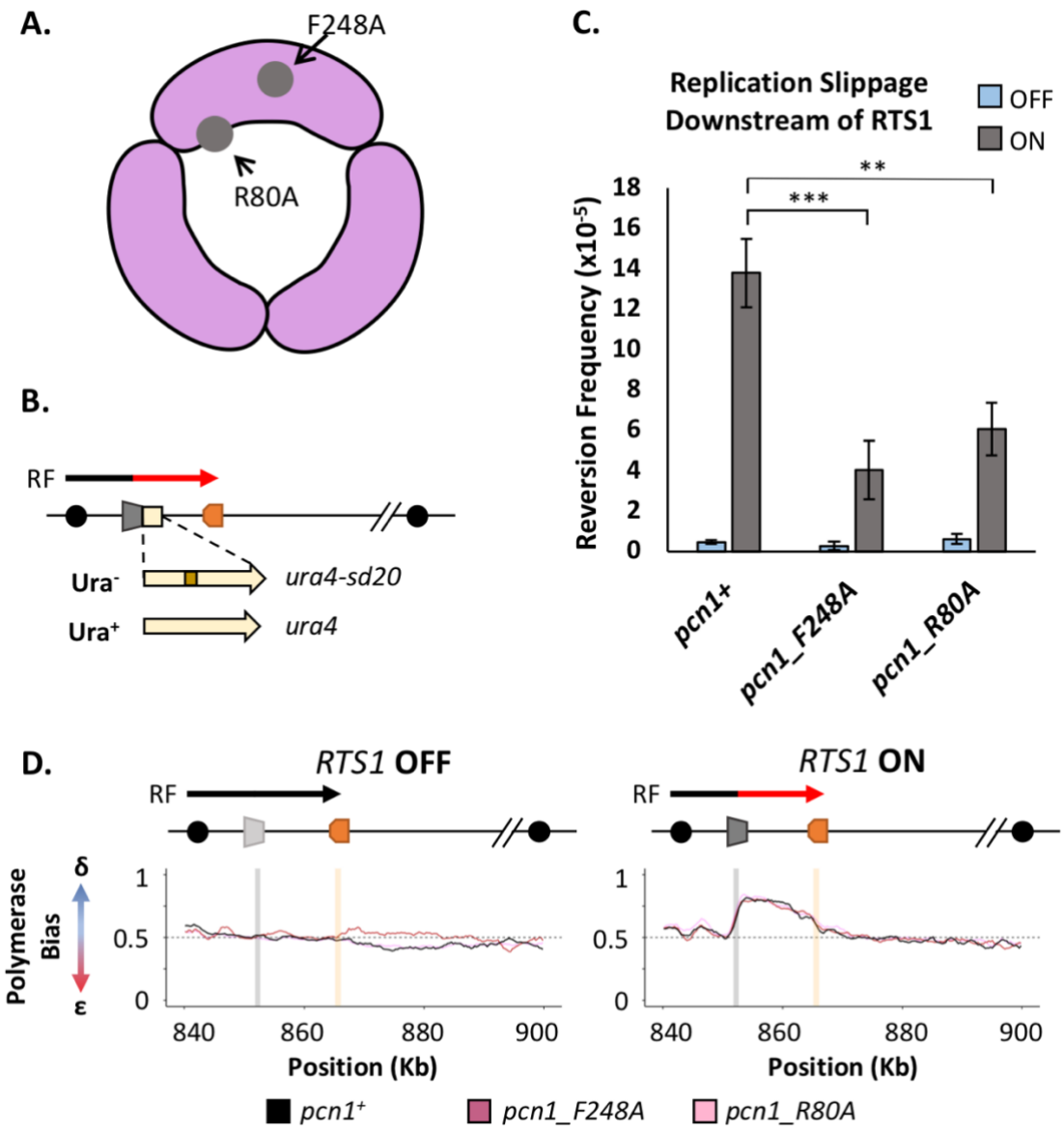

Figure 4.3. PCNA Mutants Reduce Replication Fork Slippage Downstream of Active RTS1 but Maintain Efficient Restart. A. Cartoon representation of PCNA homotrimer formed of three Pcn1 subunits and the location of each point mutation. R80A resides on the α-helices lining the hole of PCNA. F248A is a sidechain on the interdomain connector loop buried inside the structure of PCNA. **B.** *RTS1*-RFB replication slippage assay schematic. A *ura4* allele containing a 20 bp tandem repeat (*ura4sd20*) is inserted immediately downstream of the *RTS1* sequence. **C.** Replication fork slippage events scored as the frequency of *ura4* reversions over 2 cell cycles. Data from three independent experiments ± SD. Statistical analysis by two-tailed Students T Test, $p<0.05$ = *, $p<0.01$ = **, $p<0.005$ = ***) **D.** Polymerase bias graph calculated using the ratio of polymerase usage across both strands at the *RTS1* RFB; *RTS1* OFF (*left panel*), *RTS1* ON (*right panel*).

.

have previously been used as a readout for the efficiency of HR-restarted replication forks. Using an inverted repeats system, induction of the *RTS1* RFB lead to gross chromosomal rearrangements that is dependent on HR proteins (Lambert et al., 2005).

Additionally, a replication fork slippage assay has been established as a measurement for the level of HR-restart (Iraqui et al., 2012). Replication fork restart at *RTS1* induces replication fork slippage which is abolished when cells are lacking Rad51 and Rad52, which are required for the HR-restart of replication forks. In this assay, an allele of *ura4* which contains a 20 bp tandem repeat, *ura4sd20*, renders cells uracil deficient (Iraqui et al., 2012). Deletion of one tandem repeat reverts the allele to wildtype *ura4*, resulting in a uracil proficient cell. These events can be selected for and are a readout for replication fork slippage events. To test replication fork slippage associated with restart in our *RTS1* system, the *ura4sd20* allele was inserted immediately downstream of the *RTS1* sequence (Figure 4.3B). In wildtype cells, the active *RTS1* RFB results in a large increase in replication fork slippage events in the downstream region in comparison to when *RTS1* is OFF (Figure 4.3C). This increase in replication fork slippage is markedly less when either of the PCNA point mutants are introduced. This could suggest lower levels of replication fork restart at *RTS1*. To confirm the levels of replication fork slippage when *RTS1* is OFF are background levels of canonical RF slippage, in the future the *ura4sd20* allele could also be placed at a different genomic locus lacking the *RTS1* sequence to highlight it is neither *RTS1* specific, nor locus specific.

We next sought to confirm this by Pu-Seq, which provides a direct measure of the percentage of cells that replicate the locus with a restarted fork. Surprisingly, when both PCNA point mutants are analysed using Pu-Seq, the same level of Polδ bias is produced downstream of *RTS1* (Figure 4.3D). This provides direct evidence that the PCNA point mutants do not change the efficiency of restart or the ability of the restarted RF to replicate the downstream region. The reason behind the reduction in replication fork slippage events after restart at *RTS1* therefore indicates a higher fidelity of the restarted replication fork when PCNA is deficient in its interaction with Cdc27. However, these point mutants are yet to be characterised in *S. pombe*, so perhaps they do not have the same effect as is described in *S. cerevisiae*.

4.2.4 Cdc27 Truncations Deficient in Binding PCNA Reduce Replication Fork Restart at *RTS1*

Polymerase δ is a four-subunit complex consisting of the catalytic subunit Cdc6, Cdc1, Cdc27 and a small subunit Cdm1 (MacNeill et al., 1996, Reynolds et al., 1998, Zuo et al., 1997). Polymerase δ complex lacking Cdc27 greatly reduces its ability to bind PCNA and results in reduced processivity of the enzyme (Zuo et al., 2000). Similarly, reduced processivity of the enzyme complex is observed when lacking only the C-terminal portion of Cdc27 that contains the PCNA binding motif (Bermudez et al., 2002).

To investigate the contribution of Cdc27's interaction with PCNA in the restart at *RTS1,* two different C-terminally truncated versions of the protein were used (Figure 4.4A). Cdc27 is 372 amino acid residues in length, with the PCNA binding motif located in residues 353-372 (Reynolds et al., 2000). Both Cdc27 alleles (*cdc27_D1* and *cdc27_D3*) lack the PCNA binding motif, with the D3 mutant lacking only this region and D1 further truncated from residues 160-372. The larger truncation of Cdc27_D1 results in the loss of an additional conserved Polα binding motif. Replication slippage analysis downstream of *RTS1* for both Cdc27 truncations resulted in no change to the *ura4* reversion frequency when *RTS1* is ON. However, a slight increase to background levels of replication slippage are observed when the barrier is OFF. This increase is higher for Cdc27_D1, possibly reflecting an inherent mutagenic feature of these alleles that could mask a decrease in RF slippage that is seen with the PCNA point mutants.

In order to determine whether the Cdc27 truncations have the same effect as the PCNA point mutants on restart at *RTS1* and the restarted RF, Pu-Seq was conducted. When *RTS1* is ON, both Cdc27_D1 and Cdc27_D3 switch from Polε usage on the top strand to Polδ usage to replicate the region downstream of *RTS1*. The extent of the switch is, however, moderately reduced when compared to *cdc27*$^{+}$. In addition, the distance Polδ travels on the bottom strand for both mutants appears considerably less. This suggests the restarted replication fork does not replicate as far downstream of *RTS1* as in the wildtype situation. One possibility is that the restarted RF travels slower when harbouring *cdc27* truncations lacking the PCNA binding motif. Alternatively, RFs take

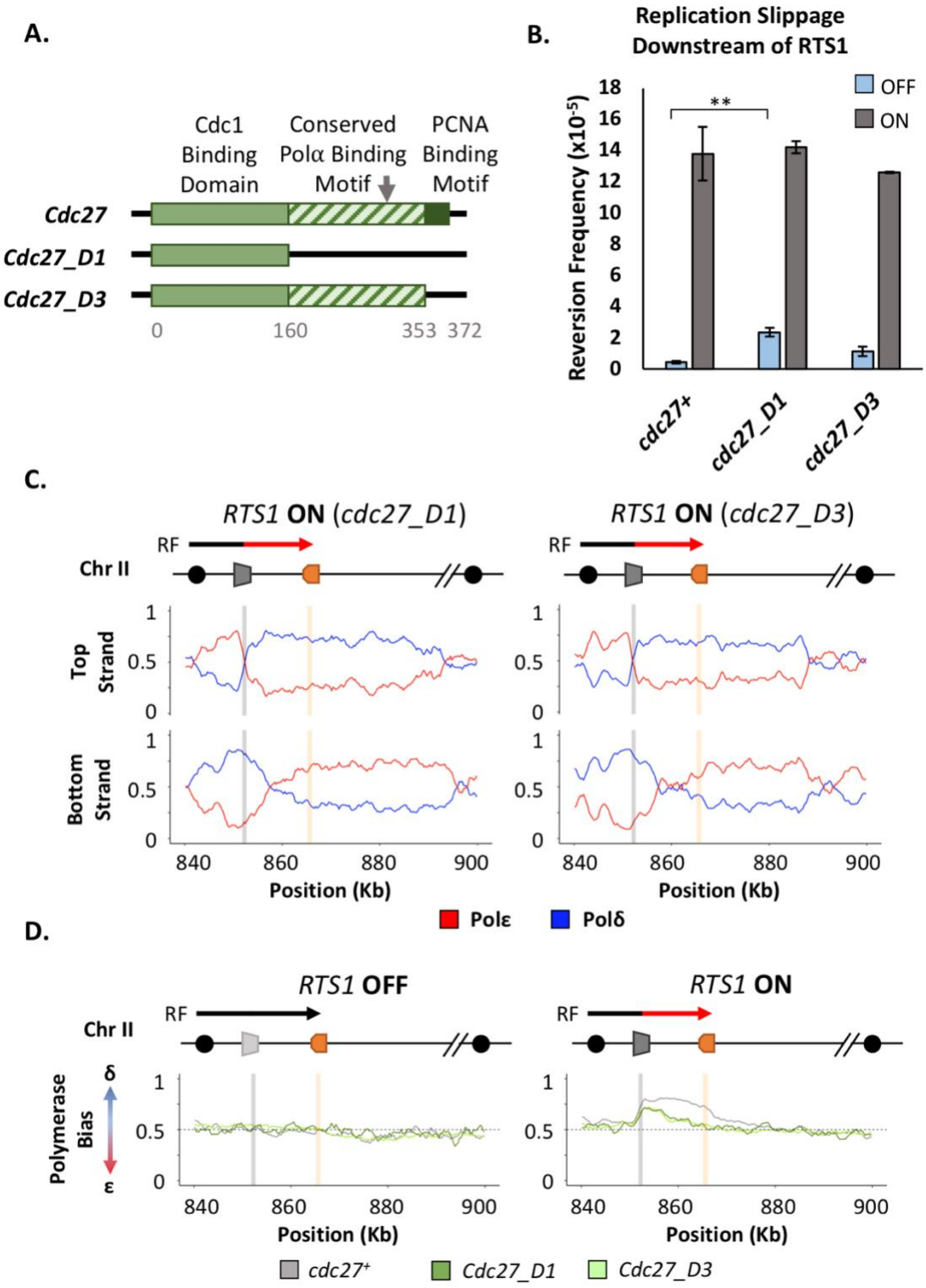
A.
Cdc1 Binding Domain
Conserved Polα Binding Motif
PCNA Binding Motif
Cdc27
Cdc27_D1
Cdc27_D3
0
160
353 372
B.
Replication Slippage Downstream of RTS1
Reversion Frequency (x10-5)
OFF
ON
**
cdc27+
cdc27_D1
cdc27_D3
C.
RTS1 ON (cdc27_D1)
RTS1 ON (cdc27_D3)
RF
Chr II
Top Strand
Bottom Strand
Position (Kb)
Polε
Polδ
D.
RTS1 OFF
RTS1 ON
Polymerase Bias
δ
ε
cdc27+
Cdc27_D1
Cdc27_D3

Figure 4.4. (previous page) Cdc27 Truncated for PCNA Binding Motif Reduces RF Restart at RTS1 while Maintaining WT Replication Fork Slippage After Restart. A. Schematic of the Cdc27 truncations. The amino acid position of each truncation is indicated. **B.** Replication fork slippage events scored as the frequency of *ura4* reversions over 2 cell cycles. Data from three independent experiments ± SD. Statistical analysis by two-tailed Students T Test, *p<0.05* = *, *p<0.01* = **) C. Polymerase usage at active (ON) *RTS1* RFB on Chr II for each Cdc27 truncation; *cdc27_D1* (left panel) and *cdc27_D3* (right panel). Ratio of Polymerase ε (red) and Polymerase δ (blue) for both the top and bottom strand is shown. **D.** Polymerase bias graph calculated using the ratio of polymerase usage across both strands at the *RTS1* RFB; *RTS1* OFF (*left panel*), *RTS1* ON (*right panel*). WT polymerase bias trace presented here uses the *cdc6_L591M* rNTP incorporation mutant.

longer to restart, resulting in fewer forks able to restart in the allotted time, allowing more convergent canonical forks to travel closer to the *RTS1* RFB. Although it could be one or the other of these possibilities, it is likely it is a combination of both reduced restart and reduced processivity that provides the results seen here. The reduced levels of restarted RFs when *RTS1* is on is visible by the reduction in Polδ bias when polymerase usage across both strands is taken into consideration. There is a reduction in both the height and width of the Polδ bias peak, suggesting both reduced restart and reduced distance travelled by the restarted RF. The conserved Polα motif is dispensable for *RTS1* restart, as both Cdc27 mutants result in the same polymerase usage profiles. However, this would need to be confirmed by using a Cdc27 truncation mutant lacking only residues 160-353. Both Cdc27 mutants also produced no Polδ bias when *RTS1* is OFF. Therefore, efficient restart at *RTS1* and replication using the restarted RF relies at least partially on the PCNA binding motif at the C terminus of Cdc27.

4.3 Discussion

Investigation into the contribution of the interaction between PCNA and Cdc27 for restart at *RTS1* has revealed stark differences between this restart in *S. pombe* and BIR in *S. cerevisiae*. Using the PCNA mutants F248A or R80A (shown to suppress BIR in budding yeast), I observed a decrease in replication fork slippage downstream of active *RTS1* by around 50%. However, Sarah Lambert's team have observed no change to

ssDNA production in both mutants compared to WT as judged by RPA enrichment across the region (unpublished data). This agrees with the Pu-Seq data presented here showing efficient replication fork restart at *RTS1*. Overall, combining the Pu-seq results with the mutational analysis of both of these PCNA mutants, it seems that PCNA's interaction with Cdc27 is not important for polymerase delta usage after restart at *RTS1*, but instead may be important for its fidelity. However, further characterisation of the PCNA point mutants' impact on binding to Cdc27 is needed. In the future it would also be interesting to construct and test the single point mutant *pcn1_Y249A* to see if this residue acts the same as *pcn1_F248A*, or whether it is this residue alone that confers increased sensitivity to the double point mutant.

When we tested the well characterised Cdc27 truncations (*cdc27_D1* and *cdc27_D3*) that lack the PCNA binding motif, replication fork slippage was unchanged after restart at *RTS1* in comparison to WT. However, higher levels of background replication fork slippage were detectable as evident from an increased *ura4* reversion frequency when *RTS1* is OFF. Therefore, the increased RF slippage observed when *RTS1* is ON may be an overestimate and could reflect more closely the reduction seen with the PCNA point mutants. This becomes evident when considering the fold increase in RF slippage between *RTS1* OFF and ON for each mutant. In a WT situation there is a roughly 30-fold increase in RF slippage when *RTS1* is ON in comparison to OFF. For the PCNA point mutants this reduces to roughly 18 (*pcn1_F248A*) and 10 (*pcn1_R80A*) fold increases. *pcn1_F248A* fold increase may be higher than *pcn1_R80A* due to it harbouring only one of the two point mutations originally characterised in *S. cerevisiae* to lose its interaction with Pol32 (Cdc27). Similarly, fold increases are reduced in comparison to WT for both *cdc27_D3* (~11 fold) and *cdc27_D1* (~6 fold), with *cdc27_D1* presenting a larger decrease, possibly due to additional loss of the Polα interaction motif. Overall, this suggests the Cdc27 truncation mutants have a similar effect as the PCNA point mutants on limiting mutagenesis downstream of active *RTS1*.

However, in contrast to the PCNA point mutants, analysis of each of the Cdc27 truncations by Pu-Seq revealed reduced RF restart and progression at active *RTS1*. Moreover, the Carr lab has previously performed Southern blots showing that Cdc27_D1

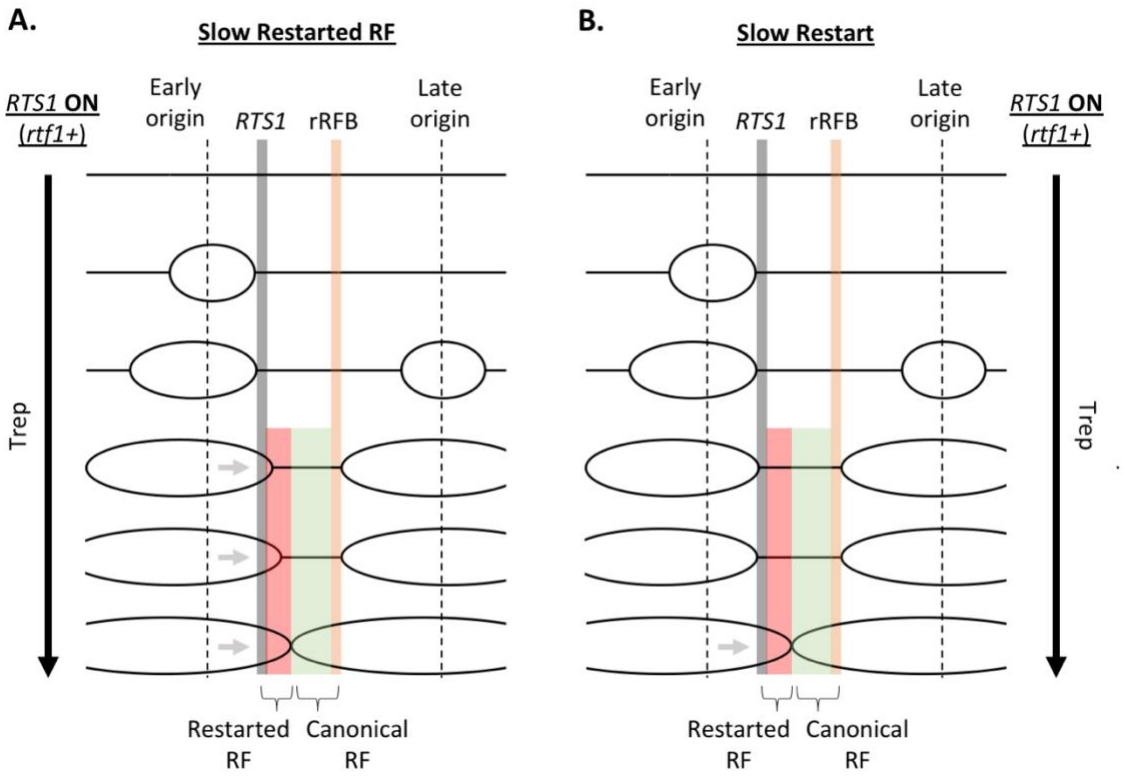

Figure 4.5. Replication Fork Movement Schematic at the RTS1 RFB for Cdc27 Mutants Lacking PCNA Binding Motif. Graphical visualisation of the possible movement of replication forks radiating from the early and late firing origins flanking the active *RTS1* construct (*RTS1* ON) when Cdc27 lacks the PCNA binding motif. Direction of replication timing (Trep) is indicated by the black arrows. Restarted replication fork movement past *RTS1* is indicated by light grey arrows. **A.** RFs stalled at *RTS1* take the same amount of time to restart as in a wildtype situation. However, the restart produces a slow-moving RF. **B.** RFs take a longer time than wildtype to restart at *RTS1* but replicate the downstream region at a speed comparable to WT.

(truncated protein lacking PCNA binding motif) decreased formation of acentric chromosomes in comparison to WT using the *RTS1* barrier in an inverted repeats system. One interpretation of this data is that replication forks are progressing through *RTS1* but replicating slowly (Figure 4.5A), or take longer to progress through the *RTS1* barrier (Figure 4.5B). This would result in the restarted RF travelling a shorter distance, allowing more cells to complete replication of the downstream region of *RTS1* with a converging replication fork. Therefore, this indicates Cdc27 is important for efficient HR-dependent restart of RFs at *RTS1* but its impact is not as dramatic as the reported role of Pol32 in BIR in *S. cerevisiae*.

Overall, the data presented here demonstrates key differences between BIR in *S. cerevisiae* and HR-dependent restart at *RTS1* in *S. pombe*. Firstly, using *cdc27* alleles truncated for the PCNA binding motif, these results confirm its importance for HR-restart at *RTS1*, but it is not as crucial as its described role in BIR in *S. cerevisiae*. Additionally, using two point mutations of PCNA shown to be important for BIR in *S. cerevisiae*, we provide clear evidence that they do not phenocopy the *cdc27* truncations. Instead, they have an interesting impact on PCNA in a way that is probably independent of Cdc27 and is yet to be fully understood.

Chapter 5 – Characterising the Role of Rtf2 in Replication Fork Restart

5.1 Introduction

Rtf2 is a protein conserved between human and fission yeast, belonging to a family of proteins that are characterised by a C2HC2 Ring Finger motif (Inagawa et al., 2009). Rtf2 is predicted to fold up into a RING-finger like structure with the ability to bind one Zn^{2+} ion. This is similar to the C3HC4 RING-finger motif found in proteins such as BRCA1, that can bind two Zn^{2+} ions and is known to mediate protein-protein interactions. Rtf2 was originally identified in *S. pombe* as being important for efficient replication fork arrest at the *RTS1* RFB (Codlin and Dalgaard, 2003). Additionally, this study identified *RTS1* to be composed of two distinct regions (Codlin and Dalgaard, 2003). Region B contains four blocking motifs' where the trans-acting factor Rtf1 binds. Region A is purine rich and identified as functioning as an enhancer region to increase Region B blocking capacity. Rtf2 was found to reduce the blocking signal at *RTS1* to the same extent as deletion of Region A of the *RTS1* sequence. Additionally, there was no additive effect of the double deletion and it was thus suggested that Rtf2 mediates its enhancing effect on the blocking signal of *RTS1* through binding at Region A. The data presented here explores this further, utilising a truncated version of *RTS1* lacking region A for Pu-Seq and replication fork slippage analysis in the presence and absence of Rtf2.

Stabilisation of replication forks upon encountering DNA damage is important for maintaining genome stability. Sumoylation of PCNA has been implicated in maintaining the stability of these RFs. Rtf2 has also been shown to interact with PCNA and it was suggested that Rtf2 possibly aid PCNA stabilisation at replication forks stalled at sites of DNA damage via sumoylation pathways. This speculation arose when deletion of *S. pombe* SUMO (Pmt3), alone or in combination with *rtf2* deletion, resulted in a similar reduction in blocking signal of *RTS1* as with the single *rtf2* deletion (Inagawa et al., 2009). This suggests a wider role for Rtf2 at stalled replisomes, not just the *RTS1* RFB. Furthermore, in human cells, the presence of Rtf2 (*Hs*RTF2) was shown to reduce the levels of replication fork restart globally, and its removal from stalled RFs via

proteasomal shuttle proteins (DDI1 and DDI2) was important to allow replication fork restart to occur (Kottemann et al., 2018). Additionally, the nuclear receptor interacting protein 3 (NIRP3) has been shown to upregulate DDI1 and increase polyubiquitylation of RTF2, promoting RTF2 removal and replication fork restart upon replication stress (Suo et al., 2020). NRIP3 has previously been shown to be upregulated in oesophageal squamous cell carcinoma and play an important role in tumour progression and resistance to chemoradiotherapy (Qin et al., 2011, Suo et al., 2020). However, a study in *S. cerevisiae*, has also suggested Ddi1 (*Hs*DDI1, *Sp*Mud1) could act directly as a protease, as HU sensitivity was rescued by mutant Ddi1 lacking both the ubiquitin-like (UBL) and ubiquitin-associated (UBA) domains important for linking the ubiquitinated protein to the 26S proteasome (Svoboda et al., 2019). Thus, it is hard to know if NIRP3 activity is acting through human RTF2.

Here, I further investigate how Rtf2 enhances the blocking signal at *RTS1* as well as its wider implications on the replisome at a genome wide scale. Additionally, a mass spectrometry method is established to allow investigation of Rtf2 protein interactors.

5.2 Results

5.2.1 Loss of Rtf2 Reduces Levels of Replication Fork Restart and Replication Fork Slippage Downstream of Active *RTS1*

Rtf2 enhances the blocking signal at active *RTS1* when visualised on 2D gels (Codlin and Dalgaard, 2003). To investigate how this affects the dynamics of polymerase usage downstream of the *RTS1* RFB Pu-Seq was conducted. In the absence of Rtf2 (*rtf2***Δ**) canonical replication is carried out across the *RTS1* RFB region when the barrier is OFF (Figure 5.1A). When *RTS1* is ON, Polε usage on the top strand reduces at the site of the *RTS1* RFB, indicating some switching to Polδ usage to replicate the region downstream of the barrier (Figure 5.1A). However, this is not to the same degree as in the WT *RTS1* ON system and Polε usage remains the predominant polymerase used to replicate this

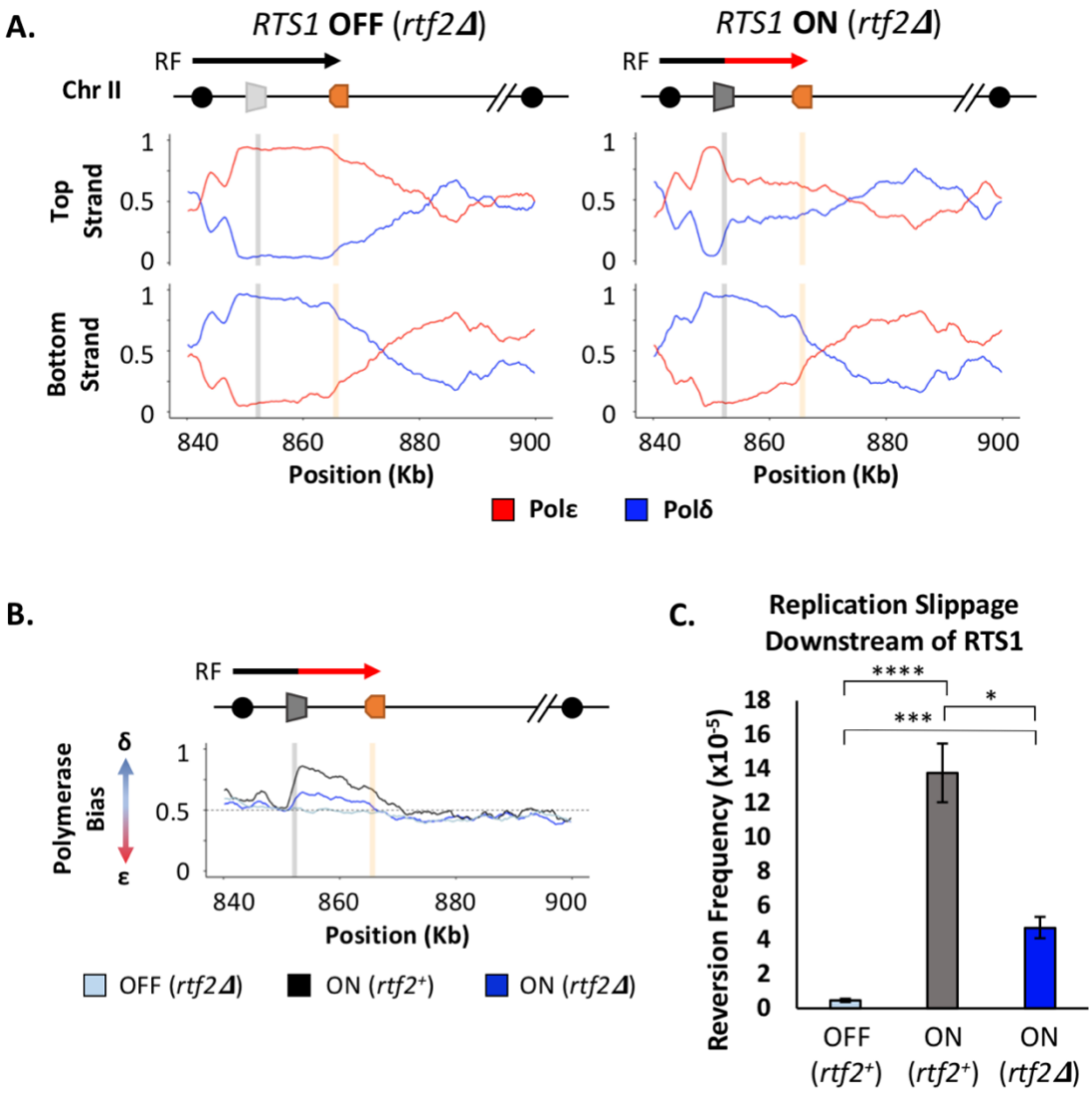

Figure 5.1. Rtf2 Deletion Reduces Replication Fork Restart at RTS1 and Levels of Downstream RF Slippage. A. Polymerase usage at the *RTS1* RFB on Chr II in rtf2**Δ** background; *RTS1* OFF (left panel) and *RTS1* ON (right panel). Ratio of Polymerase ε (red) and Polymerase δ (blue) for both the top and bottom strand is shown. **B.** Polymerase bias graph calculated using the ratio of polymerase usage across both strands at the *RTS1* RFB. **C.** Replication fork slippage events scored as the frequency of *ura4* reversions over 2 cell cycles using the *RTS1-ura4sd20* RF slippage assay. Data from three independent experiments ± SD. Statistical analysis by two-tailed Students T Test, *p<0.05* = *, *p<0.01* = **, *p<0.005* = ***, *p<0.0005* = ****)

.

top strand region. This is particularly evident when you take into consideration polymerase usage across both strands to determine the polymerase bias produced in this region. When Rtf2 is deleted the level of Polδ bias produced downstream of active *RTS1* is reduced in comparison to WT (Figure 5.1B). Additionally, there is an equivalent reduction in replication fork slippage events downstream of active *RTS1* when using the *RTS1-ura4sd20* construct (Figure 5.1C). This reduction in replication fork slippage when Rtf2 is deleted reflects the reduced levels of restarted replication forks evident in the Pu-Seq traces. These results suggest a proportion of replication forks remain canonical after encountering the *RTS1* RFB in the absence of Rtf2, with around a third of RFs restarting using δ/δ replication. Therefore, a subset of RFs block at *RTS1* and restart as in a WT situation. The other RFs either block at *RTS1* and restart as a canonical replication fork, or they do not get blocked at *RTS1* and instead continue replication across the region as in an *RTS1* OFF situation. Mathematical modelling of the efficiency of *RTS1* barrier activity in the absence of Rtf2 best fits a 10-fold reduction in efficiency when fit to the change in polymerase usage traces from Pu-Seq (Eduard Campillo-Funollet). This is a larger decrease than expected but indicates that the subset of RF's that remain canonical downstream of *RTS1* indeed do not get blocked at *RTS1* and continue replication unperturbed as a canonical RF.

5.2.2 Rtf2 Does Not Increase *RTS1* Barrier Activity by Binding to Enhancer Region A

RTS1 is composed of two main regions, A and B (Figure 5.2A). Region B has been shown to contain four blocking motifs where Rtf1 binds. Previously it has been suggested Rtf2 enhances *RTS1* barrier activity via binding to region A due to similar reductions in blocking signal of *rtf2***Δ** and *RTS1* lacking region A (*RTS1_A***Δ**) when analysed by 2D gels (Codlin and Dalgaard, 2003). To investigate if this is the case in our *RTS1* system and the impact region A plays on polymerase usage downstream of active *RTS1*, region A was deleted from the *RTS1* sequence and inserted into our locus on chromosome II containing the downstream 10xrRFBs. This truncated *RTS1* sequence was also incorporated into the replication fork slippage construct to produce *RTS1_A***Δ**-*ura4sd20.* If Rtf2 is carrying out its enhancing effect on blocking at *RTS1* the same results are expected for *rtf2***Δ** and *RTS1_A***Δ***.*

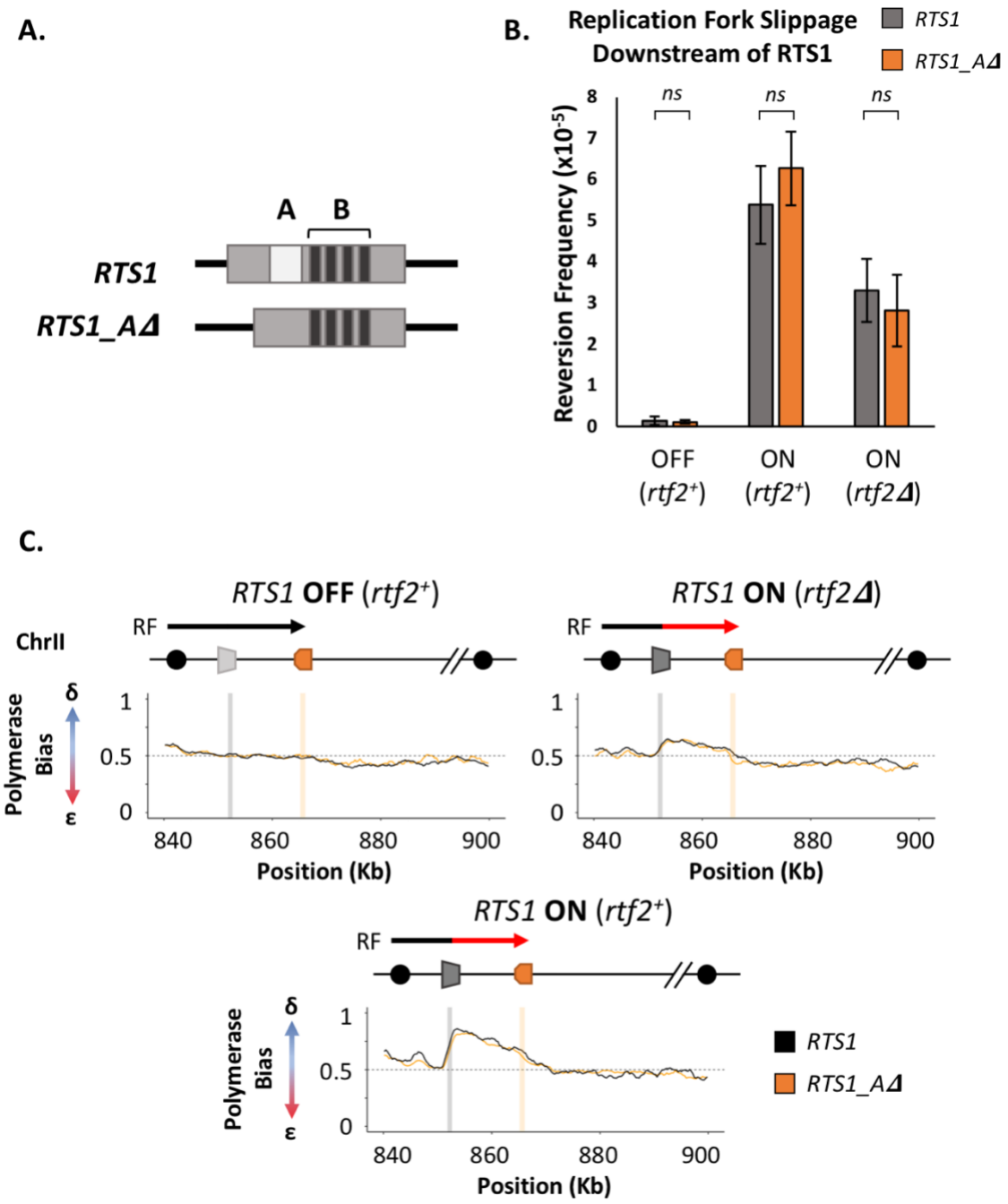

Figure 5.2. RTS1 Region A is Dispensable for Efficient Replication Fork Restart. A. Schematic of the *RTS1* RFB. Region A is a ~60 bp purine rich region and Region B is ~450 bp containing the four repeated blocking motifs essential for *RTS1* activity. **B.** Replication fork slippage events scored as the frequency of *ura4* reversions over 2 cell cycles. Data from three independent experiments ± SD. Statistical analysis by two-tailed Students T Test, *p>0.05* = not significant (*ns*). **C.** Polymerase bias graph calculated using the ratio of polymerase usage across both strands at the *RTS1* (black) and *RTS1_AΔ* (orange) RFB on Chr II; *RTS1* OFF (*left panel*), *RTS1* ON (*right and bottom panel*).

Firstly, levels of mutagenesis downstream of *RTS1* were analysed using *RTS1-ura4sd20* and *RTS1_A***Δ**-*ura4sd20* (Figure 5.2B). Similar levels of replication fork slippage were seen in both systems when *RTS1* is OFF. As expected, replication fork slippage rates were also similar when Rtf2 is deleted in both systems when the barrier is ON. However, if Region A has the same enhancing effect on blocking at *RTS1* as Rtf2, the levels of replication fork slippage would be expected to reduce to the same level as *rtf2***Δ** even in the presence of Rtf2. However, this is not the case as equivalent levels of replication fork slippage are observed when *RTS1* is ON in both systems. This suggests that Region A is dispensable for enhancing the blocking effect of *RTS1* and is not the site of Rtf2 binding.

To test this further, Pu-Seq was carried out on strains containing the *RTS1_A***Δ** system (Figure 5.2C). The same levels of Polδ bias was observed in comparison to the WT system when the barrier was both ON and OFF regardless of the presence of Rtf2. Therefore, these results indicate Rtf2 does not specifically bind to Region A and this region is dispensable for enhancing the blocking effect of active *RTS1*.

5.2.3 Confirming Activity & Function of Rtf2-GFP/13Myc/3HA

In order to further investigate the role Rtf2 plays at stalled replication forks several C-terminally tagged versions of the protein were constructed. Initially, a C-terminal tagging base strain was produced by insertion of the LoxP-*ura4*-LoxM3 sequence immediately downstream of Rtf2 5' UTR. This allows tagging of the protein using the recombination mediated cassette exchange system (Watson et al., 2008). Using this method, Rtf2 was successfully tagged with GFP, 13Myc, and 3HA. Tag functionality was confirmed via probing with the relevant antibodies from whole cell extracts of each strain (Figure 5.3A). Furthermore, Rtf2-3HA was successfully pulled down via immunoprecipitation and detected when visualised on a western blot (Figure 5.3B).

Having confirmed the functionality of each tag, their impact on Rtf2 protein function then needed to be assessed. First, each of the tagged proteins was crossed into the replication fork slippage assay (*RTS1-ura4sd20*). Levels of replication fork slippage

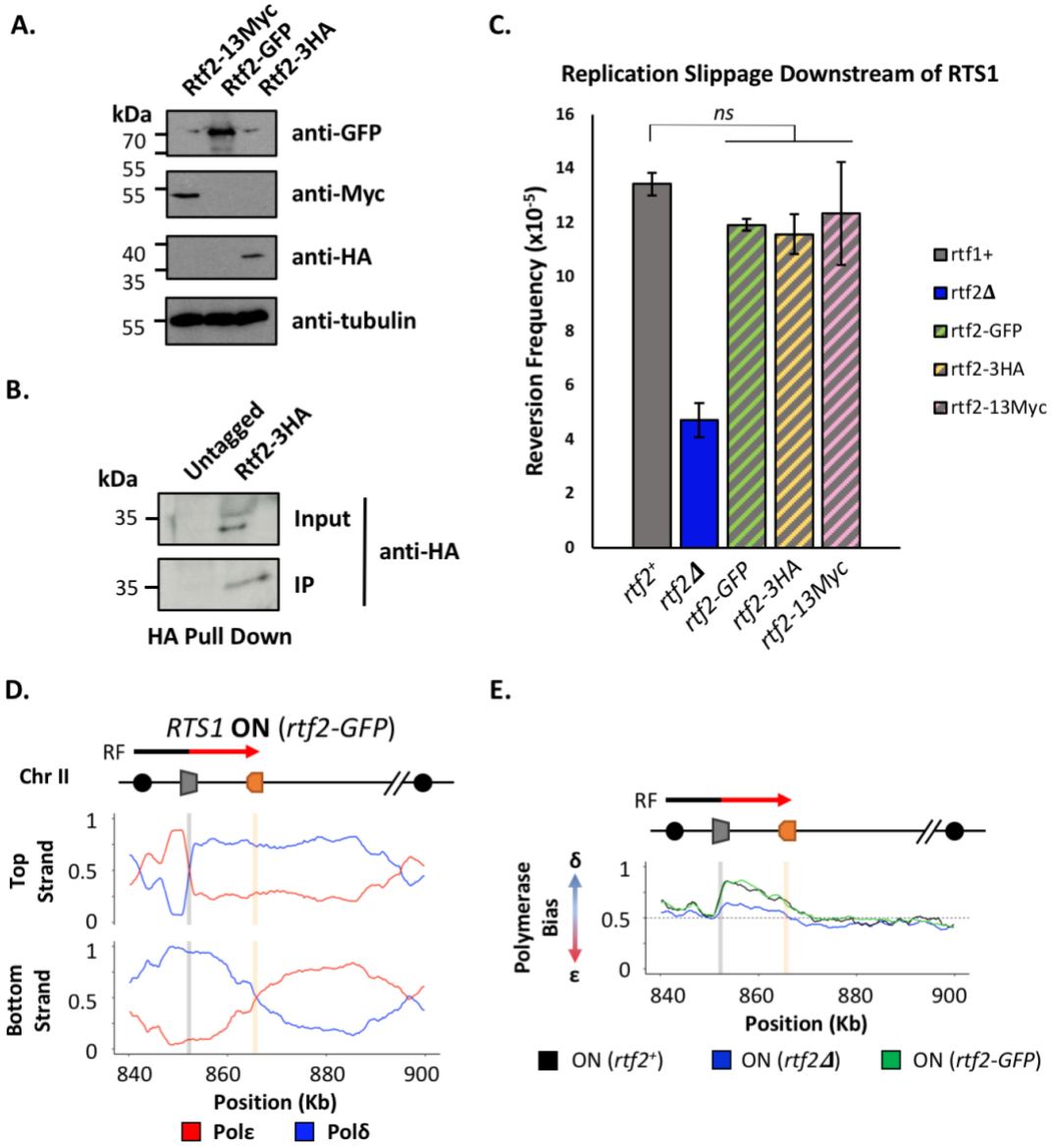

Figure 5.3. C-terminally tagged Rtf2 Activity and Functionality. A. Whole cell extracts of strains containing either Rtf2-13Myc, Rtf2-GFP, or Rtf2-3HA. Presence of each tagged protein were probed with the relevant antibodies. Tubulin was probed for as a loading control. **B.** Rtf2-3HA pull down using a HA antibody to confirm tag functionality. A WT untagged Rtf2 strain was used alongside as a control. **C.** Replication fork slippage events scored as the frequency of *ura4* reversions over 2 cell cycles. Data from three independent experiments ± SD. Statistical analysis by two-tailed Students T Test, *p>0.05* = not significant (*ns*). **D.** Polymerase usage at the active *RTS1* RFB on Chr II in a strain containing Rtf2-GFP. Ratio of Polymerase ε (red) and Polymerase δ (blue) for both the top and bottom strand is shown. **E.** Polymerase bias graph calculated using the ratio of polymerase usage across both strands at the *RTS1* RFB.

downstream of active *RTS1* were comparable to WT for each of the C-terminally tagged Rtf2 strains (Figure 5.3C). This suggests Rtf2 function is not impacted by the addition of a C-terminal tag due to the levels of RF slippage not reducing to that of r*tf2***Δ**. To confirm these results indicate efficient restart at *RTS1* due to a functioning Rtf2, Pu-Seq was conducted on the *RTS1* RFB in strains containing a tagged version of the protein (Rtf2-GFP). As in a wildtype situation, the top strand abruptly switches from Polε to Polδ replication after restart at *RTS1* as evident from the polymerase usage traces (Figure 5.4D). Direct comparison to wildtype also reveals an equivalent level of Polymerase δ bias produced across the region downstream of active *RTS1* (Figure 5.4E). Therefore, the WT levels of replication fork slippage downstream of active *RTS1* for each of the C-terminally tagged versions of Rtf2 represent efficient restart of the replication fork. Together, these results indicate both tag and Rtf2 functionality when combined on its C-terminus allowing use for further investigation into the role of Rtf2.

5.2.5 Impact of Replication Stress on Rtf2's Interaction with Chromatin and the Replisome

The importance Rtf2 has on stabilising replication forks and maintaining genome stability is yet to be fully understood. Deletion of *rtf2* confers *S. pombe* cells sensitive to high levels of MMS (Figure 5.4A). This has previously been shown, as well as no sensitivity to HU (Inagawa et al., 2009). However, in human cells removal of Rtf2 from replication forks was important for efficient replication fork restart after exposure to HU (Kottemann et al., 2018). This study suggested Rtf2 gets shuttled to the proteasome for degradation. To determine if this was the case in *S. pombe,* cells were exposed to HU synchronising them in S phase to assess whether there is a reduction in Rtf2 protein levels (Figure 5.4B). When visualised on a western blot, the levels of Rtf2 did not change after HU treatment. Additionally, the levels of Rtf2 do not appear to change across the cell cycle when comparing cells synchronised in G2 and S phase using the *cdc2asM17* allele. This suggests Rtf2 does not get degraded by the proteasome after exposure to replication stress, or that the protein is turned over rapidly.

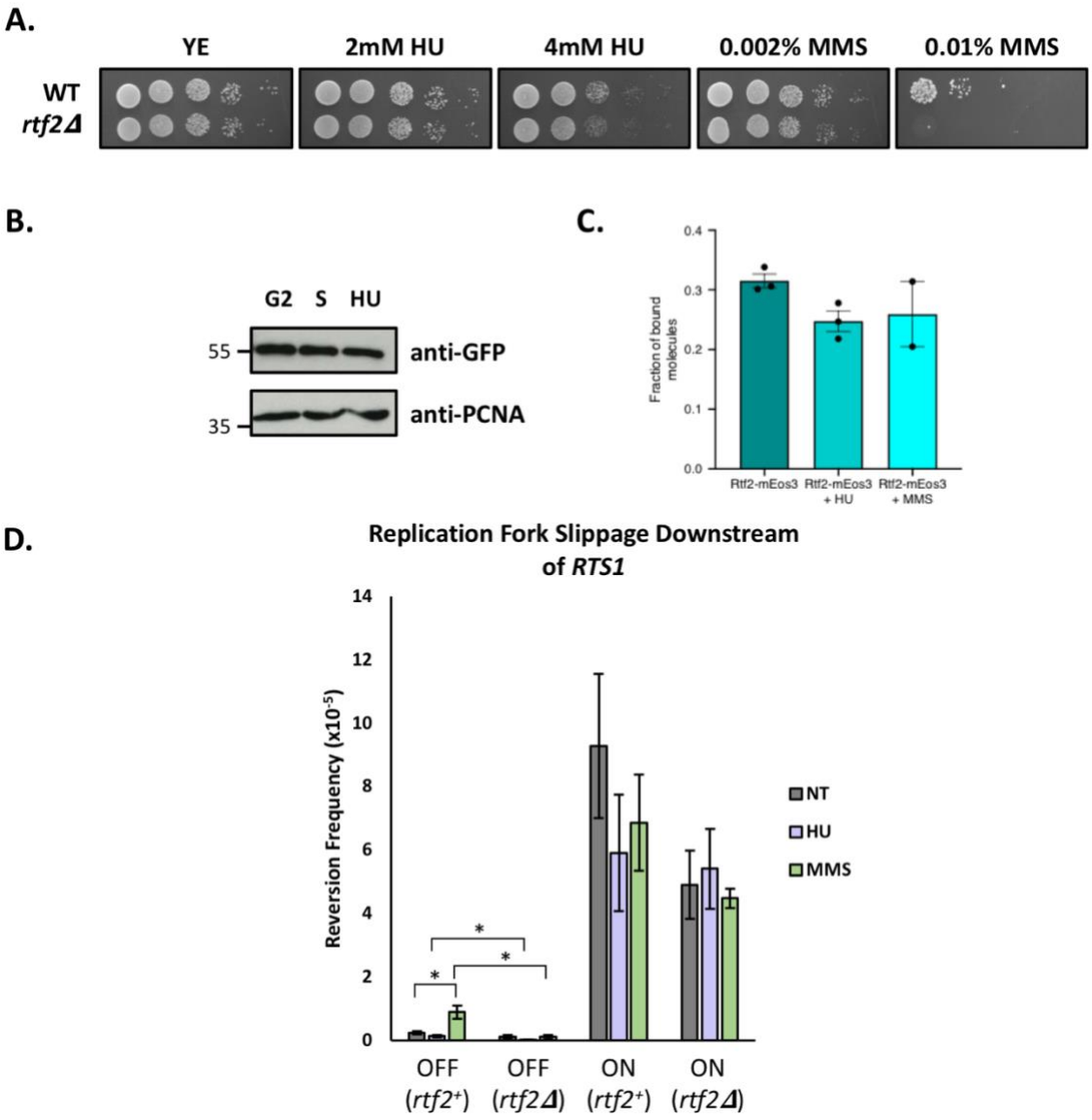

Figure 5.4. Replication Stress Induced Rtf2 Response. A. Spot test of WT and *rtf2***Δ** cells in the presence of different concentrations of HU and MMS. **B.** Whole cell extract of GFP tagged Rtf2 synchronised in G2 and S phase using cdc2asM17 allele, or grown in 10 mM HU for 4 hours. PCNA is probed for as a loading control. **C.** Single molecule microscopy data on the fraction of chromatin bound mEOS tagged Rtf2 after treatment with HU (10 mM for 4 hours) or MMS (0.03% for 5 hours). **D.** Frequency of *ura4* revertants as a measure of replication fork slippage events after 3 hrs of either: no treatment (NT); 10 mM HU; or 0.03% MMS. Data from 3-5 independent experiments ± SEM. Statistical analysis by two-tailed Students T Test, $p<0.05$ = *)

To assess whether Rtf2 indeed does get removed from replisomes, potentially to allow replication fork restart after exposure to replication stress, single molecule microscopy was conducted. An mEos tagged Rtf2 was constructed and protein functionality confirmed using the same methods outlined in section 5.2.4. Use of Rtf2-mEOS allows activation of a single fluorescently labelled molecule of Rtf2 at a time allowing tracking of its movement across a plane of the cell over three frames. Molecules that do not move across the specified time frame are classed as chromatin bound molecules, and those that have a larger trajectory across the cell are classed as freely diffusing molecules. This experiment was conducted by Thomas Etheridge using a previously published methodology (Etheridge et al., 2014). When comparing the fraction of chromatin bound molecules there is only a slight reduction after exposure to HU and MMS in comparison to untreated samples. This could suggest some removal of Rtf2 from replication forks, however these samples contain a mixed population of cells across the cell cycle and thus using synchronised cells and selecting specifically for those in S phase would be necessary to provide a clearer picture.

To get a view of Rtf2's role in restart of replication forks after exposure to replication stress the replication fork slippage assay downstream of *RTS1* was used (Figure 5.4D). Rtf1 controls the barrier activity at *RTS1* so strains lacking Rtf1 were used as a baseline level of slippage. When Rtf1 is deleted, there appears to be slightly higher levels of replication fork slippage after MMS treatment in comparison to no treatment (NT). However, when *RTS1* is active, (*rtf1+*) there is a trend toward reduced levels of replication fork slippage after both HU and MMS treatment in comparison to no treatment although this is not a significant decrease. This could be due to Rtf2 getting degraded by targeting to the proteasome after replication stress, and thus results in similar levels of replication slippage as rtf2**Δ**. The data presented here shows Rtf2 does not get substantially degraded after HU treatment but this is yet to be confirmed for MMS treatment in *S. pombe* (Figure 5.4B).

When Rtf2 is deleted in this assay, levels of replication fork slippage downstream of active *RTS1* (*rtf1+*) are the same across all three treatment conditions. Additionally, replication fork slippage for HU and MMS is similar to when the *RTS1* barrier is active

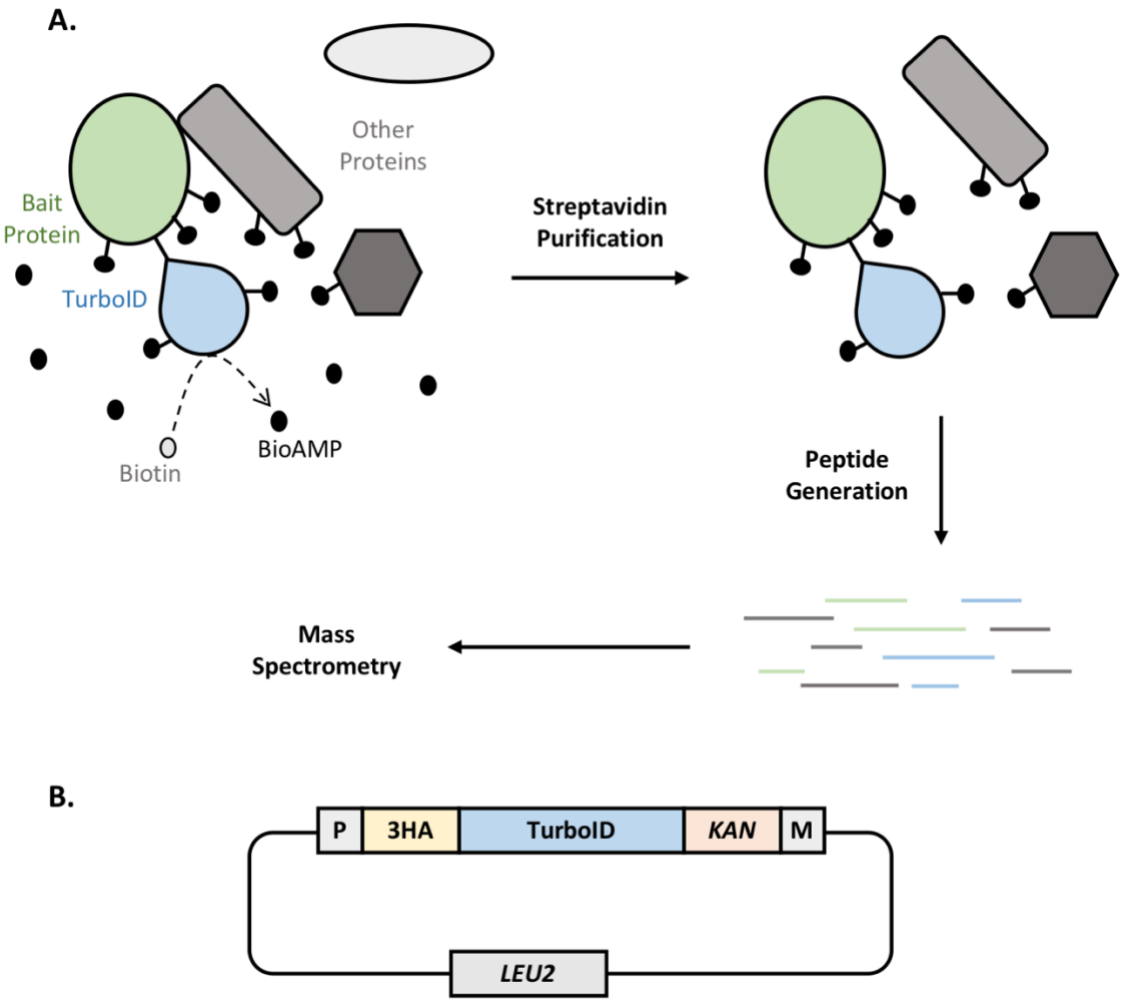

Figure 5.5. Schematic of the Proximity-Based Labelling Method for Mass Spectrometry Analysis using TurboID. A. Bait protein tagged with TurboID allows proximal proteins to be biotinylated. TurboID catalyses biotin into its active state, BioAMP, to allow biotinylation of available lysine residues. Biotinylation occurs on the bait protein and TurboID itself as well as protein interactors and proteins in close proximity. These biotinylated proteins are purified using streptavidin coated beads to remove non-biotinylated proteins. Peptides from the sample are produced and analysed by mass spectrometry. **B.** A pAW8 plasmid was constructed for C-terminal tagging of different bait proteins. The plasmid contains a 3HA internal tag, TurboID, and Kanamycin resistance marker used for selection of correct integration, between LoxP and LoxM sites to allow integration by recombination mediated cassette exchange.

regardless of the presence of Rtf2. Although, there is a trend toward a reduction for MMS treated cells in the absence of Rtf2 when compared to the presence of Rtf2. Furthermore, when the barrier is inactive the levels of replication fork slippage in all three treatment conditions is reduced in the absence of Rtf2. Therefore, the simple presence of Rtf2, particularly in the context of MMS induced replication stress, substantially changes the levels of replication fork slippage in this context. This could support the recently proposed notion in human cells that RTF2 removal is important to allow efficient restart of replication forks following replication stress (Kottemann et al., 2018).

5.2.7 Mass Spectrometry Analysis of Rtf2 Protein Interactions Using TurboID

To gain more insight into the function of Rtf2 that would allow us to design experiments to understand its role in replication restart an enzyme catalysed proximity labelling based mass spectrometry method was set up. This method utilises the *E. coli* BirA biotin ligase that catalyses biotin into biotinoyl-5'-AMP (bioAMP) in an ATP driven process (Figure 5.4A) (Chapman-Smith and Cronan, 1999, McAllister and Coon, 1966). However, this activated biotin is then only covalently attached onto its substrate when it reacts with a specific lysine residue in the recognition sequence of its substrate. In order to utilise biotin labelling for global interactors of a protein of interest, a promiscuous mutant version of BirA was identified that enables labelling of any proteins it comes into close contact with (Choi-Rhee et al., 2004, Kwon and Beckett, 2000). This mutant was used in an assay termed BioID, whereby it is fused to a protein of interest and allows biotin labelling of proximal proteins in the cell (Roux et al., 2012). These labelled proteins can then be captured using streptavidin coated beads and analysed using mass spectrometry (Figure 5.5A). Recently an optimised mutant of this protein was developed that allows faster and more selective labelling of adjacent proteins, termed TurboID (Branon et al., 2018).

In order to utilise the TurboID method to identify interactors of Rtf2, first a c-terminal tagging system was produced (Figure 5.5B). The TurboID sequence was cloned into the pAW8 vector along with an internal 3HA tag to allow protein tagging using Cre-Lox

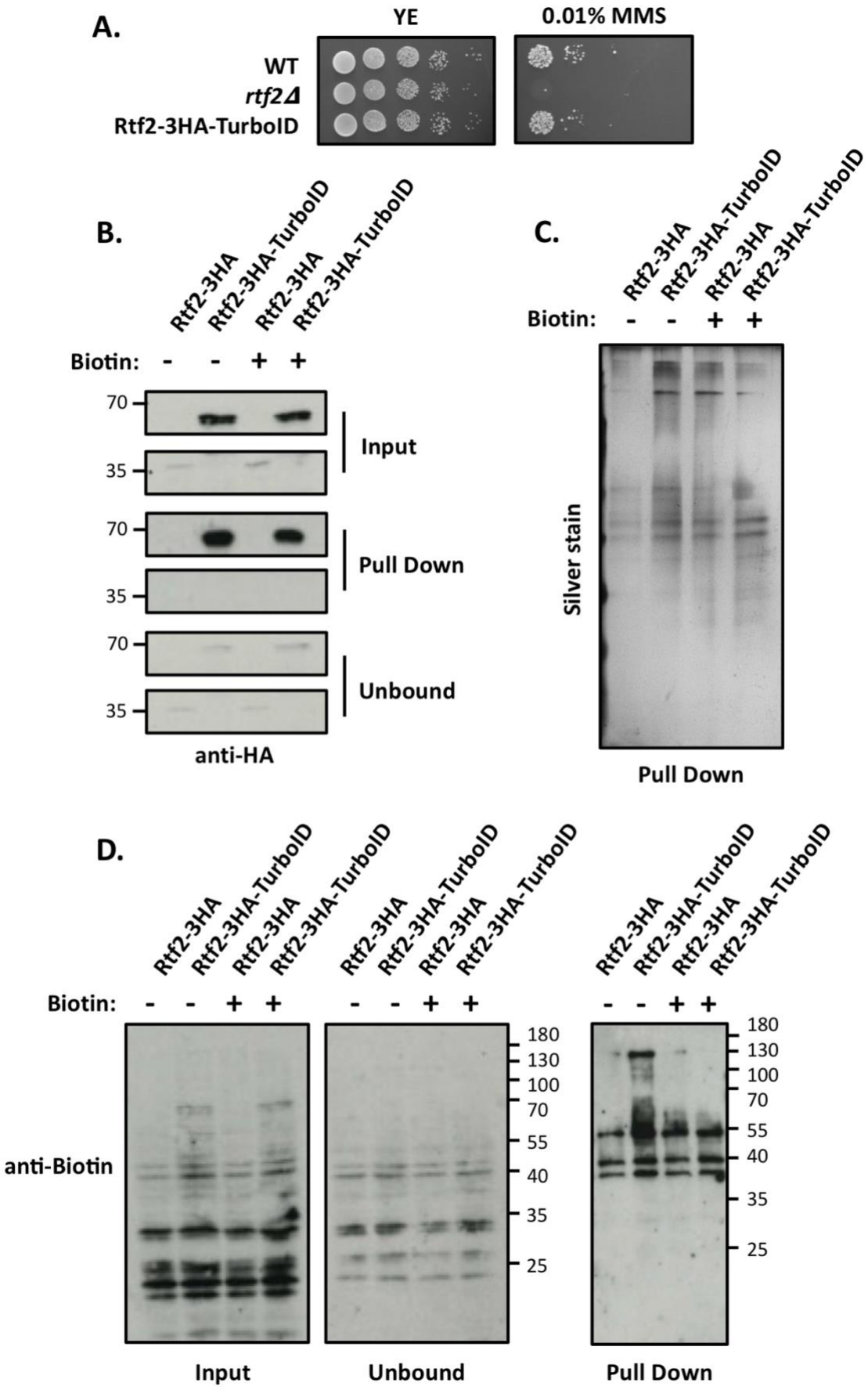
A.
YE
0.01% MMS
WT
rtf2Δ
Rtf2-3HA-TurboID
B.
Rtf2-3HA
Rtf2-3HA-TurboID
Rtf2-3HA
Rtf2-3HA-TurboID
Biotin: - - + +
70
35
Input
70
35
Pull Down
70
35
Unbound
anti-HA
C.
Rtf2-3HA
Rtf2-3HA-TurboID
Rtf2-3HA
Rtf2-3HA-TurboID
Biotin: - - + +
Silver stain
Pull Down
D.
Rtf2-3HA
Rtf2-3HA-TurboID
Rtf2-3HA
Rtf2-3HA-TurboID
Biotin: - - + +
anti-Biotin
180
130
100
70
55
40
35
25
Input
Unbound
Pull Down

Figure 5.6. (previous page) Optimisation of Protocol for Mass Spectrometry Analysis of TurboID tagged Rtf2. Streptavidin pull down of cell extracts containing Rtf2 tagged with 3HA, either with or without TurboID tag. Cells were grown in YE media in the presence or absence of excess biotin (50 µM). **A.** Spot test of WT, *rtf2***Δ** and rtf2-3HA-TurboID cells in the absence and presence of MMS. **B.** Western blot probing for the presence of Rtf2 using anti-HA. **C.** Silver stain analysis of total protein pull down using streptavidin coated beads. **D.** Western blot probed with streptavidin to assess amount of biotinylated proteins pulled down using Streptavidin coated beads.

cassette exchange. Additional cloning of the LoxM and LoxP sites at the C-terminus of the Rtf2 sequence in *S. pombe* cells allowed tagging of the protein by transformation. To ensure the tag did not affect Rtf2 function, a spot test was conducted in which loss of Rtf2 function results in sensitivity to high levels of MMS. There was no evident sensitivity of Rtf2-3HA-TurboID and so the construct could be used for further experiments (Figure 5.6A). Next, confirmation that the TurboID was functional and biotinylating both Rtf2 and other proteins in the cell was needed. Streptavidin pull down of biotinylated proteins confirmed presence of Rtf2 only when the TurboID tag was present when probing with α-HA (Figure 5.6B). Addition of excess biotin (50 µM) to YE media (already containing low levels of biotin) during the growth of the cultures did not affect pull down of biotinylated Rtf2 (Figure 5.6B). However, excess biotin did result in higher background levels of protein biotinylation, as evident from a silver stain of total proteins pulled down by streptavidin (Figure 5.6C). Additionally, when no excess biotin is added there is a clear increase in protein capture when the TurboID tag is present in comparison to Rtf2 tagged with 3HA alone (Figure 5.6C). This observation was further confirmed by probing with Streptavidin-conjugated antibody indicating a clear increase in the levels of biotinylated proteins in both input and pull down samples (Figure 5.6D). The greater capture of biotinylated proteins when the cells have been grown without excess biotin indicates an excess of free biotin may outcompete biotinylated protein binding to the streptavidin beads. Therefore, growth in standard YE media without excess biotin is the optimal condition for mass spectrometry analysis of TurboID tagged proteins.

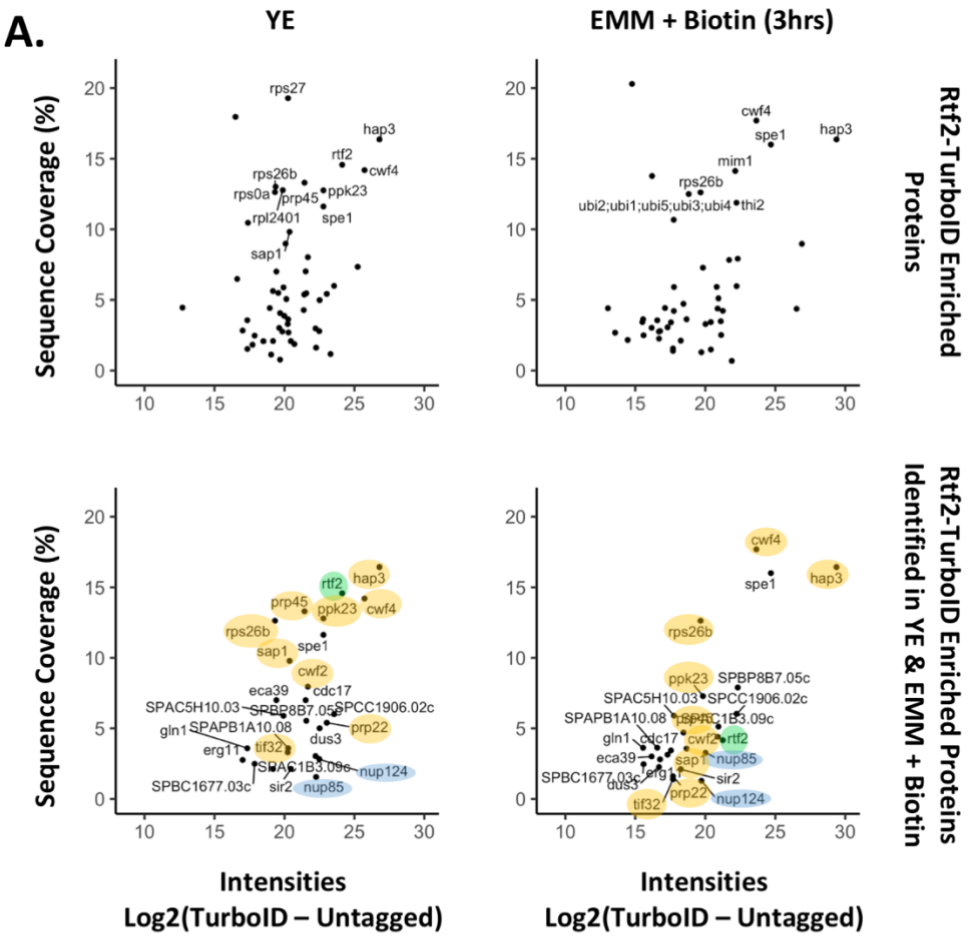
A.
YE
EMM + Biotin (3hrs)
Rtf2-TurboID Enriched Proteins
Rtf2-TurboID Enriched Proteins Identified in YE & EMM + Biotin
Sequence Coverage (%)
Intensities
Log2(TurboID – Untagged)
rps27
hap3
rtf2
cwf4
rps26b
rps0a
prp45
ppk23
rpl2401
spe1
sap1
mim1
ubi2;ubi1;ubi5;ubi3;ubi4
thi2
prp45
cwf2
eca39
cdc17
SPAC5H10.03
SPBP8B7.05c
SPCC1906.02c
gln1
SPAPB1A10.08
prp22
dus3
erg11
tif32
SPAC1B3.09c
nup124
SPBC1677.03c
sir2
nup85
ppk23
SPBP8B7.05c
SPAC5H10.03
SPCC1906.02c
SPAPB1A10.08
SPAC1B3.09c
gln1
cdc17
cwf2
rtf2
eca39
sap1
nup85
SPBC1677.03c
erg11
sir2
dus3
prp22
nup124
tif32

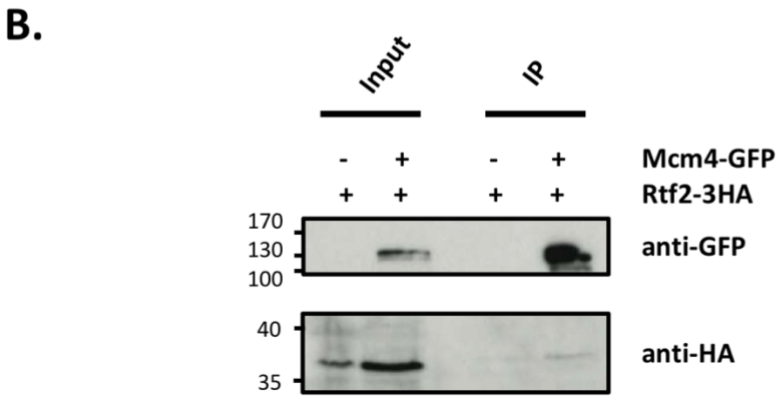
B.
Input
IP
- + - +
+ + + +
Mcm4-GFP
Rtf2-3HA
170
130
100
anti-GFP
40
35
anti-HA

Figure 5.7. (previous page) Proteins Interacting with Rtf2 identified via Co-IP and Mass Spectrometry. A. Mass spectrometry data from Rtf2-3HA-TurboID cells. Raw data was processed using MaxQuant software. Downstream analysis of the intensity values designated to each prey protein was analysed by taking the Log2 value of the difference between Rtf2-3HA and Rtf2-3HA-TurboID intensity values and plotted against protein sequence coverage. Proteins more enriched for Rtf2-3HA were discarded. The top two graphs show all proteins enriched for each experimental condition. The bottom two graphs select for only proteins that were commonly identified when grown in YE or EMM+biotin. Green = Rtf2; Yellow = protein synthesis proteins; blue = nucleoporins. **B.** Co-IP between Mcm4-GFP and Rtf2-3HA. Mcm4 was pulled down using GFP-trap beads and presence of Rtf2 analysed by probing with α-HA. Protein extract from cells containing Rtf2-3HA only was used alongside as a control.

In order to minimize background biotinylation of proteins that may be detected by mass spectrometry, cells can be starved of biotin via growth in minimal media (EMM) and biotin added for only one cell cycle (3 hrs). A preliminary mass spectrometry run (processed by Dr Benno Kuropka at the Institut für Chemie und Biochemie) was conducted using both cells grown in YE without excess biotin and EMM plus biotin for 3 hrs. Cells containing either Rtf2-3HA-TurboID or Rtf2-3HA were analysed to allow identification of proteins enriched specifically due to biotinylation from the presence of the TurboID tag. Raw mass spectrometry data was processed using the MaxQuant software (by Murat Eravci) to provide intensity values for each enriched protein. Intensity values are calculated by the sum of all peptide intensities for that group. Therefore, intensity values can be used as an indicator of the abundance of a protein in each sample. To identify proteins enriched specifically due to biotinylation from the presence of the TurboID tag, intensity values for Rtf2-3HA (untagged) were subtracted from the values for Rtf2-3HA-TurboID (TurboID). Proteins more enriched for the untagged strain were removed and Log2 values plotted against the sequence coverage calculated by MaxQuant (Figure 5.7A). Sequence coverage refers to the percentage of the total protein sequence identified from all peptides detected relating to that protein. Growth in YE media resulted in 53 positive interactors and EMM + biotin identified 49. However, between the two conditions there were 26 common proteins identified. A proportion of the proteins identified are common proteins involved in various biosynthetic pathways that will not be discussed further in this analysis (Table 5.1).

Gene Name	Description
Acs1	Predicted acetyl-CoA ligase
Dus3	Predicted tRNA dihydrouridine synthase
Eca39	Branched chain amino acid aminotransferase
Erg11	Lanosterol 14-demethylase
Gln1	Glutamate-ammonia ligase
SPAC1B3.09c	Predicted Noc complex subunit Noc202
SPAC5H10.03	Phosphoglycerate mutase/6-phosphofructo-2-kinase family
SPAPB1A10.08	Conserved fungal protein
SPBP8B7.05	Predicted carbonic anhydrase nce103
SPCC1906.02c	Predicted CUE domain protein Cue3
Spe1	Ornithine decarboxylase

Table 5.1. Other Proteins Identified as Proximal to Rtf2 via TurboID MS

These proteins are not discussed further due to their large abundance throughout the cell carrying out common biosynthetic pathways that are likely to be identified as interactors of a large proportion of proteins in the cell using this assay. Also, other proteins identified in this assay have been the subject of very little research, thus their function is only predicted and will be emitted from this analysis. As a proof of principle that the experiment was successful in identifying proximal proteins to Rtf2 specifically due to biotinylation from the TurboID tag, Rtf2 itself is expected to be identified due to autobiotinylation. Indeed, Rtf2 was successfully identified in both experimental conditions, albeit with a slightly higher sequence coverage when cells were grown in YE media (Figure 5.7A).

While these results are very preliminary and need multiple technical repeats to allow statistical analysis, a first look at the data provides some interesting observations. For example two nucleoporin proteins, Nup85 and Nup124, that are components of the nuclear pore complex, were identified as being in close proximity to Rtf2. There is an array of research indicating stalled and collapsed replication forks can be relocated to the nuclear periphery for downstream repair processes (Whalen and Freudenreich, 2020). Replication forks blocked at the *RTS1* RFB also appear to be among those that relocate to the nuclear pore complex for repair (Sarah Lambert, personal communication). This could indicate Rtf2 plays a role in directing *RTS1* stalled replication forks to the nuclear periphery. However, the reduced levels of replication fork stalling

at *RTS1* when Rtf2 is deleted may suggest it is not directly involved in directing the blocked replication forks to the nuclear pore. HR in the context of DNA breaks have previously been shown to only continue HR repair following re-location to the nuclear pore (Ryu et al., 2015). Thus, if Rtf2 was important for directing *RTS1* stalled replication forks to the nuclear pore to allow HR-restart, one would expect reduced levels of replication restart due to an inability to restart rather than reduced efficiency of the RFB as is shown here for Rtf2 delete cells.

Additionally, DSBs arising in rDNA repeats can also be relocated to the nuclear pore complex important for maintaining repeat stability (Horigome et al., 2019). The Sap1 protein was also identified which is important for the activity of the RFB located in the spacer region of rDNA repeats (Krings and Bastia, 2005), as well as Sir2 a histone deacetylase involved in heterochromatin assembly at these locations (Shankaranarayana et al., 2003). Furthermore, a 40S ribosomal protein (Rps26b) and RNA polymerase II promoter binding protein (Hap3/Php3). The serine/threonine protein kinase, ppk23 (Cdk11), was also identified, which is important for the assembly of the RNA polymerase II mediator complex and thus the downstream activation of RNA polymerase II transcription (Drogat et al., 2012). Additionally, a number of proteins identified in this mass spectrometry analysis are involved in mRNA splicing, including mRNA splicing proteins (Cwf2, Cwf4, Prp45) and a DExH-box RNA helicase (Prp22). The translation initiator protein, Tif32 (elF3α), was also identified suggesting Rtf2 may be involved in translation initiation. Perhaps Rtf2 plays a role in not only directing *RTS1* stalled replication forks to the nuclear periphery for repair, but also other stalled replication forks including those arising from replication transcription collisions.

These preliminary results did not identify any replisomes components. However, Co-IP of Rtf2 and Mcm4 revealed an interaction between the two proteins (Figure 5.7B). Previous studies have also identified an interaction between Rtf2 and PCNA (*Sp*Pcn1) (Inagawa et al., 2009). The only protein involved in DNA replication identified in the MS data was Cdc17 (DNA Ligase I), important for ligation of Okazaki fragments (Nasmyth and Nurse, 1981). Additionally, Rtf1 was expected to be identified due to both Rtf2 and

Rtf1 being important for *RTS1* barrier activity. Therefore, although these results were surprising, more repeats are needed to confidently identify proximal proteins to Rtf2.

5.3 Discussion

Investigation into the role of Rtf2 in the restart of replication forks has revealed several key characteristics. Firstly, Rtf2 is confirmed to be important to enhance the blocking capacity of the *RTS1* RFB. The data presented here add further insight into the previously published results showing a decrease in pausing signal at *RTS1* in the absence of Rtf2 when analysed by 2D gels (Codlin and Dalgaard, 2003). Polymerase usage sequencing of *RTS1* in the absence of Rtf2 lead to a reduced level of δ/δ replication downstream of active *RTS1* (Figure 5.1). Additionally, there is an equivalent reduction in the levels of replication fork slippage downstream of active *RTS1* when Rtf2 is deleted (Figure 5.1). These data suggest that a subset of replication forks do not get blocked at *RTS1* and continue replication as a canonical replication fork, or that they do get blocked but rather restart as a canonical RF. However, when taking into consideration the previously published 2D gel data showing a reduction in pausing at *RTS1* (Codlin and Dalgaard, 2003), it seems more likely that fewer replication forks stall at *RTS1* when Rtf2 is deleted. Indeed, mathematical modelling of the efficiency of the *RTS1* RFB in the absence of Rtf2 supports a reduced efficiency of the barrier to block replication forks rather than a subset of forks blocked at *RTS1* restarting as a canonical RF.

Furthermore, Rtf2 was previously suggested to produce its enhancing effect on the blocking capacity of *RTS1* via interaction with *RTS1* Region A (Codlin and Dalgaard, 2003). However, in the *RTS1* system presented here, region A is dispensable to the blocking capacity of *RTS1* as the levels of both δ/δ replication and replication fork slippage downstream of active *RTS1* are unaffected by the deletion of Region A (Figure 5.2). Exactly how Rtf2 acts at replication forks encountering *RTS1* to produce efficient replication fork stalling remains to be elucidated. To explore this further, several C-terminally tagged Rtf2 strains were successfully produced (Figure 5.3). Both tag functionality and protein functionality have been confirmed using a variety of assays and

will provide as a useful tool for future investigation into the role of Rtf2 in replication fork restart.

Removal of Rtf2 from stalled replication forks upon replication stress has recently been implicated as being important for replication fork restart and maintaining genome stability in human cells (Kottemann et al., 2018, Suo et al., 2020). In *S. pombe* deletion of Rtf2 only renders cells sensitive to high doses of MMS, but not to HU as is found in human cells (Figure 5.5). Furthermore, the studies in human cells show evidence for proteasomal degradation of RTF2 following removal from stalled replication forks. However, the levels of Rtf2 in *S. pombe* appear to remain fairly stable after HU treatment (Figure 5.5). However, this could indicate either very little or no proteasomal degradation of Rtf2, or alternatively, that Rtf2 is rapidly turned over in *S. pombe*. Another possibility is that only a small fraction of total Rtf2 in a cell is active at replication forks and the remainder is instead involved in other cell processes, thus if a small fraction only was degraded a decrease in protein levels would not be visible.

When analysing the effect of HU and MMS treatment on levels of replication fork slippage, there is a reduction in levels when Rtf2 is deleted with the most pronounced effect after MMS treatment. *S. pombe* cells are also sensitive to MMS when Rtf2 is deleted. Perhaps the overall reduction in cell survival after MMS treatment masks the true levels of mutagenicity in this context. Furthermore, both MMS and HU treatment appear to slightly reduce the levels of the fraction of chromatin bound Rtf2 molecules (Figure 5.5). This could support the notion that Rtf2 is removed from stalled replication forks to allow efficient restart. However, further experiments specifically selecting for S phase cells could provide a clearer insight into if this is the case.

To explore Rtf2's interaction with the replisome co-immunoprecipitation with the MCM subunit Mcm4 was first investigated (Figure 5.7). Rtf2 was successfully pulled down with Mcm4 which supports previous findings that Rtf2 interacts with the sliding clamp PCNA (Inagawa et al., 2009). Additional support for Rtf2 interacting with the replisome comes from experiments in human cells that find RTF2 enriched on nascent DNA and being involved in replication fork restart upon replication stress (Dungrawala et al., 2015,

Kottemann et al., 2018). Subsequently, a TurboID proximity labelling based mass spectrometry method was successfully set up in *S. pombe* to investigate into proteins that interact with Rtf2. The idea is that this might promote new ideas about how Rtf2 acts and particularly how it is involved in replication fork restart. The preliminary data has indeed provided some suggestions into the role of Rtf2. Although, preliminary mass spectrometry results did not identify replisome components, it did suggest a possible role for Rtf2 in the processing of stalled replication forks. Rtf2 is a highly abundant protein and therefore its action specifically at replication forks may only account for a small portion of its interacting partners, indicating it may have additional roles within the cell. Additional mass spectrometry experiments, studying the interaction of Rtf2 and PCNA/Mcm4 and analysis after HU/MMS treatment will provide further insight into the role of Rtf2. Further, we will follow recruitment of Rtf2 to an origin in G1/S. Moreover, analysis of Mud1 (*Hs*DDI1, *Sc*Ddi1) deleted cells by Pu-Seq and utilisation of sumoylation and ubiquitylation mutants that render the cells unable to target Rtf2 for proteasomal degradation will provide direct evidence if Rtf2 is removed from stalled replication forks as is seen in human cells. This could provide key information on the mechanism behind which the Rtf2 protein acts in replication fork stalling and restart.

Chapter 6 – Discussion

6.1 Optimised *RTS1* Replication Fork Barrier System to Investigate HR-Restarted Replication Forks

The *RTS1* replication fork barrier in *S. pombe* has been used by several laboratories to study the collapse of replication forks and their restart. A key issue with using this system to specifically study the restarted replication fork is the time it takes for replication forks to restart replication following stalling. This allows canonical replication forks travelling from the opposite direction to rescue replication forks stalled at *RTS1* before they have the chance to restart and replicate the downstream region. This project successfully produces an optimised *RTS1* system to allow the study of the restarted replication forks with significantly reduced interference from convergent canonical replication forks. The *RTS1* RFB was placed in an orientation that blocks replication forks originating from an efficient early firing origin. Downstream rDNA RFBs were positioned to delay converging replication forks from distal late firing origins. The rDNA RFBs were shown to successfully delay replication fork progression without the production of a HR-restarted replication fork, resulting in the continuing of replication in the canonical ε/δ manner.

Utilising polymerase-usage sequencing it was confirmed that the restarted replication fork was able to travel up to 10 Kb with little interference from canonical convergent replication forks. This allowed direct visualization that replication of both strands after restart at *RTS1* is conducted by Polymerase δ (Figure 6.1). This confirms previous findings that Polδ replicates both the leading and lagging strand after HR-restart at *RTS1* when tested by alkali liability of each strand after rNTP incorporation using the rNTP permissive *cdc6* and *cdc20* mutant alleles used for Pu-Seq (Miyabe et al., 2015). The Pu-Seq data presented here adds to the previous study by demonstrating that Polδ is not only utilised for initial replication fork restart, but maintains leading strand replication for at least 10 Kb, before terminating with the convergent canonical replication fork. Taking into consideration recent findings that the increased template switch events associated with HR-restarted replication forks at *RTS1* can be detected as far as 75 Kb

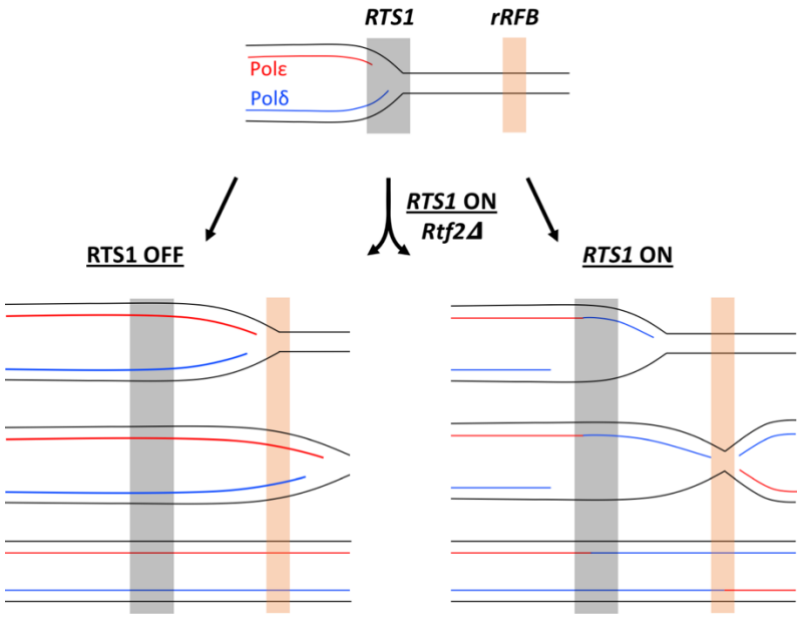

Figure 6.1. Replication Fork Movement and Polymerase Usage During HR-Restart at the Optimised RTS1 Construct. The *RTS1* RFB is ON when bound by Rtf1 and OFF when cells are deleted for Rtf1. Replication across this region travels in a predominantly rightward direction. When RTS1 is OFF (*left*), replication is conducted by the canonical ε/δ RF. When *RTS1* is ON (*right*), RFs stall at *RTS1* and restart using Polδ to replicate both leading and lagging strands. The downstream rRFB's delay the convergent canonical RF allowing time for the restarted RF to replicate the region downstream of *RTS1*. When Rtf2 is deleted, the efficiency of *RTS1* barrier activity decreases resulting in some forks restarting using a δ/δ RF, and some remaining as a canonical ε/δ RF.

downstream of restart (Jalan et al., 2019), this suggests Polδ continues replication of both strands after restart in scenarios requiring much longer range synthesis.

The Carr lab has previously shown that the production of dicentric chromosomes due to replication U-turns after restart at *RTS1* in the presence of inverted repeats decreased with distance and plateaus when the inverted repeat is placed over 2 Kb away from the RFB (Mizuno et al., 2013). One interpretation of this could be that the fork matures, possibly by switching for Polδ to Polε. It is also possible that the level of mutagenesis in this context may continue for longer distances if the assay was used in the optimised system presented here, i.e by removing any interference from convergent replication forks faithfully replicating the region. However, the observation that restarted forks retain a δ/δ configuration over ~10Kb suggests that the replication fork does not mature back into a canonical replication fork and instead remains as an error-prone δ/δ replication fork for long stretches of downstream regions before encountering a convergent replication fork or reaching the end of the template. It will be interesting to establish why the initial few kb of HR restarted replication is significantly more error prone (Mizuno et al., 2013): one possibility is it reflects a switch from the D-loop replication to semi conservative replication.

The increased levels of mutagenesis associated with *RTS1* restarted replication forks is known to not be solely due to the use of Polδ replicating both leading and lagging strands (Miyabe et al., 2015). This suggests other proteins may be involved in driving the mutagenicity of the restarted replication fork. This project exploits the optimised *RTS1* barrier to set up a synchronised ChIP-qPCR assay to allow investigation into the recruitment of proteins involved specifically in the restarted replication fork. In the future it would be interesting to probe for differences in helicase enrichment at the restarted replication fork to establish if this differs from the canonical CMG replicative helicase. There are several candidate helicases that have been reported to be involved in recombination dependent restarted replication, including Srs2, Fbh1, Rqh1, Fml1, and Pfh1. Srs2 and Fbh1 are known to have antirecombinogenic activities via dissociating Rad51 from pre-synaptic filaments (Liu et al., 2011, Tsutsui et al., 2014). Both Srs2 and Fbh1 have been show to limit ectopic recombination and template switch events that

are associated with HR-restart at *RTS1* (Jalan et al., 2019, Lorenz et al., 2009). Although the action of these two helicases compliment one another, Srs2 is found to be important to promote restart at *RTS1*, which contrasts to findings that Fbh1 is dispensible during this step (Inagawa et al., 2009, Lambert et al., 2010, Lorenz et al., 2009).

Rqh1 also limits mutagenesis of HR-restarted replication forks, possibly via D-loop dissasembly preventing multiple strand invasion events. It has been suggested that loss of Rqh1 results in a loss of recombination intermediates if chromatin cannot be formed on the D-loop to stabilise it (Pietrobon et al., 2014). Rqh1 is dispensible for restart at *RTS1* but is important for suppressing genome rearrangemets and template switches associated with the restarted replication fork (Jalan et al., 2019, Lambert et al., 2010). Fml1 deletions result in a reduction of gene conversion events associated with *RTS1* restarted replication forks without effecting deletion events, indicating Fml1 may play a role in limiting multiple strand invasion events (Jalan et al., 2019, Sun et al., 2008). Fml1 has also been implicated in limiting deleterious events associated with convergence of a canonical replication fork with a collapsed fork at *RTS1* (Morrow et al., 2017, Wong et al., 2019). The authors propose Fml1 to be important for restoring a regressed replication fork stalled at *RTS1* to counteract detrimental recombination intermediates.

It has recently been proposed that Pfh1 (*Sc*Pif1) is the helicase responsible for driving HR-restarted replication forks by analysis using mutational assays (Jalan et al., 2019). Pfh1 has previously been identified as being important in overcoming several protein-DNA barriers, including *RTS1,* rDNA RFBs, and at tRNA genes by using its sweepase activity to remove tightly bound proteins and to allow replication fork merging at the site of the barrier (Sabouri et al., 2012, Steinacher et al., 2012). Moreover, Pfh1 is important for enabling the restart of RFs stalled at *RTS1*, but was also shown to be important for suppressing template switch events when the restarted replication fork was given extra time to replicate the downstream region by deletion of distal origins (Jalan et al., 2019). Although, due to limitations of the genetic mutation assays when used on their own, it is unclear whether the suppression of template switch further downstream of *RTS1* is due to Pfh1 being important for efficient termination of a restarted and canonical replication fork.

A more definitive picture of Pfh1 involvement could be unravelled by the use of the system described here. Direct comparison of helicase enrichment downstream of *RTS1* can be directly compared to Pu-Seq traces, providing a definitive answer of Pfh1 involvement in restarted replication forks. Is Pfh1 just involved in the establishment of HR-restarted replication forks? Or is it necessary to drive the δ/δ replication fork? This system could also be used to investigate if any other replisome factors apart from helicases or polymerases are involved in HR-restart or are lost from the restarted replication fork. Additionally, incorporation of a replication fork slippage assay into the optimised *RTS1* system presented here allows for a direct read out of the mutagenicity of the restarted RF in different genetic backgrounds.

6.2 BIR vs. HR-Restart at *RTS1*

Break induced replication in *S. cerevisiae* is used to repair one-ended DSBs that can arise from the collapse of replication forks. HR-restart at *RTS1* in *S. pombe* is break independent and occurs via semi-coservative replication in contrast to conservative replication produced from BIR. A key feature that is shared between these two repair methods is the importance of Polymerase δ. Both BIR and HR-restart at *RTS1* use Polδ to complete replication of both the leading and lagging strand after replication fork restart (Donnianni et al., 2019, Miyabe et al., 2015, Naiman et al., 2020). This observation was confirmed for HR-restart in *S. pombe* by Pu-Seq of the optimised *RTS1* construct presented here (discussed above). The Pol32 subunit of Polδ is essential for BIR and its interaction with PCNA has been shown to be important to allow BIR to occur efficiently (Lydeard et al., 2007, Lydeard et al., 2010). The sub-project presented here (Chapter 4) aimed to investigate whether Cdc27 (*Sc*Pol32) and its interaction with PCNA was similarly important for HR-restart at *RTS1*.

Full deletion of Cdc27 was unable to be analysed due to it causing lethality in *S. pombe*. However, PCNA mutations shown to be defective in BIR in *S. cerevisiae*, as well as Cdc27 mutants truncated for its PCNA interaction motif could be used to investigate their impact on HR-restart at *RTS1*. Surprisingly, the PCNA mutants acted differently to the

Cdc27 truncations. This could be due to the fact that the point mutations found in *S. cerevisiae* that confer a BIR defect were mapped directly onto *S. pombe* PCNA and thus may have different impacts on the proteins function. Nevertheless, each of the PCNA single point mutants (R80A and F248A) are shown to limit mutagenesis of the restarted replication fork without effecting the levels of restart, as evident from the wildtype levels of Polδ usage downstream of active *RTS1*. The double PCNA point mutant (F248A,F249A) originally identified in *S. cerevisiae* rendered cells sick even in the absence of any replication stressing agents and thus could not be used. Potentially, different results would be obtained if this mutant was able to be further analysed and may indicate that it is a more crucial mutation with regard to its interaction with Cdc27. Despite this it is interesting and unexpected that the two separate PCNA point mutations can confer the restarted replication fork with more fidelity while not effecting the efficiency of restart.

It is known that PIP (PCNA-interacting protein) motifs are present in all three subunits of the *S. cerevisiae* Polδ holoenzyme, as well as three out of four of the *S. pombe* and *H. sapiens* subunits (Acharya et al., 2011, Bermudez et al., 2002, Ducoux et al., 2001, Li et al., 2006, Reynolds et al., 1998), and that these PIP motifs are important for the processivity of the Polδ complex. Cdc27 (*Sc*Pol32) truncation mutants deleted for the PIP motif (*cdc27_D1* and *cdc27_D3*) were used to analyse the interaction between Cdc27 and PCNA in replication fork restart at *RTS1*. Both of these mutants resulted in reduced levels of Polymerase δ bias downstream of active *RTS1*. This reduction in Polymerase δ bias may reflect several possibilities that are not mutually exclusive (Figure 6.2): (1) less replication forks able to restart in the allotted time and a proportion of arrested forks are instead rescued by convergence of a canonical replication fork; (2) replication forks take a longer time to overcome the *RTS1* RFB and thus do not replicate as far along the dowstream region in comparison to wildtype due to the increased time for converging forks to approach; (3) the restarted replication fork restarts as in a WT situation but the restarted replication fork has reduced processivity and thus does not replicate as far along the downstream region due to its slow kinetics. In the future it would be interesting to conduct 2D gel analysis of the levels of RF stalling and restart at

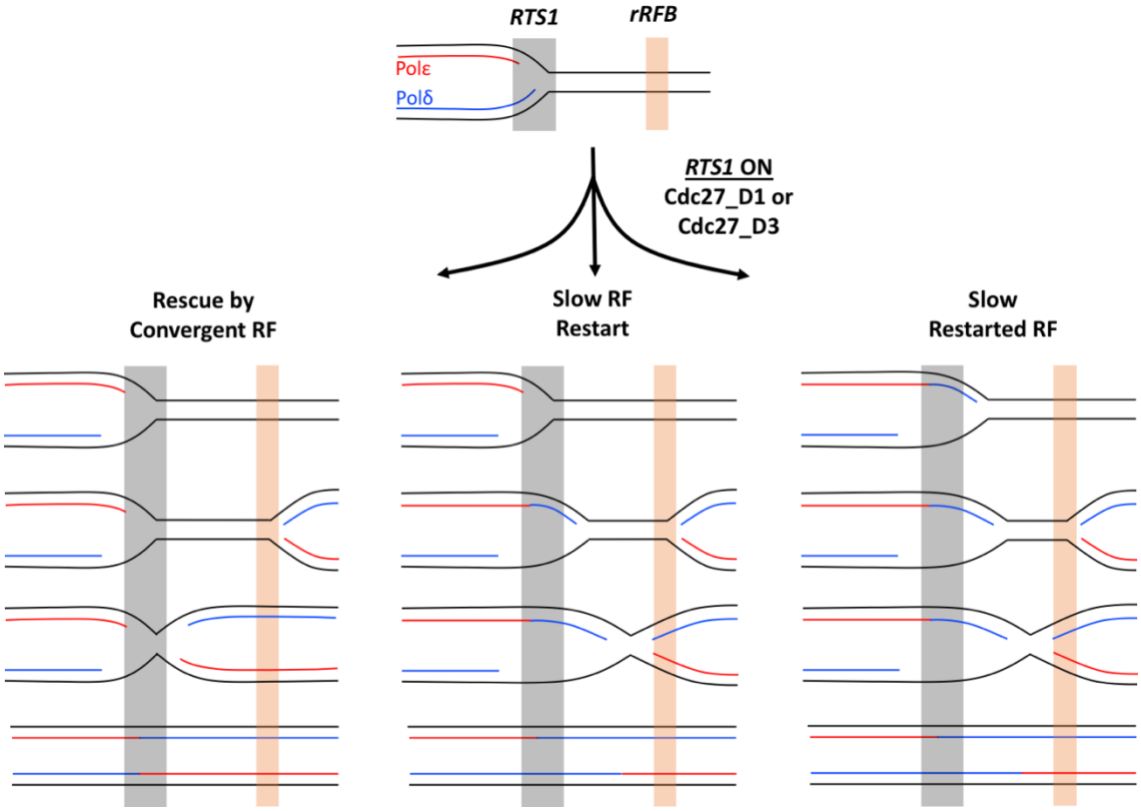

Figure 6.2. Three Modes of Replication Fork Movement and Polymerase Usage During HR-Restart at RTS1 when Cdc27 Lacks the PIP Motif. *Left*: RFs stall at *RTS1* and are unable to restart in the allotted time resulting in rescue by convergence of a canonical RF. *Middle*: RFs stall at *RTS1* and take longer to restart resulting in a shorter region replicated downstream using Polδ to replicate both leading and lagging strands. *Right*: RFs stalled at *RTS1* restart as wildtype but proceed with reduced processivity resulting in a shorter region replicated downstream using Polδ to replicate both leading and lagging strands.

RTS1 to compare with the changes found for polymerase usage. This will help us distinguish between these scenarios.

The PIP motif of Pol32 in *S. cerevisiae* (Pol32) has little impact on Polδ processivity *in vitro* (Gerik et al., 1998, Johansson et al., 2004). However, in the absence of Pol32 PIP, the PIP motifs found in the two other Polδ subunits (Pol3 and Pol31) become essential for cell survival (Acharya et al., 2011). In contrast, loss of the *S. pombe* Cdc27 PIP motif has been shown to reduce Polδ processivity *in vitro* (Bermudez et al., 2002). Therefore, the substantial reduction in the distance the restarted replication fork is able to replicate may be due to this reduction in processivity having a large impact on forks using soley Polδ for replication. Additionally, recent data from the lab has lead to the view that the leading strand of *RTS1* restarted replication forks is replicated first, with the lagging strand left as ssDNA and filled in later (Naiman et al., 2020). If this is the case, it makes sense that Polδ usage does not travel as far along the DNA on both leading and lagging strands, due to the leading strand replicated by Polδ having reduced processivity if Cdc27 is truncated for its PIP motif, and thus a shorter tract of ssDNA would also be left on the lagging strand to be replicated later by Polδ. Additionally, due to estimates of the length of time it takes to overcome the *RTS1* RFB, it has been calculated using a Monte Carlo computational modelling method that the restarted replication fork actually travels at a rate faster than canonical replication forks (Naiman et al., 2020). Therefore, proper tethering of Polδ to PCNA may be an important factor in this process.

Both Cdc27 truncations exhibited the same levels of replication fork slippage downstream of active *RTS1* in comparison to WT contrasting to the reduction seen for the PCNA point mutants. However, both Cdc27 mutants showed higher levels of replication fork slippage when *RTS1* is OFF indicating an intrinsically increased level of background mutagenesis that may mask a decrease in replication fork slippage when *RTS1* is ON. Indeed if we look at the increase between on and off rates, then there is a difference which would reflect the reduced number of times the locus is replicated by the HR-restarted fork (fold increase of slippage downstream of *RTS1* ON vs. OFF for WT = x30, Cdc27_D1 = x11, Cdc27_D3 = x6). A study in *S. cerevisiae* using Pol32 mutants defective for PCNA binding resulted in reduced levels of mutagenesis following high

levels of UV induced DNA damage (Johansson et al., 2004). However, this is likely due to its role in associating with Polymerase Zeta for translesion synthesis, not reported for Cdc27 in *S. pombe* (Acharya et al., 2009).

In *S. cerevisiae* the mere presence of PCNA has been shown to also decrease the fidelity of Polymerase δ in the context of mismatched bases (Hashimoto et al., 2003). Therefore, disruption of the Polδ-PCNA interaction could explain the decrease in replication fork slippage observed for the PCNA point mutants when *RTS1* is ON. Although, this contrasts to the Cdc27 truncations, due to increased levels of replication fork slippage when *RTS1* is OFF indicating loss of Cdc27 interaction with PCNA decreases fidelity of a canonical replication fork. It is of note that the shorter truncation (*cdc27_D3*) exhibited less background replication fork slippage than the larger truncation (*cdc27_D1*). This could be due to Cdc27_D1 also losing the Polα interaction motif. This motif appears to be dispensible for HR-restart at *RTS1* due to both Cdc27 mutants exhibiting the same levels of Polδ bias. However, this could be directly investigated using a Cdc27 mutant truncated for only this intermediate region. Although, it is unlikely any effect would be present due to Polα being found to not play a substantial role in *RTS1* restarted replication forks (Naiman et al., 2020).

Overall, the Cdc27 mutants identify key differences between BIR and HR-restart at *RTS1* in *S. pombe*. The interaction between PCNA and Cdc27 is shown to be important for restart, but are not as important as that evidenced for BIR in *S. cerevisae.* The PCNA point mutants do not exhibit the same defect as the Cdc27 mutants and require further characterisation to understand the mechanism of increased fidelity of the restarted replication fork.

6.3 Role of Rtf2 in Replication Fork Restart

The Rtf2 protein was originally identified as having a role in enhancing the blocking capacity of the *RTS1* RFB in *S. pombe* (Codlin and Dalgaard, 2003). 2D gel analysis revealed a reduced pausing signal when cells were deleted for Rtf2. Another study

identified a visible increase in large Y-intermediates and was interpreted as Rtf2 being important to allow the restart of replication forks (Inagawa et al., 2009). However, the data here confirms the reduced pausing signal at *RTS1* corresponds to a decreased level of δ/δ restarted replication forks and an increased level of forks simply passing through the barrier unperturbed. Furthermore, the increased levels of replication fork slippage that is evident when the *RTS1* barrier is ON in comparison to OFF is similary reduced when Rtf2 is deleted. The data presented here confirms Rtf2 is needed for efficient replication fork barrier activity of *RTS1* and are consistent with the interpretation that, in the absence of Rtf2, a portion of replication forks are able to bypass the barrier and continue replication as a canonical ε/δ replication fork (Figure 6.1).

Originally Rtf2 was suggested to enhance the blocking capacity of *RTS1* via interaction with Region A of the *RTS1* sequence (Codlin and Dalgaard, 2003). These researchers identified similarly reduced levels of replication fork stalling at *RTS1* when Rtf2 or *RTS1* region A was deleted when analysed using 2D gels. There was no additive effect when both deletions were combined and was thus proposed Rtf2 acts through Region A to allow efficient replication fork stalling at *RTS1.* Here, utilising these deletions for analysis of polymerase usage of the restarted replication fork identified region A to be dispensible for the blocking capacity of *RTS1*. There was no change to δ/δ replication or the levels of replication fork slippage downstream of active *RTS1* when Region A was deleted. Therefore, these results contrast to previous findings, identifying Region A of *RTS1* to be dispensible for the efficiency of barrier activity and to not be the site of Rtf2 interaction.

Other factors have previously been identified to also reduce the blocking signal at *RTS1* when analysed by 2D gels without completely abolishing it. The fork protection components Swi1/Swi3 are essential for the blocking capacity of *RTS1*, but its associated protein, Mrc1, results in a reduction in signal similar to Rtf2 (Zech et al., 2015). The reduction in replication fork stalling when Mrc1 is deleted is evident at a variety of barriers including *RTS1,* rDNA RFBs and tRNA genes, and is dependent on the DNA binding domain of Mrc1 (Zech et al., 2015). Whether Mrc1 and Rtf2 act in similar or distinct ways at *RTS1* to enhance the replication fork barrier activity are yet to be

established. Mrc1 travels with the replication fork to enact its function on replication fork protection. Rtf2 in human cells has indeed been shown to be enriched at nascent chromatin (Dungrawala et al., 2015, Kottemann et al., 2018). However, the data presented here have determined that Rtf2 at least does not act on *RTS1* via interaction with Region A, and thus, perhaps they enhance the blocking capacity of *RTS1* in distinct ways. If Rtf2 acted in a similar way to Mrc1 it could also be found to travel with the replication fork as Mrc1 does, which has been suggested for RTF2 in human cells (Kottemann et al., 2018). It would be interesting to investigate polymerase usage downstream of active *RTS1* in Mrc1 deficient cells via Pu-Seq to see if there is the same reduction in polymerase switching as is evident for Rtf2 delete cells. It is also noteworthy that although Mrc1 reduces replication fork stalling at a variety of barriers in *S. pombe*, this is not the case in *S. cerevisiae* (Hodgson et al., 2007, Mohanty et al., 2006, Tourriere et al., 2005). Additionally, Rtf2 has not been identified in *S. cerevisiae,* and thus, slightly different mechanisms of overcoming these obstacles must have evolved. Initial single molecule microscopy experiments have indicated Rtf2 may be removed from stalled replication forks due to a reduction in chromatin bound Rtf2 after treatment with the replication stressing agents HU and MMS. This supports research in human cells proposing RTF2 is targetted for the proteasome upon replication fork stalling to allow replication fork restart (Kottemann et al., 2018). Further experiments selecting for cells in S phase will provide clear evidence if Rtf2 is removed from HU/MMS stalled replication forks which could indicate its mechanism of action at *RTS1* stalled replication forks.

Rtf2 (*At*Rtf2) has also been identified in *Arabidopsis thaliana* but was found to be an essential protein that contains an additional unconsesrved N-terminal extension not present in human or *S. pombe* Rtf2 (Sasaki et al., 2015). These authors conducted mass spectrometry on *At*Rtf2 to investigate protein interacting partners and identified an array of proteins involved in mRNA splicing, Ribosome proteins, RNA binding and metabolism, as well as DNA binding proteins. They also conducted mass spectrometry on *At*Rtf2 truncated for the unconserved N-terminal domain and found many of the same proteins indicating this may be conserved between *S. pombe* and humans. Indeed, mass spectrometry conducted on *S. pombe* Rtf2 presented here also identified mRNA

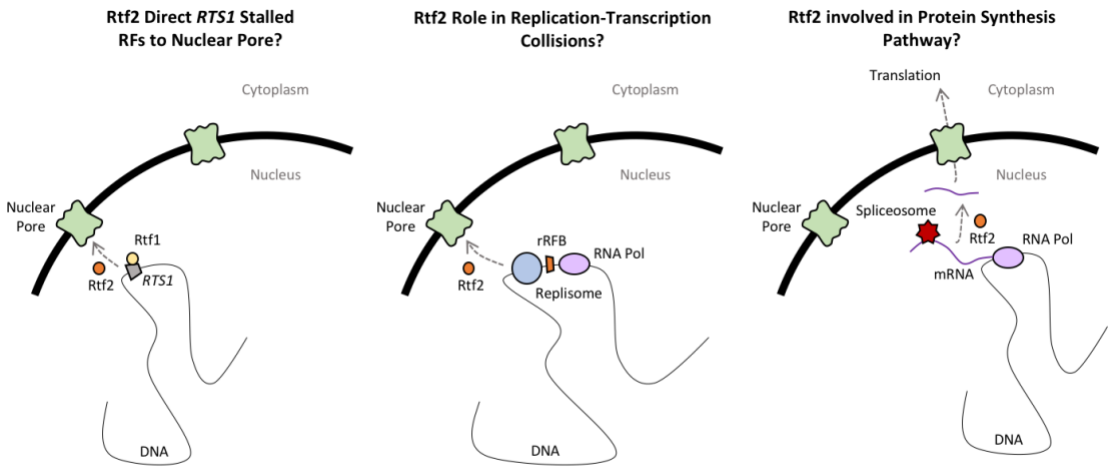

Figure 6.3. Possible Roles of Rtf2. *Left*: Rtf2 may be involved in directing RFs stalled at *RTS1* to the nuclear pore to allow efficient restart. *Middle*: Rtf2 may play a role during replication-transcription collisions, possibly stabilising the RF and directing to the nuclear pore for restart or repair. *Right*: Rtf2 may play a role during protein synthesis, regulating mRNA Splicing or translation initiation by interacting with the spliceosome, nuclear pore, or translation initiation factors.

splicing factors, ribosomal proteins, and others involved in RNA metabolism as well as translation initiation, indicating it may play a similar role to that found in *A. thaliana* (Sasaki et al., 2015).

Not only did the study in *A. thaliana* identify mRNA splicing genes, it also detected mRNA splicing defects when Rtf2 was deleted. Interestingly, a genome wide screen in *S. pombe* for factors affecting mRNA splicing also identified deletion of Rtf2 to result in splicing defects (Larson et al., 2016). Therefore, along with the identification of other splicing genes being proximal to Rtf2 in the preliminary MS experiments presented here, these results may indicate Rtf2 as having a role during mRNA splicing. In the future it would be interesting to investigate if Rtf2 is involved in the correct splicing of Rtf1 which could indicate its mechanism of action at *RTS1* to allow efficient replication fork stalling at the RFB. However, Mcm4 was also found to co-immunoprecipitate with Rtf2 supporting a role for Rtf2 at replication forks due to previous findings Rtf2 also interacts with PCNA in *S. pombe* (Inagawa et al., 2009). Further repeats of Rtf2-TurboID mass spectrometry may reveal DNA binding proteins and replisome components as has been suggested by

research in human cells (Kottemann et al., 2018). However, due to the streptavidin beads used for TurboID MS having a high affinity for biotin, this may have hindered the identification of all proximity labelled proteins. Highly biotiylated proteins may not have eluted off the beads as readily as less biotinylated proteins, and thus further optimisation of this step in the protocol may be needed. One possibility is to use on bead digestion which could reveal replisome components expected to interact with Rtf2. Additionally, treatment with HU/MMS prior to mass spectrometry may result in different capture of proteins, hopefully shedding light on the role of Rtf2 during replication stress.

Despite preliminary MS results not identifying components of the replisome as expected, several interesting factors were identified as in *A. thaliana* that could reveal other roles of Rtf2 within the cell (Figure 6.3). Identification of proteins involved in transcription as well as the rDNA RFB binding protein Sap1 could indicate Rtf2 plays a role at other stalled replication forks arising due to replication transcription collisions. Although, Pu-seq analysis of *rtf2***Δ** strains identified no obvious genome wide phenotype or changes to polymerase usage at the native rDNA loci. It would be interesting to directly test this in the future on the rRFB Pu-seq constructs in an *rtf2***Δ** background to provide a clearer picture of the involvement of Rtf2 at other stalled replication forks.

Additionally, two nucleoporins were identified that are components of the nuclear pore complex. Transcriptionally active genes have been shown to associate with nuclear pore complexes upon induction of transcription in *S. cerevisiae* (Casolari et al., 2004). This relocation of genes to the nuclear pore complex has also been shown to be important to promote transcription (Taddei et al., 2006), as well as playing a role in gene silencing (Van de Vosse et al., 2013). Furthermore, release of the transcribed gene through the nuclear pore has been indicated to be important to allow replication to continue across the region unhindered in *S. cerevisiae* (Bermejo et al., 2011). Repetitive sequences that have the possibility of forming secondary structures that can stall replication forks have also been shown to be directed to the nuclear pore to maintain repeat stability (Su et al., 2015). Moreover, HR in the context of shortened telomeres has similarly been shown to be directed to the nuclear pore for efficient repair (Churikov et al., 2016). In the

context of DSBs, HR was found to only be able to continue repair once re-located to the nuclear pore (Ryu et al., 2015). Recently, *RTS1* has also been indicated to be directed to the nuclear pore for restart (Sarah Lambert, persoal communication). Therefore, the preliminary MS results presented here may indicate Rtf2 is involved in directing not only *RTS1* restarted replication forks to the nuclear pore, but also other stalled replication forks such as those arising from replication-transcription collisions to allow RF restart and maintain genome stability.

Furthermore, it is know that the SUMO-protease Ulp1 (ubiquitin like specific protease 1) is at nuclear pores in *S. cerevisiae* (Palancade et al., 2007). This could provide a possible link between the identification that deletion of Pmt3 (*S. pombe* SUMO) results in a similar decrease in replication fork stalling at *RTS1* as Rtf2 deletion (Inagawa et al., 2009). This may suggest that relocation of *RTS1* blocked forks to the nuclear pore may be important for sumoylation of Rtf2 to allow downstream removal and restart of the replication fork. Alternatively, due to Rtf2 containing a Ring motif similar to that found in the E3 SUMO ligases Pli1 and Nse2 in *S. pombe* (Watts et al., 2007), it could itself be important for sumoylating other substrates during replication fork restart. Overall, due to the high abundance of the Rtf2 protein in *S. pombe* along with the results presented here could indicate Rtf2 as having a role in a variety of processes within the cell.

6.4 Concluding Remarks

Overall, this project successfully implements an optimised *RTS1* construct for investigation into HR-restarted replication forks without interference from caononical convergent replication forks. The restarted replication fork is shown to replicate the downstream region using Polymerase δ to replicate both leading and lagging strands. The replication fork does not mature and instead remains as a δ/δ replication fork for regions up to at least 10 Kb downstream of the barrier before termination.

The *RTS1* system was successfully used to highlight key differences between BIR in *S. cerevisiae* and HR-restart at *RTS1* in *S. pombe*. The interaction between Cdc27 and PCNA

investigated using Cdc27 mutants truncated for the PIP motif identfied its importance for HR-restart but is not as crucial as reported for BIR. The PCNA mutants did not phenocopy the Cdc27 truncations but resulted in an interesting impact on the fidelity of the restarted replication fork.

Furthermore, Rtf2 was demonstrated to be important for efficient replication fork barrier activity of *RTS1* that is independent of *RTS1* region A. Establishment of a proximity based labelling mass spectrometry method will provide important information on the role of Rtf2 at restarted replication forks and its involvement in other processes within the cell.

Publications

NAIMAN, K., CAMPILLO-FUNOLLET, E., ADAM, T. W., BUDDEN, A., MIYABE, I. & CARR, A. M. 2021. Replication dynamics of recombination-dependent replication forks. *Nature Communications. 12, 923 https://doi.org/10.1038/s41467-021-21198-0*

References

ACHARYA, N., JOHNSON, R. E., PAGES, V., PRAKASH, L. & PRAKASH, S. 2009. Yeast Rev1 protein promotes complex formation of DNA polymerase zeta with Pol32 subunit of DNA polymerase delta. *Proc Natl Acad Sci U S A,* 106**,** 9631-6.

ACHARYA, N., KLASSEN, R., JOHNSON, R. E., PRAKASH, L. & PRAKASH, S. 2011. PCNA binding domains in all three subunits of yeast DNA polymerase delta modulate its function in DNA replication. *Proc Natl Acad Sci U S A,* 108**,** 17927-32.

AHN, J. S., OSMAN, F. & WHITBY, M. C. 2005. Replication fork blockage by RTS1 at an ectopic site promotes recombination in fission yeast. *EMBO J,* 24**,** 2011-23.

AIT SAADA, A., TEIXEIRA-SILVA, A., IRAQUI, I., COSTES, A., HARDY, J., PAOLETTI, G., FREON, K. & LAMBERT, S. A. E. 2017. Unprotected Replication Forks Are Converted into Mitotic Sister Chromatid Bridges. *Mol Cell,* 66**,** 398-410 e4.

AIT-SAADA, A., KHOROSJUTINA, O., CHEN, J., KRAMARZ, K., MAKSIMOV, V., SVENSSON, J. P., LAMBERT, S. & EKWALL, K. 2019. Chromatin remodeler Fft3 plays a dual role at blocked DNA replication forks. *Life Sci Alliance,* 2.

AL-KHODAIRY, F. & CARR, A. M. 1992. DNA repair mutants defining G2 checkpoint pathways in Schizosaccharomyces pombe. *EMBO J,* 11**,** 1343-50.

ALLEN, J. B., ZHOU, Z., SIEDE, W., FRIEDBERG, E. C. & ELLEDGE, S. J. 1994. The SAD1/RAD53 protein kinase controls multiple checkpoints and DNA damage-induced transcription in yeast. *Genes Dev,* 8**,** 2401-15.

ALZU, A., BERMEJO, R., BEGNIS, M., LUCCA, C., PICCINI, D., CAROTENUTO, W., SAPONARO, M., BRAMBATI, A., COCITO, A., FOIANI, M. & LIBERI, G. 2012. Senataxin associates with replication forks to protect fork integrity across RNA-polymerase-II-transcribed genes. *Cell,* 151**,** 835-846.

AOI, Y., KAWASHIMA, S. A., SIMANIS, V., YAMAMOTO, M. & SATO, M. 2014. Optimization of the analogue-sensitive Cdc2/Cdk1 mutant by in vivo selection eliminates physiological limitations to its use in cell cycle analysis. *Open Biol,* 4.

ARCANGIOLI, B., COPELAND, T. D. & KLAR, A. J. 1994. Sap1, a protein that binds to sequences required for mating-type switching, is essential for viability in Schizosaccharomyces pombe. *Mol Cell Biol,* 14**,** 2058-65.

ARIA, V. & YEELES, J. T. P. 2018. Mechanism of Bidirectional Leading-Strand Synthesis Establishment at Eukaryotic DNA Replication Origins. *Mol Cell*.

AZVOLINSKY, A., GIRESI, P. G., LIEB, J. D. & ZAKIAN, V. A. 2009. Highly transcribed RNA polymerase II genes are impediments to replication fork progression in Saccharomyces cerevisiae. *Mol Cell,* 34**,** 722-34.

BABER-FURNARI, B. A., RHIND, N., BODDY, M. N., SHANAHAN, P., LOPEZ-GIRONA, A. & RUSSELL, P. 2000. Regulation of mitotic inhibitor Mik1 helps to enforce the DNA damage checkpoint. *Mol Biol Cell,* 11**,** 1-11.

BALMUS, G., PILGER, D., COATES, J., DEMIR, M., SCZANIECKA-CLIFT, M., BARROS, A. C., WOODS, M., FU, B., YANG, F., CHEN, E., OSTERMAIER, M., STANKOVIC, T., PONSTINGL, H., HERZOG, M., YUSA, K., MARTINEZ, F. M., DURANT, S. T., GALANTY, Y., BELI, P., ADAMS, D. J., BRADLEY, A., METZAKOPIAN, E., FORMENT, J. V. & JACKSON, S. P. 2019. ATM orchestrates the DNA-damage response to counter toxic non-homologous end-joining at broken replication forks. *Nat Commun,* 10**,** 87.

BANDO, M., KATOU, Y., KOMATA, M., TANAKA, H., ITOH, T., SUTANI, T. & SHIRAHIGE, K. 2009. Csm3, Tof1, and Mrc1 form a heterotrimeric mediator complex that associates with DNA replication forks. *J Biol Chem,* 284**,** 34355-65.

BARDWELL, A. J., BARDWELL, L., TOMKINSON, A. E. & FRIEDBERG, E. C. 1994. Specific cleavage of model recombination and repair intermediates by the yeast Rad1-Rad10 DNA endonuclease. *Science,* 265**,** 2082-5.

BARETIC, D., JENKYN-BEDFORD, M., ARIA, V., CANNONE, G., SKEHEL, M. & YEELES, J. T. P. 2020. Cryo-EM Structure of the Fork Protection Complex Bound to CMG at a Replication Fork. *Mol Cell,* 78**,** 926-940 e13.

BAUM, B., NISHITANI, H., YANOW, S. & NURSE, P. 1998. Cdc18 transcription and proteolysis couple S phase to passage through mitosis. *EMBO J,* 17**,** 5689-98.

BECK, H., NAHSE-KUMPF, V., LARSEN, M. S., O'HANLON, K. A., PATZKE, S., HOLMBERG, C., MEJLVANG, J., GROTH, A., NIELSEN, O., SYLJUASEN, R. G. & SORENSEN, C. S. 2012. Cyclin-dependent kinase suppression by WEE1 kinase protects the genome through control of replication initiation and nucleotide consumption. *Mol Cell Biol,* 32**,** 4226-36.

BEN-YEHOYADA, M., WANG, L. C., KOZEKOV, I. D., RIZZO, C. J., GOTTESMAN, M. E. & GAUTIER, J. 2009. Checkpoint signaling from a single DNA interstrand crosslink. *Mol Cell,* 35**,** 704-15.

BENSON, F. E., STASIAK, A. & WEST, S. C. 1994. Purification and characterization of the human Rad51 protein, an analogue of E. coli RecA. *EMBO J,* 13**,** 5764-71.

BERMEJO, R., CAPRA, T., JOSSEN, R., COLOSIO, A., FRATTINI, C., CAROTENUTO, W., COCITO, A., DOKSANI, Y., KLEIN, H., GOMEZ-GONZALEZ, B., AGUILERA, A., KATOU, Y., SHIRAHIGE, K. & FOIANI, M. 2011. The replication checkpoint protects fork stability by releasing transcribed genes from nuclear pores. *Cell,* 146**,** 233-46.

BERMUDEZ, V. P., MACNEILL, S. A., TAPPIN, I. & HURWITZ, J. 2002. The influence of the Cdc27 subunit on the properties of the Schizosaccharomyces pombe DNA polymerase delta. *J Biol Chem,* 277**,** 36853-62.

BHAGWAT, M. & NOSSAL, N. G. 2001. Bacteriophage T4 RNase H removes both RNA primers and adjacent DNA from the 5' end of lagging strand fragments. *J Biol Chem,* 276**,** 28516-24.

BIANCHI, J., RUDD, S. G., JOZWIAKOWSKI, S. K., BAILEY, L. J., SOURA, V., TAYLOR, E., STEVANOVIC, I., GREEN, A. J., STRACKER, T. H., LINDSAY, H. D. & DOHERTY, A. J. 2013. PrimPol bypasses UV photoproducts during eukaryotic chromosomal DNA replication. *Mol Cell,* 52**,** 566-73.

BRANON, T. C., BOSCH, J. A., SANCHEZ, A. D., UDESHI, N. D., SVINKINA, T., CARR, S. A., FELDMAN, J. L., PERRIMON, N. & TING, A. Y. 2018. Efficient proximity labeling in living cells and organisms with TurboID. *Nat Biotechnol,* 36**,** 880-887.

BYUN, T. S., PACEK, M., YEE, M. C., WALTER, J. C. & CIMPRICH, K. A. 2005. Functional uncoupling of MCM helicase and DNA polymerase activities activates the ATR-dependent checkpoint. *Genes Dev,* 19**,** 1040-52.

CASOLARI, J. M., BROWN, C. R., KOMILI, S., WEST, J., HIERONYMUS, H. & SILVER, P. A. 2004. Genome-wide localization of the nuclear transport machinery couples transcriptional status and nuclear organization. *Cell,* 117**,** 427-39.

CASPARI, T., DAHLEN, M., KANTER-SMOLER, G., LINDSAY, H. D., HOFMANN, K., PAPADIMITRIOU, K., SUNNERHAGEN, P. & CARR, A. M. 2000. Characterization of

Schizosaccharomyces pombe Hus1: a PCNA-related protein that associates with Rad1 and Rad9. *Mol Cell Biol,* 20**,** 1254-62.

CEJKA, P., PLANK, J. L., BACHRATI, C. Z., HICKSON, I. D. & KOWALCZYKOWSKI, S. C. 2010. Rmi1 stimulates decatenation of double Holliday junctions during dissolution by Sgs1-Top3. *Nat Struct Mol Biol,* 17**,** 1377-82.

CEJKA, P., PLANK, J. L., DOMBROWSKI, C. C. & KOWALCZYKOWSKI, S. C. 2012. Decatenation of DNA by the S. cerevisiae Sgs1-Top3-Rmi1 and RPA complex: a mechanism for disentangling chromosomes. *Mol Cell,* 47**,** 886-96.

CHABES, A., GEORGIEVA, B., DOMKIN, V., ZHAO, X., ROTHSTEIN, R. & THELANDER, L. 2003. Survival of DNA damage in yeast directly depends on increased dNTP levels allowed by relaxed feedback inhibition of ribonucleotide reductase. *Cell,* 112**,** 391-401.

CHAN, K. L., PALMAI-PALLAG, T., YING, S. & HICKSON, I. D. 2009. Replication stress induces sister-chromatid bridging at fragile site loci in mitosis. *Nat Cell Biol,* 11**,** 753-60.

CHAPMAN-SMITH, A. & CRONAN, J. E., JR. 1999. The enzymatic biotinylation of proteins: a post-translational modification of exceptional specificity. *Trends Biochem Sci,* 24**,** 359-63.

CHEN, L., TRUJILLO, K., RAMOS, W., SUNG, P. & TOMKINSON, A. E. 2001. Promotion of Dnl4-catalyzed DNA end-joining by the Rad50/Mre11/Xrs2 and Hdf1/Hdf2 complexes. *Mol Cell,* 8**,** 1105-15.

CHEN, S., LEVIN, M. K., SAKATO, M., ZHOU, Y. & HINGORANI, M. M. 2009. Mechanism of ATP-driven PCNA clamp loading by S. cerevisiae RFC. *J Mol Biol,* 388**,** 431-42.

CHILKOVA, O., STENLUND, P., ISOZ, I., STITH, C. M., GRABOWSKI, P., LUNDSTROM, E. B., BURGERS, P. M. & JOHANSSON, E. 2007. The eukaryotic leading and lagging strand DNA polymerases are loaded onto primer-ends via separate mechanisms but have comparable processivity in the presence of PCNA. *Nucleic Acids Res,* 35**,** 6588-97.

CHOI-RHEE, E., SCHULMAN, H. & CRONAN, J. E. 2004. Promiscuous protein biotinylation by Escherichia coli biotin protein ligase. *Protein Sci,* 13**,** 3043-50.

CHRISTENSEN, P. U., BENTLEY, N. J., MARTINHO, R. G., NIELSEN, O. & CARR, A. M. 2000. Mik1 levels accumulate in S phase and may mediate an intrinsic link between S phase and mitosis. *Proc Natl Acad Sci U S A,* 97**,** 2579-84.

CHUNG, W. H., ZHU, Z., PAPUSHA, A., MALKOVA, A. & IRA, G. 2010. Defective resection at DNA double-strand breaks leads to de novo telomere formation and enhances gene targeting. *PLoS Genet,* 6**,** e1000948.

CHURIKOV, D., CHARIFI, F., ECKERT-BOULET, N., SILVA, S., SIMON, M. N., LISBY, M. & GELI, V. 2016. SUMO-Dependent Relocalization of Eroded Telomeres to Nuclear Pore Complexes Controls Telomere Recombination. *Cell Rep,* 15**,** 1242-53.

CLAUSEN, A. R., LUJAN, S. A., BURKHOLDER, A. B., OREBAUGH, C. D., WILLIAMS, J. S., CLAUSEN, M. F., MALC, E. P., MIECZKOWSKI, P. A., FARGO, D. C., SMITH, D. J. & KUNKEL, T. A. 2015. Tracking replication enzymology in vivo by genome-wide mapping of ribonucleotide incorporation. *Nat Struct Mol Biol,* 22**,** 185-91.

CLOUD, V., CHAN, Y. L., GRUBB, J., BUDKE, B. & BISHOP, D. K. 2012. Rad51 is an accessory factor for Dmc1-mediated joint molecule formation during meiosis. *Science,* 337**,** 1222-5.

CODLIN, S. & DALGAARD, J. Z. 2003. Complex mechanism of site-specific DNA replication termination in fission yeast. *EMBO J,* 22**,** 3431-40.

CORREA-BORDES, J., GULLI, M. P. & NURSE, P. 1997. p25rum1 promotes proteolysis of the mitotic B-cyclin p56cdc13 during G1 of the fission yeast cell cycle. *EMBO J,* 16**,** 4657-64.

CORREA-BORDES, J. & NURSE, P. 1995. p25rum1 orders S phase and mitosis by acting as an inhibitor of the p34cdc2 mitotic kinase. *Cell,* 83**,** 1001-9.

CORTEZ, D., GUNTUKU, S., QIN, J. & ELLEDGE, S. J. 2001. ATR and ATRIP: partners in checkpoint signaling. *Science,* 294**,** 1713-6.

COSTER, G., FRIGOLA, J., BEURON, F., MORRIS, E. P. & DIFFLEY, J. F. 2014. Origin licensing requires ATP binding and hydrolysis by the MCM replicative helicase. *Mol Cell,* 55**,** 666-77.

COUCH, F. B., BANSBACH, C. E., DRISCOLL, R., LUZWICK, J. W., GLICK, G. G., BETOUS, R., CARROLL, C. M., JUNG, S. Y., QIN, J., CIMPRICH, K. A. & CORTEZ, D. 2013. ATR phosphorylates SMARCAL1 to prevent replication fork collapse. *Genes Dev,* 27**,** 1610-23.

COULON, S., RAMASUBRAMANYAN, S., ALIES, C., PHILIPPIN, G., LEHMANN, A. & FUCHS, R. P. 2010. Rad8Rad5/Mms2-Ubc13 ubiquitin ligase complex controls translesion synthesis in fission yeast. *EMBO J,* 29**,** 2048-58.

DABOUSSI, F., COURBET, S., BENHAMOU, S., KANNOUCHE, P., ZDZIENICKA, M. Z., DEBATISSE, M. & LOPEZ, B. S. 2008. A homologous recombination defect affects replication-fork progression in mammalian cells. *J Cell Sci,* 121**,** 162-6.

DAI, J., CHUANG, R. Y. & KELLY, T. J. 2005. DNA replication origins in the Schizosaccharomyces pombe genome. *Proc Natl Acad Sci U S A,* 102**,** 337-42.

DAIGAKU, Y., KESZTHELYI, A., MULLER, C. A., MIYABE, I., BROOKS, T., RETKUTE, R., HUBANK, M., NIEDUSZYNSKI, C. A. & CARR, A. M. 2015. A global profile of replicative polymerase usage. *Nat Struct Mol Biol,* 22**,** 192-198.

DALGAARD, J. Z. & KLAR, A. J. 2000. swi1 and swi3 perform imprinting, pausing, and termination of DNA replication in S. pombe. *Cell,* 102**,** 745-51.

DALGAARD, J. Z. & KLAR, A. J. 2001. A DNA replication-arrest site RTS1 regulates imprinting by determining the direction of replication at mat1 in S. pombe. *Genes Dev,* 15**,** 2060-8.

DAVIDSON, M. B., KATOU, Y., KESZTHELYI, A., SING, T. L., XIA, T., OU, J., VAISICA, J. A., THEVAKUMARAN, N., MARJAVAARA, L., MYERS, C. L., CHABES, A., SHIRAHIGE, K. & BROWN, G. W. 2012. Endogenous DNA replication stress results in expansion of dNTP pools and a mutator phenotype. *EMBO J,* 31**,** 895-907.

DE BRUIN, R. A., KALASHNIKOVA, T. I., ASLANIAN, A., WOHLSCHLEGEL, J., CHAHWAN, C., YATES, J. R., 3RD, RUSSELL, P. & WITTENBERG, C. 2008. DNA replication checkpoint promotes G1-S transcription by inactivating the MBF repressor Nrm1. *Proc Natl Acad Sci U S A,* 105**,** 11230-5.

DE PICCOLI, G., KATOU, Y., ITOH, T., NAKATO, R., SHIRAHIGE, K. & LABIB, K. 2012. Replisome stability at defective DNA replication forks is independent of S phase checkpoint kinases. *Mol Cell,* 45**,** 696-704.

DEEGAN, T. D., BAXTER, J., ORTIZ BAZAN, M. A., YEELES, J. T. P. & LABIB, K. P. M. 2019. Pif1-Family Helicases Support Fork Convergence during DNA Replication Termination in Eukaryotes. *Mol Cell,* 74**,** 231-244 e9.

DEEM, A., KESZTHELYI, A., BLACKGROVE, T., VAYL, A., COFFEY, B., MATHUR, R., CHABES, A. & MALKOVA, A. 2011. Break-induced replication is highly inaccurate. *PLoS Biol,* 9**,** e1000594.

DEHE, P. M., COULON, S., SCAGLIONE, S., SHANAHAN, P., TAKEDACHI, A., WOHLSCHLEGEL, J. A., YATES, J. R., 3RD, LLORENTE, B., RUSSELL, P. & GAILLARD, P. H. 2013. Regulation of Mus81-Eme1 Holliday junction resolvase in response to DNA damage. *Nat Struct Mol Biol,* 20**,** 598-603.

DELACROIX, S., WAGNER, J. M., KOBAYASHI, M., YAMAMOTO, K. & KARNITZ, L. M. 2007. The Rad9-Hus1-Rad1 (9-1-1) clamp activates checkpoint signaling via TopBP1. *Genes Dev,* 21**,** 1472-7.

DESHPANDE, A. M. & NEWLON, C. S. 1996. DNA replication fork pause sites dependent on transcription. *Science,* 272**,** 1030-3.

DEWAR, J. M., BUDZOWSKA, M. & WALTER, J. C. 2015. The mechanism of DNA replication termination in vertebrates. *Nature,* 525**,** 345-50.

DEWAR, J. M., LOW, E., MANN, M., RASCHLE, M. & WALTER, J. C. 2017. CRL2(Lrr1) promotes unloading of the vertebrate replisome from chromatin during replication termination. *Genes Dev,* 31**,** 275-290.

DISCHINGER, S., KRAPP, A., XIE, L., PAULSON, J. R. & SIMANIS, V. 2008. Chemical genetic analysis of the regulatory role of Cdc2p in the S. pombe septation initiation network. *J Cell Sci,* 121**,** 843-53.

DONNIANNI, R. A. & SYMINGTON, L. S. 2013. Break-induced replication occurs by conservative DNA synthesis. *Proc Natl Acad Sci U S A,* 110**,** 13475-80.

DONNIANNI, R. A., ZHOU, Z. X., LUJAN, S. A., AL-ZAIN, A., GARCIA, V., GLANCY, E., BURKHOLDER, A. B., KUNKEL, T. A. & SYMINGTON, L. S. 2019. DNA Polymerase Delta Synthesizes Both Strands during Break-Induced Replication. *Mol Cell,* 76**,** 371-381 e4.

DORE, A. S., KILKENNY, M. L., RZECHORZEK, N. J. & PEARL, L. H. 2009. Crystal structure of the rad9-rad1-hus1 DNA damage checkpoint complex--implications for clamp loading and regulation. *Mol Cell,* 34**,** 735-45.

DOUGLAS, M. E., ALI, F. A., COSTA, A. & DIFFLEY, J. F. X. 2018. The mechanism of eukaryotic CMG helicase activation. *Nature,* 555**,** 265-268.

DROGAT, J., MIGEOT, V., MOMMAERTS, E., MULLIER, C., DIEU, M., VAN BAKEL, H. & HERMAND, D. 2012. Cdk11-cyclinL controls the assembly of the RNA polymerase II mediator complex. *Cell Rep,* 2**,** 1068-76.

DUA, R., LEVY, D. L. & CAMPBELL, J. L. 1999. Analysis of the essential functions of the C-terminal protein/protein interaction domain of Saccharomyces cerevisiae pol epsilon and its unexpected ability to support growth in the absence of the DNA polymerase domain. *J Biol Chem,* 274**,** 22283-8.

DUCKETT, D. R., MURCHIE, A. I., DIEKMANN, S., VON KITZING, E., KEMPER, B. & LILLEY, D. M. 1988. The structure of the Holliday junction, and its resolution. *Cell,* 55**,** 79-89.

DUCOUX, M., URBACH, S., BALDACCI, G., HUBSCHER, U., KOUNDRIOUKOFF, S., CHRISTENSEN, J. & HUGHES, P. 2001. Mediation of proliferating cell nuclear antigen (PCNA)-dependent DNA replication through a conserved p21(Cip1)-like PCNA-binding motif present in the third subunit of human DNA polymerase delta. *J Biol Chem,* 276**,** 49258-66.

DUNGRAWALA, H., ROSE, K. L., BHAT, K. P., MOHNI, K. N., GLICK, G. G., COUCH, F. B. & CORTEZ, D. 2015. The Replication Checkpoint Prevents Two Types of Fork Collapse without Regulating Replisome Stability. *Mol Cell,* 59**,** 998-1010.

EDWARDS, R. J., BENTLEY, N. J. & CARR, A. M. 1999. A Rad3-Rad26 complex responds to DNA damage independently of other checkpoint proteins. *Nat Cell Biol,* 1**,** 393-8.

EGGLER, A. L., INMAN, R. B. & COX, M. M. 2002. The Rad51-dependent pairing of long DNA substrates is stabilized by replication protein A. *J Biol Chem,* 277**,** 39280-8.

EISSENBERG, J. C., AYYAGARI, R., GOMES, X. V. & BURGERS, P. M. 1997. Mutations in yeast proliferating cell nuclear antigen define distinct sites for interaction with DNA polymerase delta and DNA polymerase epsilon. *Mol Cell Biol,* 17**,** 6367-78.

ELANGO, R., SHENG, Z., JACKSON, J., DECATA, J., IBRAHIM, Y., PHAM, N. T., LIANG, D. H., SAKOFSKY, C. J., VINDIGNI, A., LOBACHEV, K. S., IRA, G. & MALKOVA, A. 2017. Break-induced replication promotes formation of lethal joint molecules dissolved by Srs2. *Nat Commun,* 8**,** 1790.

ENOCH, T., CARR, A. M. & NURSE, P. 1992. Fission yeast genes involved in coupling mitosis to completion of DNA replication. *Genes Dev,* 6**,** 2035-46.

ETHERIDGE, T. J., BOULINEAU, R. L., HERBERT, A., WATSON, A. T., DAIGAKU, Y., TUCKER, J., GEORGE, S., JONSSON, P., PALAYRET, M., LANDO, D., LAUE, E., OSBORNE, M. A., KLENERMAN, D., LEE, S. F. & CARR, A. M. 2014. Quantification of DNA-associated proteins inside eukaryotic cells using single-molecule localization microscopy. *Nucleic Acids Res,* 42**,** e146.

EVRIN, C., CLARKE, P., ZECH, J., LURZ, R., SUN, J., UHLE, S., LI, H., STILLMAN, B. & SPECK, C. 2009. A double-hexameric MCM2-7 complex is loaded onto origin DNA during licensing of eukaryotic DNA replication. *Proc Natl Acad Sci U S A,* 106**,** 20240-5.

EYDMANN, T., SOMMARIVA, E., INAGAWA, T., MIAN, S., KLAR, A. J. & DALGAARD, J. Z. 2008. Rtf1-mediated eukaryotic site-specific replication termination. *Genetics,* 180**,** 27-39.

EYKELENBOOM, J. K., HARTE, E. C., CANAVAN, L., PASTOR-PEIDRO, A., CALVO-ASENSIO, I., LLORENS-AGOST, M. & LOWNDES, N. F. 2013. ATR activates the S-M checkpoint during unperturbed growth to ensure sufficient replication prior to mitotic onset. *Cell Rep,* 5**,** 1095-107.

FABRE, F., CHAN, A., HEYER, W. D. & GANGLOFF, S. 2002. Alternate pathways involving Sgs1/Top3, Mus81/ Mms4, and Srs2 prevent formation of toxic recombination intermediates from single-stranded gaps created by DNA replication. *Proc Natl Acad Sci U S A,* 99**,** 16887-92.

FASCHING, C. L., CEJKA, P., KOWALCZYKOWSKI, S. C. & HEYER, W. D. 2015. Top3-Rmi1 dissolve Rad51-mediated D loops by a topoisomerase-based mechanism. *Mol Cell,* 57**,** 595-606.

FENG, W. & D'URSO, G. 2001. Schizosaccharomyces pombe cells lacking the amino-terminal catalytic domains of DNA polymerase epsilon are viable but require the DNA damage checkpoint control. *Mol Cell Biol,* 21**,** 4495-504.

FISHER, D. L. & NURSE, P. 1996. A single fission yeast mitotic cyclin B p34cdc2 kinase promotes both S-phase and mitosis in the absence of G1 cyclins. *EMBO J,* 15**,** 850-60.

FRICKE, W. M., BASTIN-SHANOWER, S. A. & BRILL, S. J. 2005. Substrate specificity of the Saccharomyces cerevisiae Mus81-Mms4 endonuclease. *DNA Repair (Amst),* 4**,** 243-51.

FRICKE, W. M. & BRILL, S. J. 2003. Slx1-Slx4 is a second structure-specific endonuclease functionally redundant with Sgs1-Top3. *Genes Dev,* 17**,** 1768-78.

FU, Y. V., YARDIMCI, H., LONG, D. T., HO, T. V., GUAINAZZI, A., BERMUDEZ, V. P., HURWITZ, J., VAN OIJEN, A., SCHARER, O. D. & WALTER, J. C. 2011. Selective bypass of a lagging strand roadblock by the eukaryotic replicative DNA helicase. *Cell,* 146**,** 931-41.

FUJITA, H., OHUCHIDA, K., MIZUMOTO, K., ITABA, S., ITO, T., NAKATA, K., YU, J., KAYASHIMA, T., SOUZAKI, R., TAJIRI, T., MANABE, T., OHTSUKA, T. & TANAKA, M. 2010. Gene expression levels as predictive markers of outcome in pancreatic cancer after gemcitabine-based adjuvant chemotherapy. *Neoplasia,* 12**,** 807-17.

FUKUURA, M., NAGAO, K., OBUSE, C., TAKAHASHI, T. S., NAKAGAWA, T. & MASUKATA, H. 2011. CDK promotes interactions of Sld3 and Drc1 with Cut5 for initiation of DNA replication in fission yeast. *Mol Biol Cell,* 22**,** 2620-33.

FURUYA, K., MIYABE, I., TSUTSUI, Y., PADERI, F., KAKUSHO, N., MASAI, H., NIKI, H. & CARR, A. M. 2010. DDK phosphorylates checkpoint clamp component Rad9 and promotes its release from damaged chromatin. *Mol Cell,* 40**,** 606-18.

GAINES, W. A., GODIN, S. K., KABBINAVAR, F. F., RAO, T., VANDEMARK, A. P., SUNG, P. & BERNSTEIN, K. A. 2015. Promotion of presynaptic filament assembly by the ensemble of S. cerevisiae Rad51 paralogues with Rad52. *Nat Commun,* 6**,** 7834.

GAMBUS, A., JONES, R. C., SANCHEZ-DIAZ, A., KANEMAKI, M., VAN DEURSEN, F., EDMONDSON, R. D. & LABIB, K. 2006. GINS maintains association of Cdc45 with MCM in replisome progression complexes at eukaryotic DNA replication forks. *Nat Cell Biol,* 8**,** 358-66.

GAN, W., GUAN, Z., LIU, J., GUI, T., SHEN, K., MANLEY, J. L. & LI, X. 2011. R-loop-mediated genomic instability is caused by impairment of replication fork progression. *Genes Dev,* 25**,** 2041-56.

GARBACZ, M. A., LUJAN, S. A., BURKHOLDER, A. B., COX, P. B., WU, Q., ZHOU, Z. X., HABER, J. E. & KUNKEL, T. A. 2018. Evidence that DNA polymerase delta contributes to initiating leading strand DNA replication in Saccharomyces cerevisiae. *Nat Commun,* 9**,** 858.

GE, X. Q., JACKSON, D. A. & BLOW, J. J. 2007. Dormant origins licensed by excess Mcm2-7 are required for human cells to survive replicative stress. *Genes Dev,* 21**,** 3331-41.

GEORGESCU, R., YUAN, Z., BAI, L., DE LUNA ALMEIDA SANTOS, R., SUN, J., ZHANG, D., YURIEVA, O., LI, H. & O'DONNELL, M. E. 2017. Structure of eukaryotic CMG helicase at a replication fork and implications to replisome architecture and origin initiation. *Proc Natl Acad Sci U S A,* 114**,** E697-E706.

GERIK, K. J., LI, X., PAUTZ, A. & BURGERS, P. M. 1998. Characterization of the two small subunits of Saccharomyces cerevisiae DNA polymerase delta. *J Biol Chem,* 273**,** 19747-55.

GOTTLIEB, T. M. & JACKSON, S. P. 1993. The DNA-dependent protein kinase: requirement for DNA ends and association with Ku antigen. *Cell,* 72**,** 131-42.

GOULD, K. L. & NURSE, P. 1989. Tyrosine phosphorylation of the fission yeast cdc2+ protein kinase regulates entry into mitosis. *Nature,* 342**,** 39-45.

GRIFFITHS, D. J., BARBET, N. C., MCCREADY, S., LEHMANN, A. R. & CARR, A. M. 1995. Fission yeast rad17: a homologue of budding yeast RAD24 that shares regions of sequence similarity with DNA polymerase accessory proteins. *EMBO J,* 14**,** 5812-23.

GUAN, L., HE, P., YANG, F., ZHANG, Y., HU, Y., DING, J., HUA, Y., ZHANG, Y., YE, Q., HU, J., WANG, T., JIN, C. & KONG, D. 2017. Sap1 is a replication-initiation factor essential for the assembly of pre-replicative complex in the fission yeast Schizosaccharomyces pombe. *J Biol Chem,* 292**,** 6056-6075.

HARDY, J., DAI, D., AIT SAADA, A., TEIXEIRA-SILVA, A., DUPOIRON, L., MOJALLALI, F., FREON, K., OCHSENBEIN, F., HARTMANN, B. & LAMBERT, S. 2019. Histone deposition promotes recombination-dependent replication at arrested forks. *PLoS Genet,* 15**,** e1008441.

HARTWELL, L. H. 1974. Saccharomyces cerevisiae cell cycle. *Bacteriol Rev,* 38**,** 164-98.

HARUTA, N., KUROKAWA, Y., MURAYAMA, Y., AKAMATSU, Y., UNZAI, S., TSUTSUI, Y. & IWASAKI, H. 2006. The Swi5-Sfr1 complex stimulates Rhp51/Rad51- and Dmc1-mediated DNA strand exchange in vitro. *Nat Struct Mol Biol,* 13**,** 823-30.

HASHIMOTO, K., SHIMIZU, K., NAKASHIMA, N. & SUGINO, A. 2003. Fidelity of DNA polymerase delta holoenzyme from Saccharomyces cerevisiae: the sliding clamp

proliferating cell nuclear antigen decreases its fidelity. *Biochemistry,* 42**,** 14207-13.

HAYASHI, M., KATOU, Y., ITOH, T., TAZUMI, A., YAMADA, Y., TAKAHASHI, T., NAKAGAWA, T., SHIRAHIGE, K. & MASUKATA, H. 2007. Genome-wide localization of pre-RC sites and identification of replication origins in fission yeast. *EMBO J,* 26**,** 1327-39.

HELLER, R. C., KANG, S., LAM, W. M., CHEN, S., CHAN, C. S. & BELL, S. P. 2011. Eukaryotic origin-dependent DNA replication in vitro reveals sequential action of DDK and S-CDK kinases. *Cell,* 146**,** 80-91.

HELMRICH, A., BALLARINO, M. & TORA, L. 2011. Collisions between replication and transcription complexes cause common fragile site instability at the longest human genes. *Mol Cell,* 44**,** 966-77.

HENTGES, P., WALLER, H., REIS, C. C., FERREIRA, M. G. & DOHERTY, A. J. 2014. Cdk1 restrains NHEJ through phosphorylation of XRCC4-like factor Xlf1. *Cell Rep,* 9**,** 2011-7.

HILL, T. M. & MARIANS, K. J. 1990. Escherichia coli Tus protein acts to arrest the progression of DNA replication forks in vitro. *Proc Natl Acad Sci U S A,* 87**,** 2481-5.

HIROTA, K., TSUDA, M., MOHIUDDIN, TSURIMOTO, T., COHEN, I. S., LIVNEH, Z., KOBAYASHI, K., NARITA, T., NISHIHARA, K., MURAI, J., IWAI, S., GUILBAUD, G., SALE, J. E. & TAKEDA, S. 2016. In vivo evidence for translesion synthesis by the replicative DNA polymerase delta. *Nucleic Acids Res,* 44**,** 7242-50.

HODGSON, B., CALZADA, A. & LABIB, K. 2007. Mrc1 and Tof1 regulate DNA replication forks in different ways during normal S phase. *Mol Biol Cell,* 18**,** 3894-902.

HOEGE, C., PFANDER, B., MOLDOVAN, G. L., PYROWOLAKIS, G. & JENTSCH, S. 2002. RAD6-dependent DNA repair is linked to modification of PCNA by ubiquitin and SUMO. *Nature,* 419**,** 135-41.

HOLMBERG, C., FLECK, O., HANSEN, H. A., LIU, C., SLAABY, R., CARR, A. M. & NIELSEN, O. 2005. Ddb1 controls genome stability and meiosis in fission yeast. *Genes Dev,* 19**,** 853-62.

HORIGOME, C., UNOZAWA, E., OOKI, T. & KOBAYASHI, T. 2019. Ribosomal RNA gene repeats associate with the nuclear pore complex for maintenance after DNA damage. *PLoS Genet,* 15**,** e1008103.

HU, J., SUN, L., SHEN, F., CHEN, Y., HUA, Y., LIU, Y., ZHANG, M., HU, Y., WANG, Q., XU, W., SUN, F., JI, J., MURRAY, J. M., CARR, A. M. & KONG, D. 2012. The intra-S phase checkpoint targets Dna2 to prevent stalled replication forks from reversing. *Cell,* 149**,** 1221-32.

HUANG, M., ZHOU, Z. & ELLEDGE, S. J. 1998. The DNA replication and damage checkpoint pathways induce transcription by inhibition of the Crt1 repressor. *Cell,* 94**,** 595-605.

HUERTAS, P. & AGUILERA, A. 2003. Cotranscriptionally formed DNA:RNA hybrids mediate transcription elongation impairment and transcription-associated recombination. *Mol Cell,* 12**,** 711-21.

ILVES, I., PETOJEVIC, T., PESAVENTO, J. J. & BOTCHAN, M. R. 2010. Activation of the MCM2-7 helicase by association with Cdc45 and GINS proteins. *Mol Cell,* 37**,** 247-58.

INAGAWA, T., YAMADA-INAGAWA, T., EYDMANN, T., MIAN, I. S., WANG, T. S. & DALGAARD, J. Z. 2009. Schizosaccharomyces pombe Rtf2 mediates site-specific replication termination by inhibiting replication restart. *Proc Natl Acad Sci U S A,* 106**,** 7927-32.

IRA, G., MALKOVA, A., LIBERI, G., FOIANI, M. & HABER, J. E. 2003. Srs2 and Sgs1-Top3 suppress crossovers during double-strand break repair in yeast. *Cell,* 115**,** 401-11.

IRAQUI, I., CHEKKAL, Y., JMARI, N., PIETROBON, V., FREON, K., COSTES, A. & LAMBERT, S. A. 2012. Recovery of arrested replication forks by homologous recombination is error-prone. *PLoS Genet,* 8**,** e1002976.

IVANOV, E. L., SUGAWARA, N., FISHMAN-LOBELL, J. & HABER, J. E. 1996. Genetic requirements for the single-strand annealing pathway of double-strand break repair in Saccharomyces cerevisiae. *Genetics,* 142**,** 693-704.

JAIN, S., SUGAWARA, N., MEHTA, A., RYU, T. & HABER, J. E. 2016. Sgs1 and Mph1 Helicases Enforce the Recombination Execution Checkpoint During DNA Double-Strand Break Repair in Saccharomyces cerevisiae. *Genetics,* 203**,** 667-75.

JALAN, M., OEHLER, J., MORROW, C. A., OSMAN, F. & WHITBY, M. C. 2019. Factors affecting template switch recombination associated with restarted DNA replication. *Elife,* 8.

JOHANSSON, E., GARG, P. & BURGERS, P. M. 2004. The Pol32 subunit of DNA polymerase delta contains separable domains for processive replication and proliferating cell nuclear antigen (PCNA) binding. *J Biol Chem,* 279**,** 1907-15.

JOHNSON, R. E., KLASSEN, R., PRAKASH, L. & PRAKASH, S. 2015. A Major Role of DNA Polymerase delta in Replication of Both the Leading and Lagging DNA Strands. *Mol Cell,* 59**,** 163-175.

JONES, D. T., LECHERTIER, T., MITTER, R., HERBERT, J. M., BICKNELL, R., JONES, J. L., LI, J. L., BUFFA, F., HARRIS, A. L. & HODIVALA-DILKE, K. 2012. Gene expression analysis in human breast cancer associated blood vessels. *PLoS One,* 7**,** e44294.

KAMIMURA, Y., TAK, Y. S., SUGINO, A. & ARAKI, H. 2001. Sld3, which interacts with Cdc45 (Sld4), functions for chromosomal DNA replication in Saccharomyces cerevisiae. *EMBO J,* 20**,** 2097-107.

KANG, S., WARNER, M. D. & BELL, S. P. 2014. Multiple functions for Mcm2-7 ATPase motifs during replication initiation. *Mol Cell,* 55**,** 655-65.

KANNOUCHE, P. L., WING, J. & LEHMANN, A. R. 2004. Interaction of human DNA polymerase eta with monoubiquitinated PCNA: a possible mechanism for the polymerase switch in response to DNA damage. *Mol Cell,* 14**,** 491-500.

KATOU, Y., KANOH, Y., BANDO, M., NOGUCHI, H., TANAKA, H., ASHIKARI, T., SUGIMOTO, K. & SHIRAHIGE, K. 2003. S-phase checkpoint proteins Tof1 and Mrc1 form a stable replication-pausing complex. *Nature,* 424**,** 1078-83.

KAYKOV, A. & NURSE, P. 2015. The spatial and temporal organization of origin firing during the S-phase of fission yeast. *Genome Res,* 25**,** 391-401.

KESTI, T., FLICK, K., KERANEN, S., SYVAOJA, J. E. & WITTENBERG, C. 1999. DNA polymerase epsilon catalytic domains are dispensable for DNA replication, DNA repair, and cell viability. *Mol Cell,* 3**,** 679-85.

KESZTHELYI, A., DAIGAKU, Y., PTASINSKA, K., MIYABE, I. & CARR, A. M. 2015. Mapping ribonucleotides in genomic DNA and exploring replication dynamics by polymerase usage sequencing (Pu-seq). *Nat Protoc,* 10**,** 1786-801.

KIDD, E. A., YU, J., LI, X., SHANNON, W. D., WATSON, M. A. & MCLEOD, H. L. 2005. Variance in the expression of 5-Fluorouracil pathway genes in colorectal cancer. *Clin Cancer Res,* 11**,** 2612-9.

KOH, K. D., BALACHANDER, S., HESSELBERTH, J. R. & STORICI, F. 2015. Ribose-seq: global mapping of ribonucleotides embedded in genomic DNA. *Nat Methods,* 12**,** 251-7, 3 p following 257.

KOLINJIVADI, A. M., SANNINO, V., DE ANTONI, A., ZADOROZHNY, K., KILKENNY, M., TECHER, H., BALDI, G., SHEN, R., CICCIA, A., PELLEGRINI, L., KREJCI, L. & COSTANZO, V. 2017. Smarcal1-Mediated Fork Reversal Triggers Mre11-Dependent Degradation of Nascent DNA in the Absence of Brca2 and Stable Rad51 Nucleofilaments. *Mol Cell,* 67**,** 867-881 e7.

KOTTEMANN, M. C., CONTI, B. A., LACH, F. P. & SMOGORZEWSKA, A. 2018. Removal of RTF2 from Stalled Replisomes Promotes Maintenance of Genome Integrity. *Mol Cell,* 69**,** 24-35 e5.

KOUNDRIOUKOFF, S., CARIGNON, S., TECHER, H., LETESSIER, A., BRISON, O. & DEBATISSE, M. 2013. Stepwise activation of the ATR signaling pathway upon increasing replication stress impacts fragile site integrity. *PLoS Genet,* 9**,** e1003643.

KRINGS, G. & BASTIA, D. 2004. swi1- and swi3-dependent and independent replication fork arrest at the ribosomal DNA of Schizosaccharomyces pombe. *Proc Natl Acad Sci U S A,* 101**,** 14085-90.

KRINGS, G. & BASTIA, D. 2005. Sap1p binds to Ter1 at the ribosomal DNA of Schizosaccharomyces pombe and causes polar replication fork arrest. *J Biol Chem,* 280**,** 39135-42.

KUMAR, S. & BURGERS, P. M. 2013. Lagging strand maturation factor Dna2 is a component of the replication checkpoint initiation machinery. *Genes Dev,* 27**,** 313-21.

KUMAR, S. & HUBERMAN, J. A. 2009. Checkpoint-dependent regulation of origin firing and replication fork movement in response to DNA damage in fission yeast. *Mol Cell Biol,* 29**,** 602-11.

KUROKAWA, Y., MURAYAMA, Y., HARUTA-TAKAHASHI, N., URABE, I. & IWASAKI, H. 2008. Reconstitution of DNA strand exchange mediated by Rhp51 recombinase and two mediators. *PLoS Biol,* 6**,** e88.

KWON, K. & BECKETT, D. 2000. Function of a conserved sequence motif in biotin holoenzyme synthetases. *Protein Sci,* 9**,** 1530-9.

LAMBERT, S., MIZUNO, K., BLAISONNEAU, J., MARTINEAU, S., CHANET, R., FREON, K., MURRAY, J. M., CARR, A. M. & BALDACCI, G. 2010. Homologous recombination restarts blocked replication forks at the expense of genome rearrangements by template exchange. *Mol Cell,* 39**,** 346-59.

LAMBERT, S., WATSON, A., SHEEDY, D. M., MARTIN, B. & CARR, A. M. 2005. Gross chromosomal rearrangements and elevated recombination at an inducible site-specific replication fork barrier. *Cell,* 121**,** 689-702.

LANGSTON, L. D., ZHANG, D., YURIEVA, O., GEORGESCU, R. E., FINKELSTEIN, J., YAO, N. Y., INDIANI, C. & O'DONNELL, M. E. 2014. CMG helicase and DNA polymerase epsilon form a functional 15-subunit holoenzyme for eukaryotic leading-strand DNA replication. *Proc Natl Acad Sci U S A,* 111**,** 15390-5.

LAROCQUE, J. R., STARK, J. M., OH, J., BOJILOVA, E., YUSA, K., HORIE, K., TAKEDA, J. & JASIN, M. 2011. Interhomolog recombination and loss of heterozygosity in wild-type and Bloom syndrome helicase (BLM)-deficient mammalian cells. *Proc Natl Acad Sci U S A,* 108**,** 11971-6.

LARSEN, N. B., SASS, E., SUSKI, C., MANKOURI, H. W. & HICKSON, I. D. 2014. The Escherichia coli Tus-Ter replication fork barrier causes site-specific DNA replication perturbation in yeast. *Nat Commun,* 5**,** 3574.

LARSON, A., FAIR, B. J. & PLEISS, J. A. 2016. Interconnections Between RNA-Processing Pathways Revealed by a Sequencing-Based Genetic Screen for Pre-mRNA Splicing Mutants in Fission Yeast. *G3 (Bethesda),* 6**,** 1513-23.

LEE, J., KUMAGAI, A. & DUNPHY, W. G. 2007. The Rad9-Hus1-Rad1 checkpoint clamp regulates interaction of TopBP1 with ATR. *J Biol Chem,* 282**,** 28036-44.

LEE, J. K., MOON, K. Y., JIANG, Y. & HURWITZ, J. 2001. The Schizosaccharomyces pombe origin recognition complex interacts with multiple AT-rich regions of the replication origin DNA by means of the AT-hook domains of the spOrc4 protein. *Proc Natl Acad Sci U S A,* 98**,** 13589-94.

LEHMANN, A. R. 1972. Postreplication repair of DNA in ultraviolet-irradiated mammalian cells. *J Mol Biol,* 66**,** 319-37.

LI, H., XIE, B., ZHOU, Y., RAHMEH, A., TRUSA, S., ZHANG, S., GAO, Y., LEE, E. Y. & LEE, M. Y. 2006. Functional roles of p12, the fourth subunit of human DNA polymerase delta. *J Biol Chem,* 281**,** 14748-55.

LILLEY, D. M. 1980. The inverted repeat as a recognizable structural feature in supercoiled DNA molecules. *Proc Natl Acad Sci U S A,* 77**,** 6468-72.

LINDSAY, H. D., GRIFFITHS, D. J., EDWARDS, R. J., CHRISTENSEN, P. U., MURRAY, J. M., OSMAN, F., WALWORTH, N. & CARR, A. M. 1998. S-phase-specific activation of Cds1 kinase defines a subpathway of the checkpoint response in Schizosaccharomyces pombe. *Genes Dev,* 12**,** 382-95.

LINSKENS, M. H. & HUBERMAN, J. A. 1988. Organization of replication of ribosomal DNA in Saccharomyces cerevisiae. *Mol Cell Biol,* 8**,** 4927-35.

LIU, C., POITELEA, M., WATSON, A., YOSHIDA, S. H., SHIMODA, C., HOLMBERG, C., NIELSEN, O. & CARR, A. M. 2005. Transactivation of Schizosaccharomyces pombe cdt2+ stimulates a Pcu4-Ddb1-CSN ubiquitin ligase. *EMBO J,* 24**,** 3940-51.

LIU, J., RENAULT, L., VEAUTE, X., FABRE, F., STAHLBERG, H. & HEYER, W. D. 2011. Rad51 paralogues Rad55-Rad57 balance the antirecombinase Srs2 in Rad51 filament formation. *Nature,* 479**,** 245-8.

LOBACHEV, K. S., GORDENIN, D. A. & RESNICK, M. A. 2002. The Mre11 complex is required for repair of hairpin-capped double-strand breaks and prevention of chromosome rearrangements. *Cell,* 108**,** 183-93.

LOPES, J., PIAZZA, A., BERMEJO, R., KRIEGSMAN, B., COLOSIO, A., TEULADE-FICHOU, M. P., FOIANI, M. & NICOLAS, A. 2011. G-quadruplex-induced instability during leading-strand replication. *EMBO J,* 30**,** 4033-46.

LORENZ, A., OSMAN, F., FOLKYTE, V., SOFUEVA, S. & WHITBY, M. C. 2009. Fbh1 limits Rad51-dependent recombination at blocked replication forks. *Mol Cell Biol,* 29**,** 4742-56.

LORENZ, A., OSMAN, F., SUN, W., NANDI, S., STEINACHER, R. & WHITBY, M. C. 2012. The fission yeast FANCM ortholog directs non-crossover recombination during meiosis. *Science,* 336**,** 1585-8.

LUKAS, C., SAVIC, V., BEKKER-JENSEN, S., DOIL, C., NEUMANN, B., PEDERSEN, R. S., GROFTE, M., CHAN, K. L., HICKSON, I. D., BARTEK, J. & LUKAS, J. 2011. 53BP1 nuclear bodies form around DNA lesions generated by mitotic transmission of chromosomes under replication stress. *Nat Cell Biol,* 13**,** 243-53.

LUNDGREN, K., WALWORTH, N., BOOHER, R., DEMBSKI, M., KIRSCHNER, M. & BEACH, D. 1991. mik1 and wee1 cooperate in the inhibitory tyrosine phosphorylation of cdc2. *Cell,* 64**,** 1111-22.

LYDEARD, J. R., JAIN, S., YAMAGUCHI, M. & HABER, J. E. 2007. Break-induced replication and telomerase-independent telomere maintenance require Pol32. *Nature,* 448**,** 820-3.

LYDEARD, J. R., LIPKIN-MOORE, Z., SHEU, Y. J., STILLMAN, B., BURGERS, P. M. & HABER, J. E. 2010. Break-induced replication requires all essential DNA replication factors except those specific for pre-RC assembly. *Genes Dev,* 24**,** 1133-44.

MACNEILL, S. A., MORENO, S., REYNOLDS, N., NURSE, P. & FANTES, P. A. 1996. The fission yeast Cdc1 protein, a homologue of the small subunit of DNA polymerase delta, binds to Pol3 and Cdc27. *EMBO J,* 15**,** 4613-28.

MAJKA, J., BINZ, S. K., WOLD, M. S. & BURGERS, P. M. 2006. Replication protein A directs loading of the DNA damage checkpoint clamp to 5'-DNA junctions. *J Biol Chem,* 281**,** 27855-61.

MALKOVA, A., IVANOV, E. L. & HABER, J. E. 1996. Double-strand break repair in the absence of RAD51 in yeast: a possible role for break-induced DNA replication. *Proc Natl Acad Sci U S A,* 93**,** 7131-6.

MALKOVA, A., NAYLOR, M. L., YAMAGUCHI, M., IRA, G. & HABER, J. E. 2005. RAD51-dependent break-induced replication differs in kinetics and checkpoint responses from RAD51-mediated gene conversion. *Mol Cell Biol,* 25**,** 933-44.

MANOLIS, K. G., NIMMO, E. R., HARTSUIKER, E., CARR, A. M., JEGGO, P. A. & ALLSHIRE, R. C. 2001. Novel functional requirements for non-homologous DNA end joining in Schizosaccharomyces pombe. *EMBO J,* 20**,** 210-21.

MARIC, M., MACULINS, T., DE PICCOLI, G. & LABIB, K. 2014. Cdc48 and a ubiquitin ligase drive disassembly of the CMG helicase at the end of DNA replication. *Science,* 346**,** 1253596.

MARTINHO, R. G., LINDSAY, H. D., FLAGGS, G., DEMAGGIO, A. J., HOEKSTRA, M. F., CARR, A. M. & BENTLEY, N. J. 1998. Analysis of Rad3 and Chk1 protein kinases defines different checkpoint responses. *EMBO J,* 17**,** 7239-49.

MASTRO, T. L., TRIPATHI, V. P. & FORSBURG, S. L. 2020. Translesion synthesis polymerases contribute to meiotic chromosome segregation and cohesin dynamics in S chizosaccharomyces pombe. *J Cell Sci,* 133.

MAYLE, R., CAMPBELL, I. M., BECK, C. R., YU, Y., WILSON, M., SHAW, C. A., BJERGBAEK, L., LUPSKI, J. R. & IRA, G. 2015. DNA REPAIR. Mus81 and converging forks limit the mutagenicity of replication fork breakage. *Science,* 349**,** 742-7.

MCALLISTER, H. C. & COON, M. J. 1966. Further studies on the properties of liver propionyl coenzyme A holocarboxylase synthetase and the specificity of holocarboxylase formation. *J Biol Chem,* 241**,** 2855-61.

MCEACHERN, M. J. & HABER, J. E. 2006. Break-induced replication and recombinational telomere elongation in yeast. *Annu Rev Biochem,* 75**,** 111-35.

MCILWRAITH, M. J. & WEST, S. C. 2008. DNA repair synthesis facilitates RAD52-mediated second-end capture during DSB repair. *Mol Cell,* 29**,** 510-6.

MCNALLY, R., BOWMAN, G. D., GOEDKEN, E. R., O'DONNELL, M. & KURIYAN, J. 2010. Analysis of the role of PCNA-DNA contacts during clamp loading. *BMC Struct Biol,* 10**,** 3.

MINE-HATTAB, J. & ROTHSTEIN, R. 2012. Increased chromosome mobility facilitates homology search during recombination. *Nat Cell Biol,* 14**,** 510-7.

MITCHISON, J. M. & CREANOR, J. 1971. Further measurements of DNA synthesis and enzyme potential during cell cycle of fission yeast Schizosaccharomyces pombe. *Exp Cell Res,* 69**,** 244-7.

MIYABE, I., KUNKEL, T. A. & CARR, A. M. 2011. The major roles of DNA polymerases epsilon and delta at the eukaryotic replication fork are evolutionarily conserved. *PLoS Genet,* 7**,** e1002407.

MIYABE, I., MIZUNO, K., KESZTHELYI, A., DAIGAKU, Y., SKOUTERI, M., MOHEBI, S., KUNKEL, T. A., MURRAY, J. M. & CARR, A. M. 2015. Polymerase delta replicates both strands after homologous recombination-dependent fork restart. *Nat Struct Mol Biol,* 22**,** 932-8.

MIZUNO, K., LAMBERT, S., BALDACCI, G., MURRAY, J. M. & CARR, A. M. 2009. Nearby inverted repeats fuse to generate acentric and dicentric palindromic chromosomes by a replication template exchange mechanism. *Genes Dev,* 23**,** 2876-86.

MIZUNO, K., MIYABE, I., SCHALBETTER, S. A., CARR, A. M. & MURRAY, J. M. 2013. Recombination-restarted replication makes inverted chromosome fusions at inverted repeats. *Nature,* 493**,** 246-9.

MOHANTY, B. K., BAIRWA, N. K. & BASTIA, D. 2006. The Tof1p-Csm3p protein complex counteracts the Rrm3p helicase to control replication termination of Saccharomyces cerevisiae. *Proc Natl Acad Sci U S A,* 103**,** 897-902.

MOHEBI, S., MIZUNO, K., WATSON, A., CARR, A. M. & MURRAY, J. M. 2015. Checkpoints are blind to replication restart and recombination intermediates that result in gross chromosomal rearrangements. *Nat Commun,* 6**,** 6357.

MORENO, A., CARRINGTON, J. T., ALBERGANTE, L., AL MAMUN, M., HAAGENSEN, E. J., KOMSELI, E. S., GORGOULIS, V. G., NEWMAN, T. J. & BLOW, J. J. 2016. Unreplicated DNA remaining from unperturbed S phases passes through mitosis for resolution in daughter cells. *Proc Natl Acad Sci U S A,* 113**,** E5757-64.

MORROW, C. A., NGUYEN, M. O., FOWER, A., WONG, I. N., OSMAN, F., BRYER, C. & WHITBY, M. C. 2017. Inter-Fork Strand Annealing causes genomic deletions during the termination of DNA replication. *Elife,* 6.

MOYER, S. E., LEWIS, P. W. & BOTCHAN, M. R. 2006. Isolation of the Cdc45/Mcm2-7/GINS (CMG) complex, a candidate for the eukaryotic DNA replication fork helicase. *Proc Natl Acad Sci U S A,* 103**,** 10236-10241.

MURAMATSU, S., HIRAI, K., TAK, Y. S., KAMIMURA, Y. & ARAKI, H. 2010. CDK-dependent complex formation between replication proteins Dpb11, Sld2, Pol (epsilon}, and GINS in budding yeast. *Genes Dev,* 24**,** 602-12.

MUZI FALCONI, M., BROWN, G. W. & KELLY, T. J. 1996. cdc18+ regulates initiation of DNA replication in Schizosaccharomyces pombe. *Proc Natl Acad Sci U S A,* 93**,** 1566-70.

NAIMAN, K., CAMPILLO-FUNOLLET, E., ADAM, T. W., BUDDEN, A., MIYABE, I. & CARR, A. M. 2020. Replication dynamics of recombination-dependent replication forks. *BioRxiv*.

NAKAJIMA, R. & MASUKATA, H. 2002. SpSld3 is required for loading and maintenance of SpCdc45 on chromatin in DNA replication in fission yeast. *Mol Biol Cell,* 13**,** 1462-72.

NASMYTH, K. & NURSE, P. 1981. Cell division cycle mutants altered in DNA replication and mitosis in the fission yeast Schizosaccharomyces pombe. *Mol Gen Genet,* 182**,** 119-24.

NGUYEN, M. O., JALAN, M., MORROW, C. A., OSMAN, F. & WHITBY, M. C. 2015. Recombination occurs within minutes of replication blockage by RTS1 producing restarted forks that are prone to collapse. *Elife,* 4**,** e04539.

NICK MCELHINNY, S. A., GORDENIN, D. A., STITH, C. M., BURGERS, P. M. & KUNKEL, T. A. 2008. Division of labor at the eukaryotic replication fork. *Mol Cell,* 30**,** 137-44.

NIMONKAR, A. V., SICA, R. A. & KOWALCZYKOWSKI, S. C. 2009. Rad52 promotes second-end DNA capture in double-stranded break repair to form complement-stabilized joint molecules. *Proc Natl Acad Sci U S A,* 106**,** 3077-82.

NISHITANI, H., LYGEROU, Z., NISHIMOTO, T. & NURSE, P. 2000. The Cdt1 protein is required to license DNA for replication in fission yeast. *Nature,* 404**,** 625-8.

NISHITANI, H. & NURSE, P. 1995. p65cdc18 plays a major role controlling the initiation of DNA replication in fission yeast. *Cell,* 83**,** 397-405.

NOGUCHI, C. & NOGUCHI, E. 2007. Sap1 promotes the association of the replication fork protection complex with chromatin and is involved in the replication checkpoint in Schizosaccharomyces pombe. *Genetics,* 175**,** 553-66.

NOGUCHI, E., NOGUCHI, C., DU, L. L. & RUSSELL, P. 2003. Swi1 prevents replication fork collapse and controls checkpoint kinase Cds1. *Mol Cell Biol,* 23**,** 7861-74.

NOGUCHI, E., NOGUCHI, C., MCDONALD, W. H., YATES, J. R., 3RD & RUSSELL, P. 2004. Swi1 and Swi3 are components of a replication fork protection complex in fission yeast. *Mol Cell Biol,* 24**,** 8342-55.

NOGUCHI, E., SHANAHAN, P., NOGUCHI, C. & RUSSELL, P. 2002. CDK phosphorylation of Drc1 regulates DNA replication in fission yeast. *Curr Biol,* 12**,** 599-605.

NURSE, P. & BISSETT, Y. 1981. Gene required in G1 for commitment to cell cycle and in G2 for control of mitosis in fission yeast. *Nature,* 292**,** 558-60.

OKAZAKI, R., OKAZAKI, T., SAKABE, K., SUGIMOTO, K. & SUGINO, A. 1968. Mechanism of DNA chain growth. I. Possible discontinuity and unusual secondary structure of newly synthesized chains. *Proc Natl Acad Sci U S A,* 59**,** 598-605.

OZERI-GALAI, E., LEBOFSKY, R., RAHAT, A., BESTER, A. C., BENSIMON, A. & KEREM, B. 2011. Failure of origin activation in response to fork stalling leads to chromosomal instability at fragile sites. *Mol Cell,* 43**,** 122-31.

PAESCHKE, K., BOCHMAN, M. L., GARCIA, P. D., CEJKA, P., FRIEDMAN, K. L., KOWALCZYKOWSKI, S. C. & ZAKIAN, V. A. 2013. Pif1 family helicases suppress genome instability at G-quadruplex motifs. *Nature,* 497**,** 458-62.

PAESCHKE, K., CAPRA, J. A. & ZAKIAN, V. A. 2011. DNA replication through G-quadruplex motifs is promoted by the Saccharomyces cerevisiae Pif1 DNA helicase. *Cell,* 145**,** 678-91.

PAI, C. C., GARCIA, I., WANG, S. W., COTTERILL, S., MACNEILL, S. A. & KEARSEY, S. E. 2009. GINS inactivation phenotypes reveal two pathways for chromatin association of replicative alpha and epsilon DNA polymerases in fission yeast. *Mol Biol Cell,* 20**,** 1213-22.

PALAKODETI, A., LUCAS, I., JIANG, Y., YOUNG, D. J., FERNALD, A. A., KARRISON, T. & LE BEAU, M. M. 2010. Impaired replication dynamics at the FRA3B common fragile site. *Hum Mol Genet,* 19**,** 99-110.

PALANCADE, B., LIU, X., GARCIA-RUBIO, M., AGUILERA, A., ZHAO, X. & DOYE, V. 2007. Nucleoporins prevent DNA damage accumulation by modulating Ulp1-dependent sumoylation processes. *Mol Biol Cell,* 18**,** 2912-23.

PANAYOTATOS, N. & WELLS, R. D. 1981. Cruciform structures in supercoiled DNA. *Nature,* 289**,** 466-70.

PATEL, P. K., ARCANGIOLI, B., BAKER, S. P., BENSIMON, A. & RHIND, N. 2006. DNA replication origins fire stochastically in fission yeast. *Mol Biol Cell,* 17**,** 308-16.

PIETROBON, V., FREON, K., HARDY, J., COSTES, A., IRAQUI, I., OCHSENBEIN, F. & LAMBERT, S. A. 2014. The chromatin assembly factor 1 promotes Rad51-dependent template switches at replication forks by counteracting D-loop disassembly by the RecQ-type helicase Rqh1. *PLoS Biol,* 12**,** e1001968.

POLI, J., TSAPONINA, O., CRABBE, L., KESZTHELYI, A., PANTESCO, V., CHABES, A., LENGRONNE, A. & PASERO, P. 2012. dNTP pools determine fork progression and origin usage under replication stress. *EMBO J,* 31**,** 883-94.

POMERANTZ, R. T. & O'DONNELL, M. 2008. The replisome uses mRNA as a primer after colliding with RNA polymerase. *Nature,* 456**,** 762-6.

PRADO, F. & AGUILERA, A. 2005. Impairment of replication fork progression mediates RNA polII transcription-associated recombination. *EMBO J,* 24**,** 1267-76.

PRAKASH, R., SATORY, D., DRAY, E., PAPUSHA, A., SCHELLER, J., KRAMER, W., KREJCI, L., KLEIN, H., HABER, J. E., SUNG, P. & IRA, G. 2009. Yeast Mph1 helicase dissociates Rad51-made D-loops: implications for crossover control in mitotic recombination. *Genes Dev,* 23**,** 67-79.

PRAKASH, S., JOHNSON, R. E. & PRAKASH, L. 2005. Eukaryotic translesion synthesis DNA polymerases: specificity of structure and function. *Annu Rev Biochem,* 74**,** 317-53.

PURSELL, Z. F., ISOZ, I., LUNDSTROM, E. B., JOHANSSON, E. & KUNKEL, T. A. 2007. Yeast DNA polymerase epsilon participates in leading-strand DNA replication. *Science,* 317**,** 127-30.

QI, Z., REDDING, S., LEE, J. Y., GIBB, B., KWON, Y., NIU, H., GAINES, W. A., SUNG, P. & GREENE, E. C. 2015. DNA sequence alignment by microhomology sampling during homologous recombination. *Cell,* 160**,** 856-869.

QIN, Y. R., TANG, H., XIE, F., LIU, H., ZHU, Y., AI, J., CHEN, L., LI, Y., KWONG, D. L., FU, L. & GUAN, X. Y. 2011. Characterization of tumor-suppressive function of SOX6 in human esophageal squamous cell carcinoma. *Clin Cancer Res,* 17**,** 46-55.

RALPH, E., BOYE, E. & KEARSEY, S. E. 2006. DNA damage induces Cdt1 proteolysis in fission yeast through a pathway dependent on Cdt2 and Ddb1. *EMBO Rep,* 7**,** 1134-9.

RASS, U., COMPTON, S. A., MATOS, J., SINGLETON, M. R., IP, S. C., BLANCO, M. G., GRIFFITH, J. D. & WEST, S. C. 2010. Mechanism of Holliday junction resolution by the human GEN1 protein. *Genes Dev,* 24**,** 1559-69.

REIJNS, M. A. M., KEMP, H., DING, J., DE PROCE, S. M., JACKSON, A. P. & TAYLOR, M. S. 2015. Lagging-strand replication shapes the mutational landscape of the genome. *Nature,* 518**,** 502-506.

REMUS, D., BEURON, F., TOLUN, G., GRIFFITH, J. D., MORRIS, E. P. & DIFFLEY, J. F. 2009. Concerted loading of Mcm2-7 double hexamers around DNA during DNA replication origin licensing. *Cell,* 139**,** 719-30.

REYNOLDS, N., WARBRICK, E., FANTES, P. A. & MACNEILL, S. A. 2000. Essential interaction between the fission yeast DNA polymerase delta subunit Cdc27 and Pcn1 (PCNA) mediated through a C-terminal p21(Cip1)-like PCNA binding motif. *EMBO J,* 19**,** 1108-18.

REYNOLDS, N., WATT, A., FANTES, P. A. & MACNEILL, S. A. 1998. Cdm1, the smallest subunit of DNA polymerase d in the fission yeast Schizosaccharomyces pombe, is non-essential for growth and division. *Curr Genet,* 34**,** 250-8.

ROUX, K. J., KIM, D. I., RAIDA, M. & BURKE, B. 2012. A promiscuous biotin ligase fusion protein identifies proximal and interacting proteins in mammalian cells. *J Cell Biol,* 196**,** 801-10.

ROZENZHAK, S., MEJIA-RAMIREZ, E., WILLIAMS, J. S., SCHAFFER, L., HAMMOND, J. A., HEAD, S. R. & RUSSELL, P. 2010. Rad3 decorates critical chromosomal domains with gammaH2A to protect genome integrity during S-Phase in fission yeast. *PLoS Genet,* 6**,** e1001032.

RUFF, P., DONNIANNI, R. A., GLANCY, E., OH, J. & SYMINGTON, L. S. 2016. RPA Stabilization of Single-Stranded DNA Is Critical for Break-Induced Replication. *Cell Rep,* 17**,** 3359-3368.

RUNGE, K. W. & LI, Y. 2018. A curious new role for MRN in Schizosaccharomyces pombe non-homologous end-joining. *Curr Genet,* 64**,** 359-364.

RUPP, W. D. & HOWARD-FLANDERS, P. 1968. Discontinuities in the DNA synthesized in an excision-defective strain of Escherichia coli following ultraviolet irradiation. *J Mol Biol,* 31**,** 291-304.

RUSSELL, P. & NURSE, P. 1986. cdc25+ functions as an inducer in the mitotic control of fission yeast. *Cell,* 45**,** 145-53.

RYU, T., SPATOLA, B., DELABAERE, L., BOWLIN, K., HOPP, H., KUNITAKE, R., KARPEN, G. H. & CHIOLO, I. 2015. Heterochromatic breaks move to the nuclear periphery to continue recombinational repair. *Nat Cell Biol,* 17**,** 1401-11.

SABOURI, N., MCDONALD, K. R., WEBB, C. J., CRISTEA, I. M. & ZAKIAN, V. A. 2012. DNA replication through hard-to-replicate sites, including both highly transcribed RNA

Pol II and Pol III genes, requires the S. pombe Pfh1 helicase. *Genes Dev,* 26**,** 581-93.

SAINI, N., RAMAKRISHNAN, S., ELANGO, R., AYYAR, S., ZHANG, Y., DEEM, A., IRA, G., HABER, J. E., LOBACHEV, K. S. & MALKOVA, A. 2013. Migrating bubble during break-induced replication drives conservative DNA synthesis. *Nature,* 502**,** 389-92.

SANCHEZ-GOROSTIAGA, A., LOPEZ-ESTRANO, C., KRIMER, D. B., SCHVARTZMAN, J. B. & HERNANDEZ, P. 2004. Transcription termination factor reb1p causes two replication fork barriers at its cognate sites in fission yeast ribosomal DNA in vivo. *Mol Cell Biol,* 24**,** 398-406.

SASAKI, T., KANNO, T., LIANG, S. C., CHEN, P. Y., LIAO, W. W., LIN, W. D., MATZKE, A. J. & MATZKE, M. 2015. An Rtf2 Domain-Containing Protein Influences Pre-mRNA Splicing and Is Essential for Embryonic Development in Arabidopsis thaliana. *Genetics,* 200**,** 523-35.

SAUVAGEAU, S., STASIAK, A. Z., BANVILLE, I., PLOQUIN, M., STASIAK, A. & MASSON, J. Y. 2005. Fission yeast rad51 and dmc1, two efficient DNA recombinases forming helical nucleoprotein filaments. *Mol Cell Biol,* 25**,** 4377-87.

SEGURADO, M., DE LUIS, A. & ANTEQUERA, F. 2003. Genome-wide distribution of DNA replication origins at A+T-rich islands in Schizosaccharomyces pombe. *EMBO Rep,* 4**,** 1048-53.

SEONG, C., SEHORN, M. G., PLATE, I., SHI, I., SONG, B., CHI, P., MORTENSEN, U., SUNG, P. & KREJCI, L. 2008. Molecular anatomy of the recombination mediator function of Saccharomyces cerevisiae Rad52. *J Biol Chem,* 283**,** 12166-74.

SHANKARANARAYANA, G. D., MOTAMEDI, M. R., MOAZED, D. & GREWAL, S. I. 2003. Sir2 regulates histone H3 lysine 9 methylation and heterochromatin assembly in fission yeast. *Curr Biol,* 13**,** 1240-6.

SHIMMOTO, M., MATSUMOTO, S., ODAGIRI, Y., NOGUCHI, E., RUSSELL, P. & MASAI, H. 2009. Interactions between Swi1-Swi3, Mrc1 and S phase kinase, Hsk1 may regulate cellular responses to stalled replication forks in fission yeast. *Genes Cells,* 14**,** 669-82.

SHINOHARA, A., OGAWA, H. & OGAWA, T. 1992. Rad51 protein involved in repair and recombination in S. cerevisiae is a RecA-like protein. *Cell,* 69**,** 457-70.

SHINOHARA, A., SHINOHARA, M., OHTA, T., MATSUDA, S. & OGAWA, T. 1998. Rad52 forms ring structures and co-operates with RPA in single-strand DNA annealing. *Genes Cells,* 3**,** 145-56.

SHOR, E., WEINSTEIN, J. & ROTHSTEIN, R. 2005. A genetic screen for top3 suppressors in Saccharomyces cerevisiae identifies SHU1, SHU2, PSY3 and CSM2: four genes involved in error-free DNA repair. *Genetics,* 169**,** 1275-89.

SMITH, C. E., LLORENTE, B. & SYMINGTON, L. S. 2007. Template switching during break-induced replication. *Nature,* 447**,** 102-5.

SOGO, J. M., LOPES, M. & FOIANI, M. 2002. Fork reversal and ssDNA accumulation at stalled replication forks owing to checkpoint defects. *Science,* 297**,** 599-602.

SOLINGER, J. A., KIIANITSA, K. & HEYER, W. D. 2002. Rad54, a Swi2/Snf2-like recombinational repair protein, disassembles Rad51:dsDNA filaments. *Mol Cell,* 10**,** 1175-88.

SONG, B. & SUNG, P. 2000. Functional interactions among yeast Rad51 recombinase, Rad52 mediator, and replication protein A in DNA strand exchange. *J Biol Chem,* 275**,** 15895-904.

SPARKS, J. L., CHON, H., CERRITELLI, S. M., KUNKEL, T. A., JOHANSSON, E., CROUCH, R. J. & BURGERS, P. M. 2012. RNase H2-initiated ribonucleotide excision repair. *Mol Cell,* 47**,** 980-6.

STAFA, A., DONNIANNI, R. A., TIMASHEV, L. A., LAM, A. F. & SYMINGTON, L. S. 2014. Template switching during break-induced replication is promoted by the Mph1 helicase in Saccharomyces cerevisiae. *Genetics,* 196**,** 1017-28.

STEINACHER, R., OSMAN, F., DALGAARD, J. Z., LORENZ, A. & WHITBY, M. C. 2012. The DNA helicase Pfh1 promotes fork merging at replication termination sites to ensure genome stability. *Genes Dev,* 26**,** 594-602.

STERN, B. & NURSE, P. 1996. A quantitative model for the cdc2 control of S phase and mitosis in fission yeast. *Trends Genet,* 12**,** 345-50.

STITH, C. M., STERLING, J., RESNICK, M. A., GORDENIN, D. A. & BURGERS, P. M. 2008. Flexibility of eukaryotic Okazaki fragment maturation through regulated strand displacement synthesis. *J Biol Chem,* 283**,** 34129-40.

STODOLA, J. L. & BURGERS, P. M. 2016. Resolving individual steps of Okazaki-fragment maturation at a millisecond timescale. *Nat Struct Mol Biol,* 23**,** 402-8.

SU, X. A., DION, V., GASSER, S. M. & FREUDENREICH, C. H. 2015. Regulation of recombination at yeast nuclear pores controls repair and triplet repeat stability. *Genes Dev,* 29**,** 1006-17.

SUGIYAMA, T., ZAITSEVA, E. M. & KOWALCZYKOWSKI, S. C. 1997. A single-stranded DNA-binding protein is needed for efficient presynaptic complex formation by the Saccharomyces cerevisiae Rad51 protein. *J Biol Chem,* 272**,** 7940-5.

SUN, W., NANDI, S., OSMAN, F., AHN, J. S., JAKOVLESKA, J., LORENZ, A. & WHITBY, M. C. 2008. The FANCM ortholog Fml1 promotes recombination at stalled replication forks and limits crossing over during DNA double-strand break repair. *Mol Cell,* 32**,** 118-28.

SUNG, P. 1997. Yeast Rad55 and Rad57 proteins form a heterodimer that functions with replication protein A to promote DNA strand exchange by Rad51 recombinase. *Genes Dev,* 11**,** 1111-21.

SUNG, P. & ROBBERSON, D. L. 1995. DNA strand exchange mediated by a RAD51-ssDNA nucleoprotein filament with polarity opposite to that of RecA. *Cell,* 82**,** 453-61.

SUO, D., WANG, L., ZENG, T., ZHANG, H., LI, L., LIU, J., YUN, J., GUAN, X. Y. & LI, Y. 2020. NRIP3 upregulation confers resistance to chemoradiotherapy in ESCC via RTF2 removal by accelerating ubiquitination and degradation of RTF2. *Oncogenesis,* 9**,** 75.

SVOBODA, M., KONVALINKA, J., TREMPE, J. F. & GRANTZ SASKOVA, K. 2019. The yeast proteases Ddi1 and Wss1 are both involved in the DNA replication stress response. *DNA Repair (Amst),* 80**,** 45-51.

TADDEI, A., VAN HOUWE, G., HEDIGER, F., KALCK, V., CUBIZOLLES, F., SCHOBER, H. & GASSER, S. M. 2006. Nuclear pore association confers optimal expression levels for an inducible yeast gene. *Nature,* 441**,** 774-8.

TAKAHASHI, T. S., WOLLSCHEID, H. P., LOWTHER, J. & ULRICH, H. D. 2020. Effects of chain length and geometry on the activation of DNA damage bypass by polyubiquitylated PCNA. *Nucleic Acids Res,* 48**,** 3042-3052.

TAMANG, S., KISHKEVICH, A., MORROW, C. A., OSMAN, F., JALAN, M. & WHITBY, M. C. 2019. The PCNA unloader Elg1 promotes recombination at collapsed replication forks in fission yeast. *Elife,* 8.

TANAKA, H., RYU, G. H., SEO, Y. S. & MACNEILL, S. A. 2004. Genetics of lagging strand DNA synthesis and maturation in fission yeast: suppression analysis links the Dna2-Cdc24 complex to DNA polymerase delta. *Nucleic Acids Res,* 32**,** 6367-77.

TANAKA, K. & RUSSELL, P. 2001. Mrc1 channels the DNA replication arrest signal to checkpoint kinase Cds1. *Nat Cell Biol,* 3**,** 966-72.

TANAKA, S., NAKATO, R., KATOU, Y., SHIRAHIGE, K. & ARAKI, H. 2011. Origin association of Sld3, Sld7, and Cdc45 proteins is a key step for determination of origin-firing timing. *Curr Biol,* 21**,** 2055-63.

TANAKA, T., YOKOYAMA, M., MATSUMOTO, S., FUKATSU, R., YOU, Z. & MASAI, H. 2010. Fission yeast Swi1-Swi3 complex facilitates DNA binding of Mrc1. *J Biol Chem,* 285**,** 39609-22.

TANG, S., WU, M. K. Y., ZHANG, R. & HUNTER, N. 2015. Pervasive and essential roles of the Top3-Rmi1 decatenase orchestrate recombination and facilitate chromosome segregation in meiosis. *Mol Cell,* 57**,** 607-621.

TAYLOR, M. R. G. & YEELES, J. T. P. 2018. The Initial Response of a Eukaryotic Replisome to DNA Damage. *Mol Cell,* 70**,** 1067-1080 e12.

TEIXEIRA-SILVA, A., AIT SAADA, A., HARDY, J., IRAQUI, I., NOCENTE, M. C., FREON, K. & LAMBERT, S. A. E. 2017. The end-joining factor Ku acts in the end-resection of double strand break-free arrested replication forks. *Nat Commun,* 8**,** 1982.

TOURRIERE, H., VERSINI, G., CORDON-PRECIADO, V., ALABERT, C. & PASERO, P. 2005. Mrc1 and Tof1 promote replication fork progression and recovery independently of Rad53. *Mol Cell,* 19**,** 699-706.

TSANG, E., MIYABE, I., IRAQUI, I., ZHENG, J., LAMBERT, S. A. & CARR, A. M. 2014. The extent of error-prone replication restart by homologous recombination is controlled by Exo1 and checkpoint proteins. *J Cell Sci,* 127**,** 2983-94.

TSUTSUI, Y., KUROKAWA, Y., ITO, K., SIDDIQUE, M. S., KAWANO, Y., YAMAO, F. & IWASAKI, H. 2014. Multiple regulation of Rad51-mediated homologous recombination by fission yeast Fbh1. *PLoS Genet,* 10**,** e1004542.

TUDURI, S., CRABBE, L., CONTI, C., TOURRIERE, H., HOLTGREVE-GREZ, H., JAUCH, A., PANTESCO, V., DE VOS, J., THOMAS, A., THEILLET, C., POMMIER, Y., TAZI, J., COQUELLE, A. & PASERO, P. 2009. Topoisomerase I suppresses genomic

instability by preventing interference between replication and transcription. *Nat Cell Biol,* 11**,** 1315-24.

VAN DE VOSSE, D. W., WAN, Y., LAPETINA, D. L., CHEN, W. M., CHIANG, J. H., AITCHISON, J. D. & WOZNIAK, R. W. 2013. A role for the nucleoporin Nup170p in chromatin structure and gene silencing. *Cell,* 152**,** 969-83.

VAS, A., MOK, W. & LEATHERWOOD, J. 2001. Control of DNA rereplication via Cdc2 phosphorylation sites in the origin recognition complex. *Mol Cell Biol,* 21**,** 5767-77.

VOINEAGU, I., NARAYANAN, V., LOBACHEV, K. S. & MIRKIN, S. M. 2008. Replication stalling at unstable inverted repeats: interplay between DNA hairpins and fork stabilizing proteins. *Proc Natl Acad Sci U S A,* 105**,** 9936-41.

WALKER, J. R., CORPINA, R. A. & GOLDBERG, J. 2001. Structure of the Ku heterodimer bound to DNA and its implications for double-strand break repair. *Nature,* 412**,** 607-14.

WALLGREN, M., MOHAMMAD, J. B., YAN, K. P., POURBOZORGI-LANGROUDI, P., EBRAHIMI, M. & SABOURI, N. 2016. G-rich telomeric and ribosomal DNA sequences from the fission yeast genome form stable G-quadruplex DNA structures in vitro and are unwound by the Pfh1 DNA helicase. *Nucleic Acids Res,* 44**,** 6213-31.

WATANABE, K., TATEISHI, S., KAWASUJI, M., TSURIMOTO, T., INOUE, H. & YAMAIZUMI, M. 2004. Rad18 guides poleta to replication stalling sites through physical interaction and PCNA monoubiquitination. *EMBO J,* 23**,** 3886-96.

WATSON, A. T., GARCIA, V., BONE, N., CARR, A. M. & ARMSTRONG, J. 2008. Gene tagging and gene replacement using recombinase-mediated cassette exchange in Schizosaccharomyces pombe. *Gene,* 407**,** 63-74.

WATT, D. L., JOHANSSON, E., BURGERS, P. M. & KUNKEL, T. A. 2011. Replication of ribonucleotide-containing DNA templates by yeast replicative polymerases. *DNA Repair (Amst),* 10**,** 897-902.

WATTS, F. Z., SKILTON, A., HO, J. C., BOYD, L. K., TRICKEY, M. A., GARDNER, L., OGI, F. X. & OUTWIN, E. A. 2007. The role of Schizosaccharomyces pombe SUMO ligases in genome stability. *Biochem Soc Trans,* 35**,** 1379-84.

WECHSLER, T., NEWMAN, S. & WEST, S. C. 2011. Aberrant chromosome morphology in human cells defective for Holliday junction resolution. *Nature,* 471**,** 642-6.

WHALEN, J. M. & FREUDENREICH, C. H. 2020. Location, Location, Location: The Role of Nuclear Positioning in the Repair of Collapsed Forks and Protection of Genome Stability. *Genes (Basel),* 11.

WILLIS, N. A., PANDAY, A., DUFFEY, E. E. & SCULLY, R. 2018. Rad51 recruitment and exclusion of non-homologous end joining during homologous recombination at a Tus/Ter mammalian replication fork barrier. *PLoS Genet,* 14**,** e1007486.

WILLIS, N. A., ZHOU, C., ELIA, A. E., MURRAY, J. M., CARR, A. M., ELLEDGE, S. J. & RHIND, N. 2016. Identification of S-phase DNA damage-response targets in fission yeast reveals conservation of damage-response networks. *Proc Natl Acad Sci U S A,* 113**,** E3676-85.

WILSON, M. A., KWON, Y., XU, Y., CHUNG, W. H., CHI, P., NIU, H., MAYLE, R., CHEN, X., MALKOVA, A., SUNG, P. & IRA, G. 2013. Pif1 helicase and Poldelta promote recombination-coupled DNA synthesis via bubble migration. *Nature,* 502**,** 393-6.

WONG, I. N., NEO, J. P., OEHLER, J., SCHAFHAUSER, S., OSMAN, F., CARR, S. B. & WHITBY, M. C. 2019. The Fml1-MHF complex suppresses inter-fork strand annealing in fission yeast. *Elife,* 8.

WOODWARD, A. M., GOHLER, T., LUCIANI, M. G., OEHLMANN, M., GE, X., GARTNER, A., JACKSON, D. A. & BLOW, J. J. 2006. Excess Mcm2-7 license dormant origins of replication that can be used under conditions of replicative stress. *J Cell Biol,* 173**,** 673-83.

WRIGHT, W. D. & HEYER, W. D. 2014. Rad54 functions as a heteroduplex DNA pump modulated by its DNA substrates and Rad51 during D loop formation. *Mol Cell,* 53**,** 420-32.

WU, P. Y. & NURSE, P. 2009. Establishing the program of origin firing during S phase in fission Yeast. *Cell,* 136**,** 852-64.

XU, J., YANAGISAWA, Y., TSANKOV, A. M., HART, C., AOKI, K., KOMMAJOSYULA, N., STEINMANN, K. E., BOCHICCHIO, J., RUSS, C., REGEV, A., RANDO, O. J., NUSBAUM, C., NIKI, H., MILOS, P., WENG, Z. & RHIND, N. 2012. Genome-wide identification and characterization of replication origins by deep sequencing. *Genome Biol,* 13**,** R27.

XU, X., PAGE, J. L., SURTEES, J. A., LIU, H., LAGEDROST, S., LU, Y., BRONSON, R., ALANI, E., NIKITIN, A. Y. & WEISS, R. S. 2008. Broad overexpression of ribonucleotide reductase genes in mice specifically induces lung neoplasms. *Cancer Res,* 68**,** 2652-60.

YABUUCHI, H., YAMADA, Y., UCHIDA, T., SUNATHVANICHKUL, T., NAKAGAWA, T. & MASUKATA, H. 2006. Ordered assembly of Sld3, GINS and Cdc45 is distinctly regulated by DDK and CDK for activation of replication origins. *EMBO J,* 25**,** 4663-74.

YAN, S. & MICHAEL, W. M. 2009. TopBP1 and DNA polymerase alpha-mediated recruitment of the 9-1-1 complex to stalled replication forks: implications for a replication restart-based mechanism for ATR checkpoint activation. *Cell Cycle,* 8**,** 2877-84.

YANEVA, M., KOWALEWSKI, T. & LIEBER, M. R. 1997. Interaction of DNA-dependent protein kinase with DNA and with Ku: biochemical and atomic-force microscopy studies. *EMBO J,* 16**,** 5098-112.

YANG, K., GONG, P., GOKHALE, P. & ZHUANG, Z. 2014. Chemical protein polyubiquitination reveals the role of a noncanonical polyubiquitin chain in DNA damage tolerance. *ACS Chem Biol,* 9**,** 1685-91.

YEELES, J. T., DEEGAN, T. D., JANSKA, A., EARLY, A. & DIFFLEY, J. F. 2015. Regulated eukaryotic DNA replication origin firing with purified proteins. *Nature,* 519**,** 431-5.

YEELES, J. T. P., JANSKA, A., EARLY, A. & DIFFLEY, J. F. X. 2017. How the Eukaryotic Replisome Achieves Rapid and Efficient DNA Replication. *Mol Cell,* 65**,** 105-116.

ZARATIEGUI, M., CASTEL, S. E., IRVINE, D. V., KLOC, A., REN, J., LI, F., DE CASTRO, E., MARIN, L., CHANG, A. Y., GOTO, D., CANDE, W. Z., ANTEQUERA, F., ARCANGIOLI, B. & MARTIENSSEN, R. A. 2011. RNAi promotes heterochromatic silencing through replication-coupled release of RNA Pol II. *Nature,* 479**,** 135-8.

ZECH, J., GODFREY, E. L., MASAI, H., HARTSUIKER, E. & DALGAARD, J. Z. 2015. The DNA-Binding Domain of S. pombe Mrc1 (Claspin) Acts to Enhance Stalling at Replication Barriers. *PLoS One,* 10**,** e0132595.

ZHOU, Z. X., LUJAN, S. A., BURKHOLDER, A. B., GARBACZ, M. A. & KUNKEL, T. A. 2019. Roles for DNA polymerase delta in initiating and terminating leading strand DNA replication. *Nat Commun,* 10**,** 3992.

ZOU, L., CORTEZ, D. & ELLEDGE, S. J. 2002. Regulation of ATR substrate selection by Rad17-dependent loading of Rad9 complexes onto chromatin. *Genes Dev,* 16**,** 198-208.

ZOU, L., LIU, D. & ELLEDGE, S. J. 2003. Replication protein A-mediated recruitment and activation of Rad17 complexes. *Proc Natl Acad Sci U S A,* 100**,** 13827-32.

ZUO, S., BERMUDEZ, V., ZHANG, G., KELMAN, Z. & HURWITZ, J. 2000. Structure and activity associated with multiple forms of Schizosaccharomyces pombe DNA polymerase delta. *J Biol Chem,* 275**,** 5153-62.

ZUO, S., GIBBS, E., KELMAN, Z., WANG, T. S., O'DONNELL, M., MACNEILL, S. A. & HURWITZ, J. 1997. DNA polymerase delta isolated from Schizosaccharomyces pombe contains five subunits. *Proc Natl Acad Sci U S A,* 94**,** 11244-9.